University of Twente

MSc Thesis Biomedical Engineering

Evaluation of linear regression models for minimal IMU based estimation of aCOM in gait and non-gait activities

Mathieu van der Donck

EECMS faculty, Department of Biomedical Signals and Systems

Examination Committee:

Bert-Jan van Beijnum	Committee Chair
Frank Wouda	Daily Supervisor
Bart Koopman	External Member

ABSTRACT

An estimation of center of mass acceleration(aCOM) using a small number of inertial measurement units(IMUs) can potentially be used to estimate energy expenditure in daily living for the purpose of monitoring users in their daily lives. IMU data and reference aCOM was gathered for a variety of gait and non-gait activities using the MVN Link suit. Linear regression models were trained on segment acceleration, angular acceleration, angular velocity and orientation data obtained from this IMU data via the MVN record software. The performance of activity specific instantaneous linear regression models for the estimation of aCOM using segment acceleration was investigated for models using inputs from the pelvis segment in addition to one other segment, the pelvis segment in addition to two symmetrical limb segments and the pelvis segment in addition to two symmetrical limb segments and the head or sternum segment. The performance of models using inputs based on the tangential and centripetal acceleration as well as linear acceleration from the pelvis segment in addition to one other segment was also tested. Models using inputs from the head, sternum and shoulder segments performed the best overall. Models using linear acceleration from symmetrical lower leg segments were necessary to obtain better performance than pelvis only models for a balancing task but did not perform well for other activities without the addition of a head or sternum segment. The addition of inputs based on the tangential and centripetal acceleration significantly improved the performance of models using inputs from the upper legs, but such models were still outperformed by models using the head, shoulders or sternum. Large differences in performance for data from different subjects was detected. It was found that such differences were not exacerbated by the addition of inputs based on the tangential and centripetal acceleration.

CONTENTS

1 INTRODUCTION

This report describes an investigation into the estimation of center of mass acceleration(aCOM) of the human body during a variety of activities. This introduction will first provide some context on why this investigation is relevant by explaining the relevance of energy expenditure estimation and then relating aCOM estimation to energy expenditure estimation. It will then establish the research question of the thesis and the limitations placed on this scope. Finally, this introduction will provide the structure of the rest of the report.

1.1 Context

To understand the relevance of aCOM estimation, it is first necessary to understand the relevance of energy expenditure and how it relates to aCOM. Energy expenditure is a measure of the metabolic energy that the human body converts into mechanical work and heat [1]. The measurement of energy expenditure has a wide variety of applications such as informing the nutrition of both critically ill patients and athletes [2, 3]. It is also used in assessing the effects of certain weight loss interventions [4].

Energy expenditure measurements in daily living would be useful since it can be used for providing feedback for patients trying to lose weight [5], monitoring the health of the elderly persons [6], providing insulin dosage recommendations for diabetics [7], or simply as a method to gather epidemiological data [8].

Energy expenditure can currently be measured using the gold standard of indirect calorimetry and the highly accurate method of doubly labeled water [9, 10]. Indirect calorimetry and doubly labeled water are obtrusive methods since indirect calorimetry requires continuous measurement of the subject's respiratory gasses via a hood or mask, and doubly labeled water requires the collection and expensive analysis of bodily liquids [10]. This makes these methods unsuitable for measuring energy expenditure in daily living, so a less obtrusive method for measuring energy expenditure in daily living is desired.

One potential less obtrusive method for estimating energy expenditure is via the motion of the body's center of mass (COM), specifically via aCOM. aCOM can be used to estimate the mechanical work done by the subject, and a difference in mechanical work can create a difference in energy expenditure [11, 12]. As such, aCOM can also contribute to the estimation of energy expenditure. aCOM has been shown to be linked to the the energy expenditure of prosthetic and brace users [12, 13], making it a promising parameter for energy expenditure estimation.

aCOM can be measured in multiple ways. The golden standard is force plates [14], which measure the ground reaction forces that act on the human body [15]. Ground reaction forces can also be measured via force shoes [16]. Another method is via the use of inertial or optical

motion capture. Optical motion capture uses camera recordings of reflected markers and is able to provide very accurate estimates of COM movement [14]. Inertial motion capture uses inertial measurement units (IMUs), sensors that combine gyroscopes and accelerometers to estimate movement [17]. aCOM estimation using full body inertial motion capture using has been validated against visual motion capture to a high degree of accuracy [18].

Inertial motion capture is the preferred method for measuring aCOM in daily living, since it is relatively unobtrusive and does not require a dedicated measuring environment. In contrast, optical motion capture and force plates come at the are location bound [16, 19] and force shoes obtrusively require large force transducers to be added to the sole of the foot [15]. Several studies have already used IMUs to estimate energy expenditure directly without make use of an estimation of aCOM [6, 20, 21].

While the aCOM estimation of full body IMU measurement setups has been validated against visual motion capture to a high degree of accuracy [18], such setups are still too obtrusive to be used repeatedly and for extended periods of time in daily life. Some studies have used the assumption that COM is contained within the pelvis, and have attempted to measure aCOM in gait using only a pelvis IMU [13, 16]. This has resulted in an estimation of aCOM that is notably of lower accuracy in the mediolateral direction relative to the vertical and posterior directions [13, 16], illustrating a need for sensor setups that measure a greater portion of the human body in order to measure mediolateral aCOM accurately.

Another issue with studies on setups with fewer IMUs is that they have often been limited to normal gait [22, 23], or specific sports tasks [24, 25]. Some studies of minimal IMU estimation of non-gait activities exist, for instance in investigating a bathtub exiting task [26], but information on non-gait tasks is sparse. Since daily living activities involve a wide variety of tasks, creating a model for estimating aCOM that can function for a variety of gait and non-gait tasks is essential for the estimation of aCOM in daily living.

1.2 Research question

Now that it is established that it would be useful to investigate models for the estimation of aCOM using a small set of IMUs in a variety of tasks, a research question can be formulated to perform such an investigation. Before this research question is formulated, the scope of the investigation will first be narrowed to create a feasible research question for an exploratory study.

The first narrowing of the scope concerns the activities. Multiple activities will be investigated, but this investigation will not concern itself with the generalisability of the model over multiple activities. The investigated models will also not include automatic activity detection in order to reduce the complexity of the implemented model. Instead, data will manually be labeled as an activity type, and activity specific models will be trained and evaluated on data that belongs to one activity label. This means that these models will have the assumption that an activity detection model has first selected which model to use. In addition to activity recognition, the model will also assume step detection: Data for gait-based activities will be segmented into individual steps before being used for training and evaluation.

The second narrowing of the scope happens through the IMUs that are considered. As established, using only one IMU does not produce sufficiently accurate results, but it is nevertheless desirable to limit the amount of IMUs used as much as possible. As such, the amount of IMUs

that provide inputs to the investigated models will initially be limited to 2, and models using more IMUs will only be investigated where it is warranted. As the pelvis IMU can provide a moderately accurate estimate on its own, all models that are investigated will include an IMU on the pelvis as a sensor providing input data. This means that the thesis will investigate the performance of models using input from IMUs placed in different locations of the body when combined with an IMU on the pelvis.

Lastly, a final narrowing of the scope will be performed by limiting the type of model that is considered. As it is sensible to start by investigating the simplest possible model, only variations on linear regression models will be investigated in this study. The data from these IMUs will additionally be used in ways that are based on the kinematics of the human body, as these are the most likely to produce useful results.

With these three limitations applied, the research question becomes as follows: What is the performance of activity specific linear regression models for the estimation of whole body aCOM using a pelvis mounted IMU and at least one other IMU, using inputs based on the kinematic properties of human motion, and which IMUs are the most suitable to use in addition to the pelvis with these models?

1.3 Structure

Now that the goal of this thesis has been established, the investigation of this goal will be detailed as follows: First the rigid body model (RBM) which informs the biomechanical basis for the input parameters of the linear regression models will be described, followed by the means by which the data for the models was collected. Then the models themselves will be described, including preprocessing steps and their mathematical description. The process of evaluating the models and selecting input IMUs for evaluation will be described and the results of the evaluation will be described and then summarized using a number of tables. Finally the limitations, potential follow ups and other considerations for the results will be discussed.

2 BACKGROUND

This section contains background information on the models used in this thesis. First a general formulation for a linear regression model(LRM) will be provided. Then number of kinematic definitions used within this thesis will be established. These definitions will be then be used to define a rigid body model (RBM), which functions as a simplified model of the human body. It will be shown that the motion described by this rigid body model can be used to calculate aCOM of the simulated body, and this kinematic relation between the motion of the RBM and aCOM will be used in the methods section to derive biomechanically valid input parameters for the LRMs used to estimate aCOM.

2.1 Linear regression models

This thesis aims to estimate aCOM using a simple linear regression model(LRM), as it is the easiest possible model to use aside from simply assuming that an IMU measures aCOM directly. This section will provide a basic description of how LRMs work.

An LRM estimates a target(u) by multiplying a series of basis functions($f_n()$) based on inputs (v_n) with corresponding coefficients(w_n) [27].

$$\bar{u} = w_0 + \sum_{n=1}^{N} w_n * f_n(v_n) \tag{2.1}$$

Here N is the amount of basis functions used in the model. The coefficients of the LRM are chosen such that an error function is minimized. When the target data has a gaussian noise distribution, the best estimate is given by minimizing the root mean square error, which is as follows [27]:

$$E = \sqrt{(\bar{u} - u)^2} \tag{2.2}$$

Through basis functions, LRMs can be used to model nonlinear relationships, on the condition that these relationships are known [27]. The models investigated in thesis will use three types of basis functions, the exact form of which will be discussed in section 3.4.

2.2 Kinematic notation

To explain the equations and models used in this thesis, it is first necessary to establish the notation for the kinematic concepts that will be used. This section will define the notation used for the vectors, coordinate systems and rotations used to define the rigid body model.

2.2.1 Coordinate systems and vectors

A coordinate system is a method of representing the distances between different points in space. All coordinate systems used in this thesis are Cartesian and are denoted using one or more capital letters. (For example, frame A.) Cartesian coordinate systems consist of an origin and a number of perpendicular axes. In the case of three dimensional coordinates, these axes will be denoted as the x-, y- and z-axis.

Coordinate systems have origins, denoted by O_A, where O indicates that it is an origin and the subscript indicates the coordinate system to which the origin belongs. The coordinates of points are defined in relation to the origin, as a sum of multiples of the unit vectors along each of the three axes.

$$\vec{r}_A = \begin{bmatrix} r_{A,x} \\ r_{A,y} \\ r_{A,z} \end{bmatrix} \tag{2.3}$$

Here r is a point, $\overrightarrow{r_A}$ is the point described as vector coordinates within A, and $r_{A,x}$, $r_{A,y}$, $r_{A,z}$ are the components of $\overrightarrow{r_A}$ along the x, y and z axes, respectively. As the origin of a coordinate system has zero distance from itself, the position of the origin within its corresponding coordinate system is as follows:

$$\vec{O}_{A,A} = \begin{bmatrix} 0 \\ 0 \\ 0 \end{bmatrix} \tag{2.4}$$

As with eq. 2.3, the second subscript here indicates that $\vec{O}_{A,A}$ is a vector within coordinate system A.

2.2.2 Rotation matrices and translating between coordinate systems

Vectors that are defined within one coordinate system can be transformed into coordinates within another coordinate system when the two coordinate systems are defined in relation to one another. This is done using a translation, which is the simple addition of a coordinate vector, and a rotation. The vector used for translation is the location of the origin of the original coordinate system in the target coordinate system, $\vec{O}_{A,B}$ for a translation from A to B. A rotation describes a difference in the direction of the x y and z axes of the coordinate frame, and can be described by both a rotation matrix and a unit quaternion. A rotation matrix that describes a rotation from coordinate system A to coordinate system B is denoted as $\mathbf{R}^{\mathbf{AB}}$, with the first superscript denoting the original coordinate system and the second superscript denoting the target coordinate system. A rotation of a vector is performed by performing a matrix multiplication with the rotation matrix and the vector.

$$\vec{r}_B = \boldsymbol{R^{AB}} * \vec{r} + \overrightarrow{O}_{A,B} \tag{2.5}$$

A rotation matrix is a 3 by 3 matrix, but can be written as a function of Euler angles. In 3D space, these are 3 angles that each represent a rotation around one of the axes of the coordinate system. They are depicted in figure 2.1. These angles are named pitch(α),roll(β) and heading(γ) and are depicted in . A 3D rotation matrix based on the euler angles can be seen as the rotation that would result from a rotation around each of the three axes in sequence. When applying rotations in sequence in this way, the result depends on the order in which the rotations are applied.

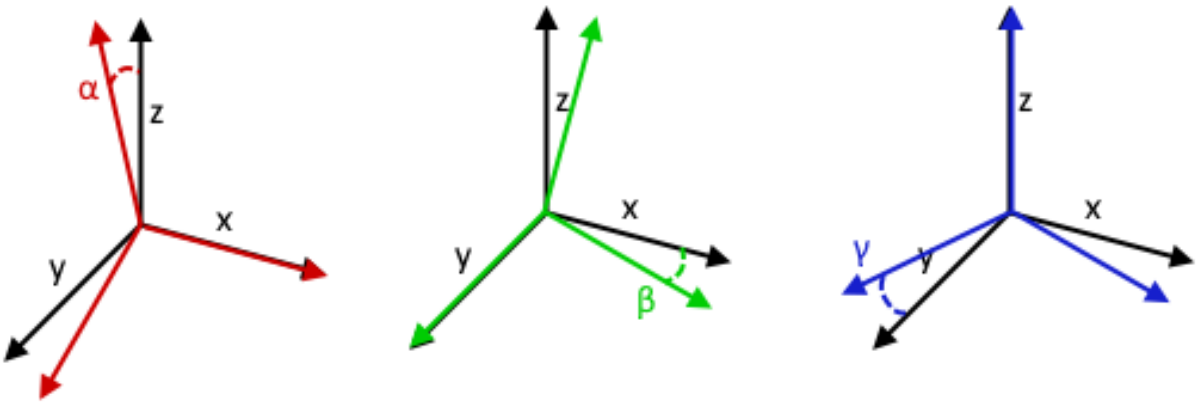

Figure 2.1: A depiction of the pitch roll and heading angles.

$$\boldsymbol{R}_{\gamma}^{\boldsymbol{AB}} \boldsymbol{R}_{\beta}^{\boldsymbol{AB}} \boldsymbol{R}_{\alpha}^{AB} = \boldsymbol{R^{AB}} = f(\alpha, \beta, \gamma) \tag{2.6}$$

Rotation matrices are a more intuitive representation of rotation than quaternions and will therefore be used in the description of the rigid body model. Note however that any rotation described by a rotation matrix can be described by a unit quaternion. Unit quaternions are 4 dimensional vectors with components denoted q_0 through q_3. The first step in performing rotation using a unit quaternion is creating the quaternion representation of the vector:

$$\begin{bmatrix} r_A, x \\ r_A, y \\ r_A, z \end{bmatrix} \longrightarrow \begin{bmatrix} 0 \\ r_A, x \\ r_A, y \\ r_A, z \end{bmatrix} \tag{2.7}$$

Once the vector is in quaternion representation, it can be rotated by performing the following quaternion multiplication using the unit quaternion.

$$\begin{bmatrix} 0 \\ r_B, x \\ r_B, y \\ r_B, z \end{bmatrix} = \vec{q}^{AB} \begin{bmatrix} 0 \\ r_A, x \\ r_A, y \\ r_A, z \end{bmatrix} \vec{q}^{AB-1} \tag{2.8}$$

Here again the superscripts on $\vec{q}^{AB}$ indicate that $\vec{q}^{AB}$ describes a rotation from coordinate system A to coordinate system B. $\vec{q}^{AB-1}$ is the inverse of $\vec{q}^{AB}$. Quaternion multiplication is different

from matrix multiplication but the specifics of the process are not required to understand of the work done in this thesis. It is sufficient to understand that the quaternion multiplication in eq. 2.8 describes a rotation of the vector $\vec{r}_A$.

2.3 Rigid body model

Now that the notation for vectors and coordinate systems has been established, they will be used to describe a rigid body model. Subsequently, the relation between the motion of an RBM and its center of mass will be shown.

2.3.1 Segments and coordinate systems

An RMB is a simplified model of the human body that consists of linked rigid segments, each of which represents a bone or group of bones within the human body. RBMs are commonly used in the description and measurement of human motion, including in MVN [28, 29].

In order to describe the movement of the body relative to the world, the RBM is modelled within a stationary local frame (L) which represents the outside world. Defined in relation to this local frame is the root segment, which can be any arbitrarily chosen segment of the rigid body model. A schematic depiction of this relation is shown in figure 2.2. The root segment is modelled via its frame (Sr), which is defined in relation to the local frame via a rotation and translation.

$$\overrightarrow{p_L} = \boldsymbol{R^{SrL}} * \vec{p}_{Sr} + \overrightarrow{O}_{Sr,L} \tag{2.9}$$

Here $\vec{p}$ is a point that is defined in relation to the root segment. The root segment has 3 rotational and 3 Cartesian degrees of freedom. This means that each of the axial components of $\overrightarrow{O}_{Sr,L}$ and each of the Euler angles that describe $\boldsymbol{R^{SrL}}$ can change depending on the position and pose of the body that is being modelled [28].

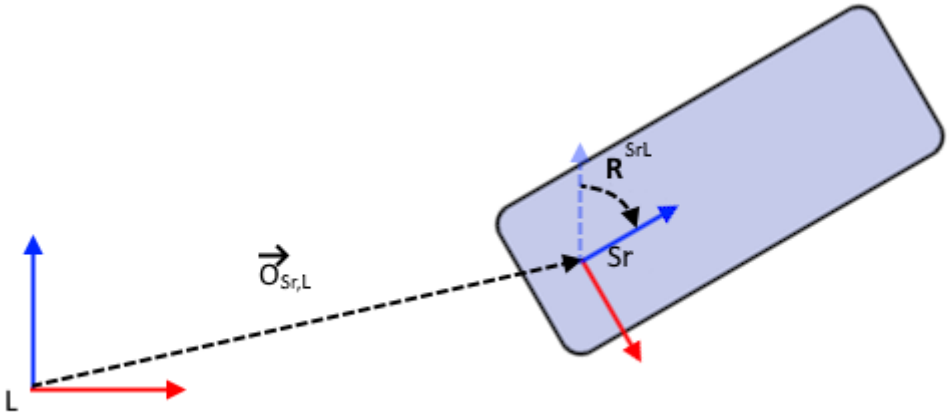

Figure 2.2: A schematic illustration of the definition of a root segment within the local frame.

Segments other than the root segment are defined in relation to another segment. A rigid body model with a parent segment and other segmnets is depicted in figure 2.3. The segment that a segment is defined in relation to is its parent segment. A segment is also called the child segment of its parent segment. The relation between a segment and its parent segment can be described in a fashion similar to eq.2.9 [28].

$$\vec{p}_{Sb} = \boldsymbol{R^{AB}} * \vec{p}_{Sa} + \overrightarrow{O}_{Sa,Sb} \tag{2.10}$$

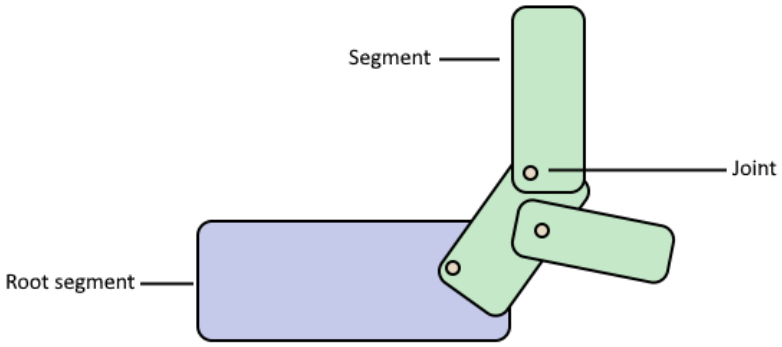

Figure 2.3: A schematic illustration of a 2D rigid body model.

Here Sb is the frame of the parent segment of the segment defined by the frame Sa. The difference between the relations defined through parent segments and the relation between the local frame and the parent segment is that non-root segments only have rotational degrees of freedom. The position of a segment's origin within its parent frame remains constant. The positions of these segment origins are normally chosen to represent joints, and the rotational degrees of freedom may be limited to represent a joint with limited rotational degrees of freedom such as the elbow joint. The segments in the RBM are additionally linked in a hierarchical manner: Any segment within the RBM is defined in relation to the root segment through a chain of parent segments [28].

Due to the hierarchical character of the RBM segments, eq. 2.10 can be applied repeatedly to a point defined on any segment in order to find its location in the root segment frame, followed by eq. 2.9 to find its position in the local frame. As such, an RBM describes every point defined on each of its segment frames within the local frame.

Aditionally there are a number of parameters that describe motion that are used in the description of the models used in this thesis. The segment acceleration is the second time derivative of the position of the segment origin in the local frame, the segment orientation is the difference in orientation between the segment frame and local frame, and the segment angular velocity and angular acceleration are respectively the first and second time derivatives of the segment orientation.

2.3.2 Rigid body model motion and aCOM

Now that the RBM is defined, it can be shown that motion described by an RBM can be used to calculate aCOM. To do this, it will first be shown that an RBM can be used to calculate COM

position in the Local frame ($\vec{p}_{COM}$).

Using the assumption that both the mass and distribution of mass of a segment do not change over time, it is possible define a segment mass (m_n) and the coordinates of a segment center of mass within the segment frame($\vec{p}_{COM,Sn,Sn}$). Here n denotes the nth segment from a list of segments of an RBM, Sn denotes the coordinate frame of segment n. As established, the coordinates of the segment center of mass can be translated to the local frame by repeatedly applying eqs. 2.9 and 2.10, resulting in ($\vec{p}_{COM,Sn,L}$). The segment masses and the segment positions in the local frame can be used to calculate the position of the whole body center of mass in the local frame via the definition of the center of mass of an object consisting of number of discrete volumes [30].

$$\vec{p}_{COM,L} = \frac{1}{M} \sum_{n=1}^{N} m_n * \vec{p}_{COM,Sn,L} \tag{2.11}$$

Here M is the sum of the segment masses and N is the total number of segments. Taking the second derivative of eq. 2.11 produces an equation for the object's center of mass acceleration based on the acceleration of the centers of mass of its constituent volumes.

$$\vec{a}_{COM,L} = \frac{1}{M} \sum_{n=1}^{N} m_n * \vec{a}_{COM,Sn,L} \tag{2.12}$$

As such, it is possible to calculate the aCOM of a rigid body model that describes the motion of points within its segment frames. Eq. 2.12 will be used in section 3.4.1 to formulate linear regression models in such a way that the parameters and coefficients estimate m_n/M and $\vec{a}_{COM,Sn,L}$.

3 METHODS

To investigate which IMU placement locations are the best to use for the estimation of aCOM, linear regression models were trained on IMU measurements and measurements of reference aCOM data from a number of activities. This section will first describe the system used to acquire the IMU and reference aCOM data and the protocol of the activities it was used in. Then, it will detail the preprocessing steps used before training the models, the models themselves and their mathematical justifications, and then lastly the analysis used to evaluate the models. An overview of these steps can be seen in figure 3.1.

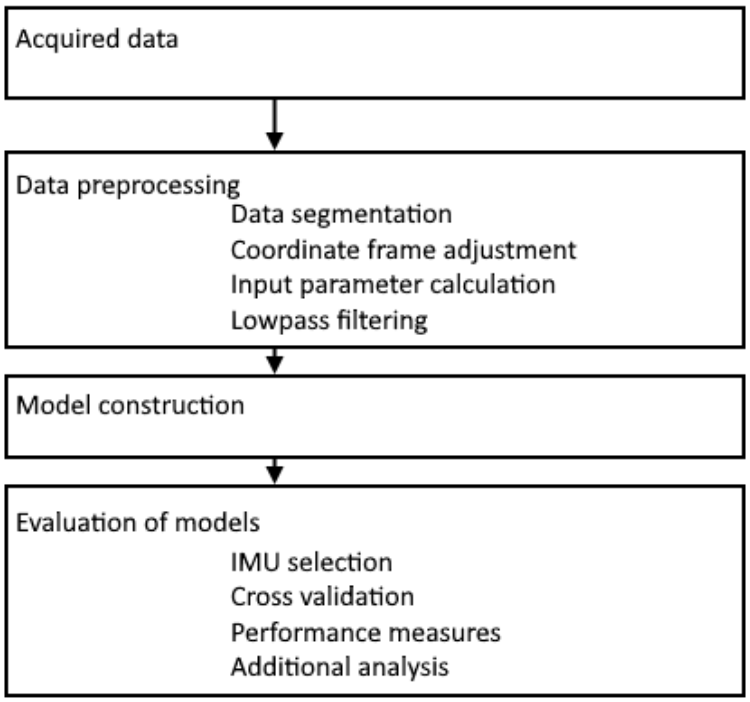

Figure 3.1: A schematic overview of the steps taken to evaluate different linear regression models.

3.1 Data acquisition system

To acquire the IMU data and reference aCOM data used to train and evaluate the models, the MVN Link suit was used [29]. It is a measurement system which consists of 17 IMUs placed in different locations on the body [29]. The MVN Link suit transmits information to a wireless receiver connected to a PC running the MVN analyze software, which processes the data.

Recordings made via in this way provide an estimate of aCOM that is close in accuracy to visual motion capture [18, 29]. IMUs were attached to the body using a headband, double sided tape and velcro straps[†], on the locations shown in figure 3.2. A photo of the setup can be seen in figure 3.3. Aside from IMUs, the Link suit requires the subject to wear a body pack which transmits the data to the receiver and a battery pack which powers the suit [29]. These were also attached using double sided tape and velcro straps.

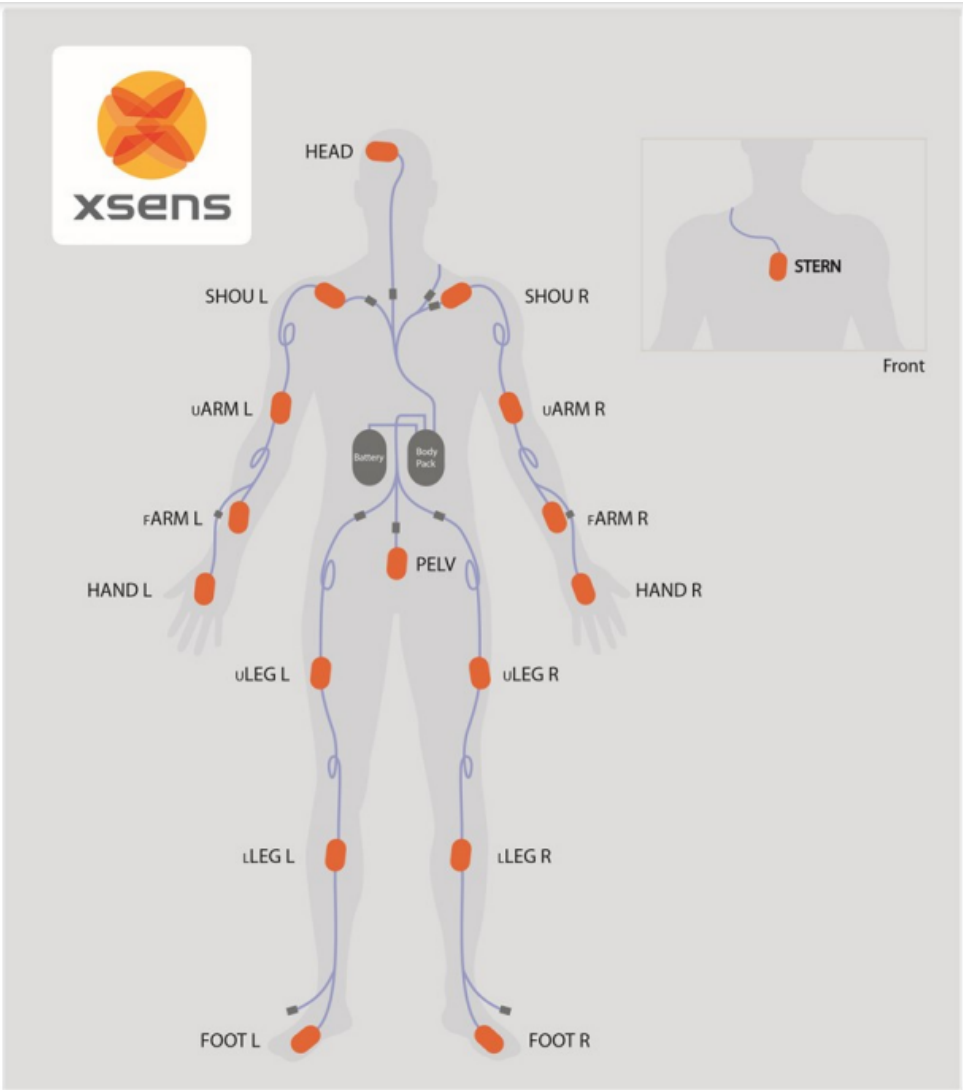

Figure 3.2: A schematic depiction of the different placement locations of the IMUs used in the MVN Link suit. Source: Xsens MVN quick setup sheet [31].

The MVN analyze software processes the data transmitted to it using the subjects body dimensions, data from the magnetometer included in the IMUs of the MVN Link system, as well as detected contacts between subject's body and the floor to improve the estimate of the captured motion. After the processing the recorded data be exported, creating a file containing among other things the aforementioned detected contacts and center of mass acceleration data, the ac-

[†]The Link suit IMU's were attached using double sided tape and velcro straps instead of the lycra suit that is normally used because the Link measurements were taken in tandem with VICON optical motion capture measurements for a different study, and the lycra suit was incompatible with the marker clusters used in thee optical motion capture measurements. These optical motion capture measurements were not used in this thesis except to detect when the subject stepped off the beam in the beam walk recording, as the difference between standing on the beam and standing on the ground detectable in the MVN recordings.

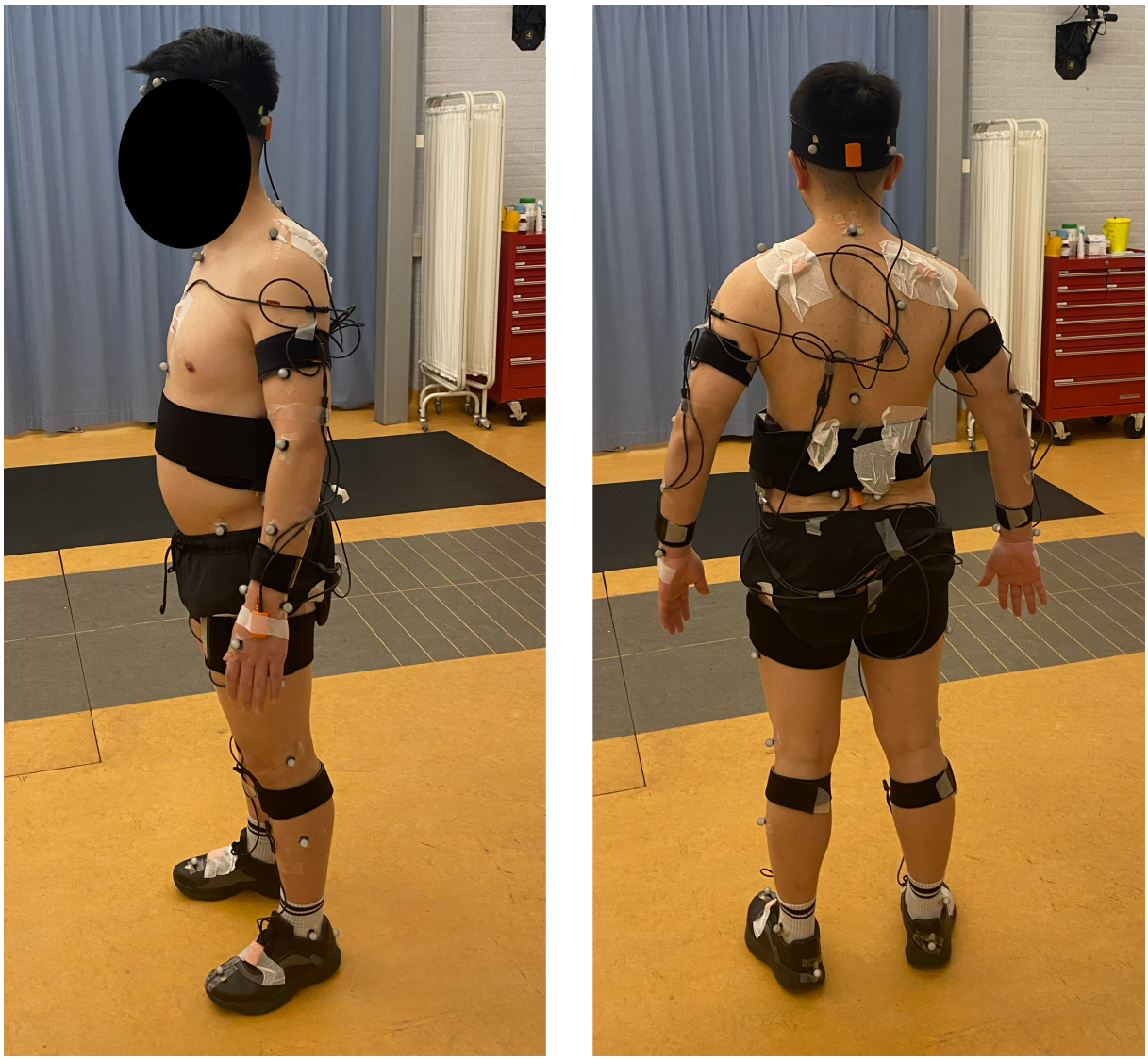

Figure 3.3: Pictures of a subject wearing the measurement setup attached with double sided tape and velcro straps, taken from the front and side.

celeration and angular velocity of the body segment frames within the local frame(body segment data) and processed sensor acceleration and angular velocity within the sensor frame(sensor data) [29].

Although the sensor data is closer to what a minimal IMU setup would measure, the body segment data is still a reasonable approximation of IMU data that is calibrated to equalize the data for varying IMU positions on the body segment. Due to the exploratory nature of this thesis, the models were trained and evaluated using the body segment data rather than the sensor data in order to reduce the amount of processing that needed to be performed.

3.2 Measurement protocol

To accomplish the goal of evaluating different models in gait and non-gait activities, a protocol was created[‡] to encompass multiple variations of gait and multiple non-gait activities. First the Link suit was put on the subject as described in the previous section. Once the subject was wearing the Link suit, the calibration of the MVN software was performed. This calibration involved the subject standing in N pose, walking forward, turning around and then walking back. After the calibration was performed, the other activities in the protocol were performed and recorded using the Link suit.

The activities performed in the protocol were performed in sequence and are listed below. The performance of each activity by the subject was first preceded by instructions on how to perform the activity. The activities were performed three times each before moving to the next and for each repetition the subject was told to start the activity via a verbal start signal. The subject was instructed to stand in place prior to the start of each activity, and would stand in place until the start signal was given. Every activity involving gait was performed at the subjects preferred pace.

1. Natural walking: The subjects walked forward until the subjects was several steps outside of a threshold in the measurement area.
2. Slalom walking: The subjects walked around several plastic markers on the floor following a slalom pattern. The markers were placed in a straight line, approximately 75 cm apart.
3. Zigzag: The subjects walked around several plastic markers on the floor following a slalom pattern. The markers were placed approximately 60 cm apart in the direction of travel and approximately 150cm perpendicular to the direction of travel, so that the subjects alternated between walking in a straight line and walking around the markers.
4. Walk and turn: The subjects walked up to a plastic marker on the floor, walked around it and then continued to walk for several steps.
5. Sit down and Stand up: The subjects stood in front of a stool, sat down on it for 3-5 seconds and then stood up. The stool did not have armrests or a backrest.
6. Jump: The subject jumped forwards by pushing off the floor with both legs simultaneously. After landing, the subjects remained standing until given a stop signal.
7. Beam walking: The subjects stepped onto a narrow beam and walks across it, balancing themselves. The subjects kept walking after they have stepped off the beam until they were past a threshold in the measurement area.
8. Terrain walking: The subjects stepped onto a section of uneven terrain and walked across it. The subjects will kept walking after they stepped off the terrain until they were past a threshold in the measurement area.
9. Stairs walking: The subjects approached and then walked up a set of stairs, onto a platform. The subjects took a few steps after reaching the platform and then turned around and walked back down the stairs. The subjects did not make use of the railing during the activity.

[‡]Courtesy to Junhao Zhang, who defined the lion's share of the activities.

The activities were performed by 11 young healthy adults, 8 male and 3 female. All anthropometric measurements available for input to MVN were taken and used in the processing of the measurements. Subjects were assigned a number (1 to 11) and the processed trial data was exported with a subject number, trial number, and activity type attached. The zigzag and turn activities were not performed for subject 1.

3.3 Preprocessing

Before models could be trained on the data, some processing had to be performed first. First, the part of the recording that encompassed the activity was extracted in order to exclude non-activity related motion. Then, the data was rotated to an anatomical coordinate frame to keep the posterior and mediolateral directions consistent with rotation of the body. The basis functions for the input of the linear model were selected or calculated. And finally, a 10Hz lowpass filter was applied to the data to filter out noise.

3.3.1 Data segmentation

In order to include only the relevant data in the training and evaluation of the model, the data that corresponded to the activities had to be extracted from the recordings. This was performed in two steps: First, a section of the recording encompassing the activity was selected, then this selection was trimmed down further and segmented into steps using estimated foot contacts.

To prevent activities from being contaminated with sections of standing still, or walking or turning where these were not the activity of interest, the recordings were visually evaluated via the render provided by MVN analyze. From this evaluation, a range of samples that encapsulated only the activity of interest was determined and extracted from the recording. As step detection would be used to trim the recording down to a precise start and end, ranges of samples that were slightly wider than the section containing the activity of interest were determined.

Two notable alterations are made through this extraction process: The stairs walking recordings were divided into two activities: One where the subject is walking up the stairs, and one where the subject is walking down the stairs. This was done because walking downstairs and walking upstairs result in distinct types of motion. The walk and turn activity was also trimmed in such a way that the extracted data only contained the turning part of the recording and not the straight line walking part, because the recordings from the natural walking activity already included straight line walking. The two parts of the stairs walking recording will be referred to as 'Stairs walking up' and 'Stairs walking down', and the data extracted from the walk and turn activity will be referred to as the 'turn' activity. The criteria for the start and of all activities can be found in appendix A.

Since the models created in this thesis assume accurate step detection, step detection was used to further trim down and segment the extracted data for the gait based activities. Usage of MVN's foot contact detection failed to work for certain stairs walking recordings, so instead the magnitude of the foot velocity of the foot segment was used to detect foot contacts. An absolute velocity below a 10% of the maximum foot velocity within the recording was treated as a foot contact. The time series segments that were extracted, shown in figure 3.4, were defined as the frames between the end of a foot contact(foot-off) of one foot and the foot-off of the other foot and extracted from the recordings. If the recording contained a new foot contact after the

final foot-off in that recording, the extraction was performed as shown in figure 3.5: the frames between that foot-off and the new foot contact were treated as an additional time series segment and extracted. The jump and sit down and stand up activities were not segmented in this way and the section of the recording that extracted using the start and end criteria was used as a single time series segment.

In addition to preparing the data for the next step in the processing, the data segmentation was also used to examine the step length and exclude extremely slow or quick steps in certain activities. A more in-depth description of this process can be found in appendix B.

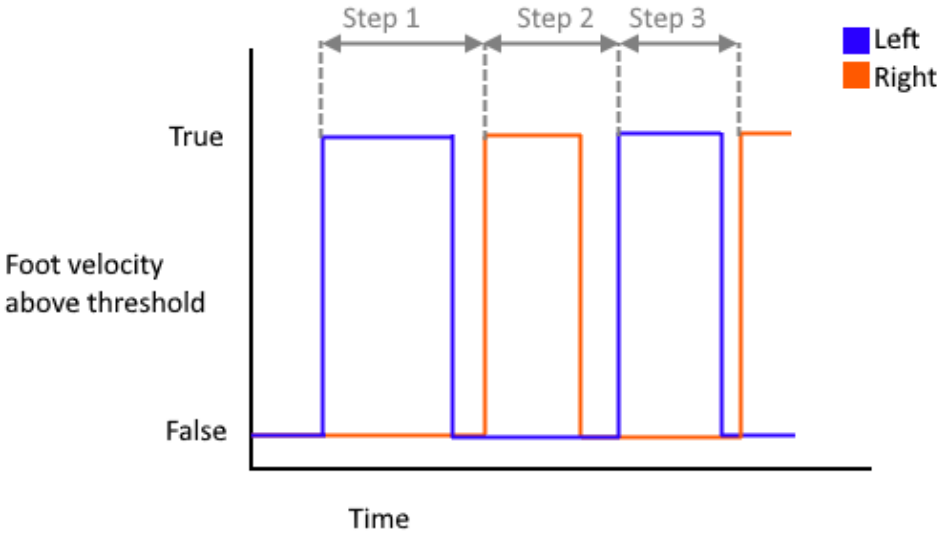

Figure 3.4: A schematic depiction of the time series segment start and end criteria.

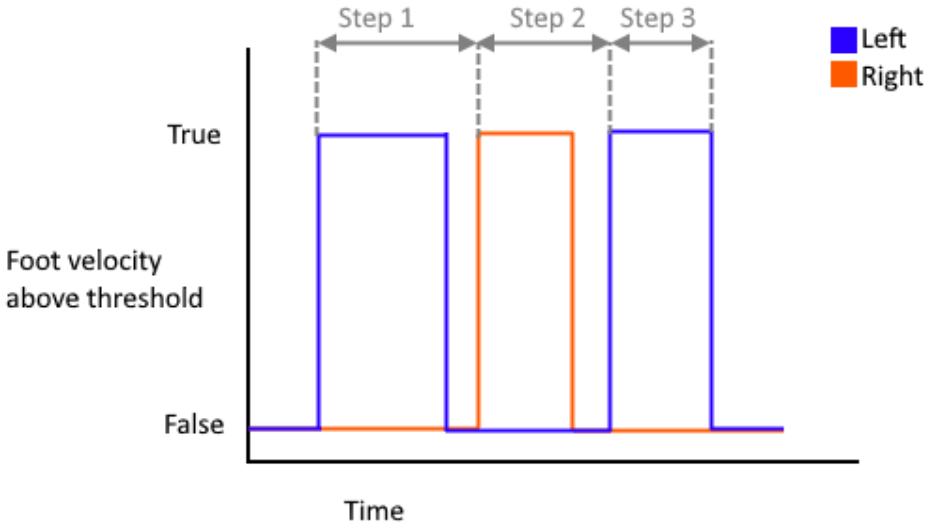

Figure 3.5: A schematic depiction of the time series segment start and end criteria in the case where the recording ends after a new foot contact but before a foot-off.

3.3.2 Coordinate frame adjustment

After the relevant data was extracted, the data was converted from the local frame to an anatomical frame. This was necessary since the body segment data from the exported recordings are defined in the local frame, and the local frame allows the subject's body to freely rotate within it. This creates a situation where it is inconsistent whether an axis corresponds to the anterioposterior direction, the mediolateral direction, or a combination of both. To create a frame where the axes consistently correspond to the anterioposterior and mediolateral directions, shown in figure 3.6, a frame defined by the vertical vector of the local frame and the heading of the pelvis frame as defined in the MVN manual[29] were used to create a frame called the anatomical frame(P). This heading of the pelvis is defined as an orthogonal vector to a line between the left and right anterior superior iliac spine and is based on established anatomical definitions [29].

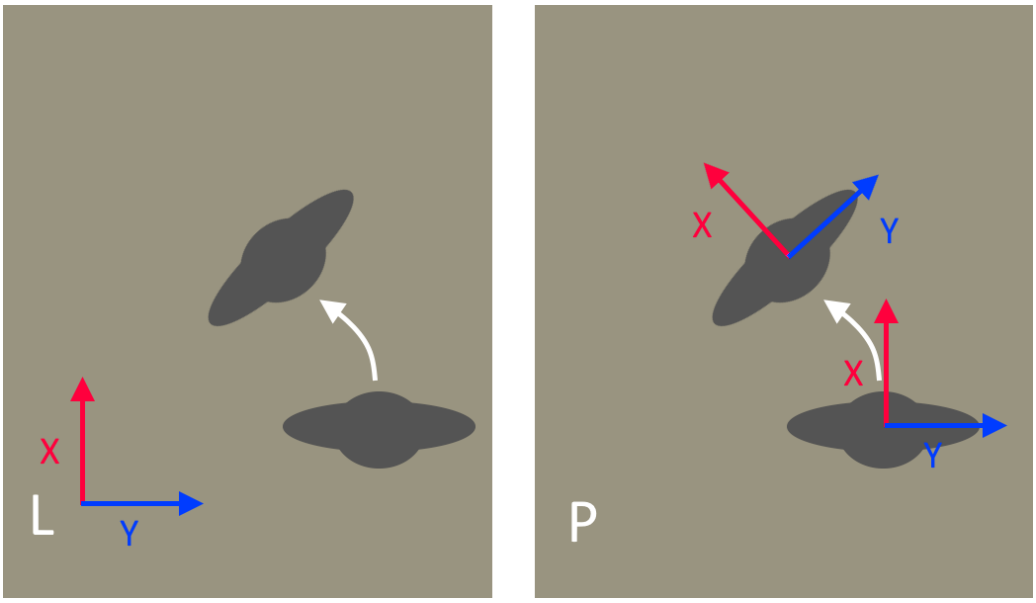

Figure 3.6: A comparison between the local frame(L) and the anatomical frame(P) when the subject rotates.

The vertical axis from the global frame was kept instead of placing all vectors in the pelvic coordinate frame, because this vertical axis is based on the gravity [29], which is both measurable in minimal IMU setups and physiologically meaningful, since it is a force that the human body must counteract. Due to its availability and relevance, using a combination of the gravity vector and the pelvis heading has value compared to using a purely pelvis based coordinate system.

In order to place the body segment data in the pelvis heading based frame, the heading was first extracted from the pelvis orientation. Since the MVN provides the orientation as a quaternion, the heading can be extracted using the formula for heading angle from quaternions [32].

$$\gamma = atan2(q_1 + q_3, q_0 - q_2) + atan2(q_3 - q_1, q_2 + q_0) \tag{3.1}$$

A quaternion is constructed from the negative of this heading angle and used to rotate all global frame variables provided by MVN. This quaternion can be constructed using the formula to convert euler angles to quaternions [33].

$$
\begin{aligned}
q_0 &= cos(\frac{\alpha}{2})cos(\frac{\beta}{2})cos(\frac{\gamma}{2}) + sin(\frac{\alpha}{2})sin(\frac{\beta}{2})sin(\frac{\gamma}{2}) \\
q_1 &= cos(\frac{\alpha}{2})cos(\frac{\beta}{2})sin(\frac{\gamma}{2}) - sin(\frac{\alpha}{2})sin(\frac{\beta}{2})cos(\frac{\gamma}{2}) \\
q_2 &= cos(\frac{\alpha}{2})sin(\frac{\beta}{2})cos(\frac{\gamma}{2}) + sin(\frac{\alpha}{2})cos(\frac{\beta}{2})sin(\frac{\gamma}{2}) \\
q_3 &= sin(\frac{\alpha}{2})cos(\frac{\beta}{2})cos(\frac{\gamma}{2}) - cos(\frac{\alpha}{2})sin(\frac{\beta}{2})sin(\frac{\gamma}{2})
\end{aligned}
\tag{3.2}
$$

Since the only rotation that occurs is a negation of the pelvis heading and α and β remain unchanged, the equation becomes as follows:

$$
\begin{aligned}
q_0 &= cos(\frac{-\gamma_{pelvis}}{2}) \\
q_1 &= 0 \\
q_2 &= 0 \\
q_3 &= sin(\frac{-\gamma_{pelvis}}{2})
\end{aligned}
\tag{3.3}
$$

This quaternion was used to rotate all body segment data as well as aCOM, resulting in IMU data in a frame where the heading angle of the pelvis is always 0. Since a change in the heading angle represents a rotation around the z axis, the direction of the z axis in this new frame is consistent with its direction in the local frame defined by MVN.

3.4 Analysis

To compare the linear models that have been established as well as the possible input body segments, the models need to be evaluated. This section will first describe which combinations of input parameters were evaluated, and how describe how a selection of input body segments for these models was made. Then it will describe the performance metrics that were used to evaluate the models, and how cross validation was used to evaluate the generalizability of the models. Finally, a number of additional plots used in the analysis of the models will be described.

3.4.1 Model types

Four types of models were investigated in this thesis, three of which use only body segment acceleration and one which uses a combination of body segment acceleration and the variables based on the tangential and centripetal acceleration. For every combination of activity, body segment combination and model type that was investigated, three seperate sets of coefficients were calculated, each of which was used to estimate a different axial component of aCOM in the anatomical frame. This section provides the formulation of each of these four model types.

Body segment acceleration models

For the first model type based on body segment acceleration, the ”one direction acceleration model”, only body segment acceleration in the same direction as the estimated component of aCOM is considered. This is done by a model of the following form:

$$\vec{\bar{a}}_{COM} = w_0 + \sum_{n=1}^{N} w_n * \vec{a}_{Sn} \tag{3.4}$$

Here a_{Sn} is the linear acceleration of segment n The mathematical justification that relates a model of this format to the kinematics of the RBM can be found in appendix C. Since a_{COM} is a three dimensional vector, the components of a_{COM} ($a_{COM,x}$, $a_{COM,y}$, $a_{COM,z}$) are each estimated separately in the implementation of this model.

$$\begin{aligned} a_{COM,x} &= w_{x,0} + \sum_{n=1}^{N} w_{x,n} * a_{Sn,x} \\ a_{COM,y} &= w_{y,0} + \sum_{n=1}^{N} w_{y,n} * a_{Sn,y} \\ a_{COM,z} &= w_{z,0} + \sum_{n=1}^{N} w_{z,n} * a_{Sn,z} \end{aligned} \tag{3.5}$$

Here $w_{x,n}$,$w_{y,n}$ and $w_{z,n}$ are the coefficients that correspond to the estimation of the x, y and z axis components of $\vec{a}_{COM}$, respectively.

Although the only kinematic relation between aCOM and body segment linear accelerations is between accelerations along the same axis, there might nevertheless be cross axis correlations between the accelerations due to the periodic nature of human movement. Since using linear accelerations from different axes still satisfies dimensional analysis, and the addition of extra inputs of linear acceleration is trivial, the body segment linear accelerations along all axes can be considered for each axial component of aCOM. In the second model type based purely on body segment acceleration, the ”all direction acceleration model”, all three axial components are used. This produces a model of the following form:

$$\sum_{n} w_{x,n} * alin_{seg_n} = w_{x,1} * a_{S1,x} + w_{x,2} * a_{S1,y} + w_{x,3} * a_{S1,z} + w_{x,4} * a_{S2,x} + ... \tag{3.6}$$

Additional body segments

While most of the models that were investigated use only data from the pelvis and one other body segment, a model using three body segments was employed in the case of the beam walk activity where all models performed poorly for the mediolateral direction. This third model type, the ’multi segment model’ were models to the form of eq.3.6 using body segment acceleration from symmetrical limb segments(Ex. Both upper leg segments) in addition to the pelvis.

Body segment angular velocity and angular acceleration models

The fourth model type, the 'gyroscope based model', aims to make use of information about aCOM contained in the gyroscope data in addition to the body segment acceleration. While body segment orientation data is used in calculating the body segment acceleration, since the body segment orientation is used to rotate the direction of this acceleration into the anatomical frame, data corresponding to the gyroscope measurements is otherwise not utilized in the two previous models. The gyroscope based model uses body segment angular velocity and body segment angular acceleration via a set of nine features in addition to the body segment acceleration data. These nine features were derived via the kinematic equations for centripetal acceleration(a_c) and tangential acceleration(a_t). These two equations are as follows [30]:

$$a_{c,a} = -r_a * \dot{\theta_b}^2 \tag{3.7}$$

$$a_{t,a} = r_b * \ddot{\theta_c} \tag{3.8}$$

Here a, b and c denote three orthogonal axes, r_a is the a axis component of the distance between the point where the acceleration is calculated in and the axis of rotation, and $\dot{\theta}_b$ and $\ddot{\theta}_c$ are the angular velocity and angular acceleration around the b and c axes, respectively. a_c is always perpendicular to the axis of rotation and pointing towards it, and a_t is always perpendicular to both the axis of rotation and the vector between the axis of rotation and the point [30]. The direction of these vectors in relation to the axis of rotation are shown in figure 3.7.

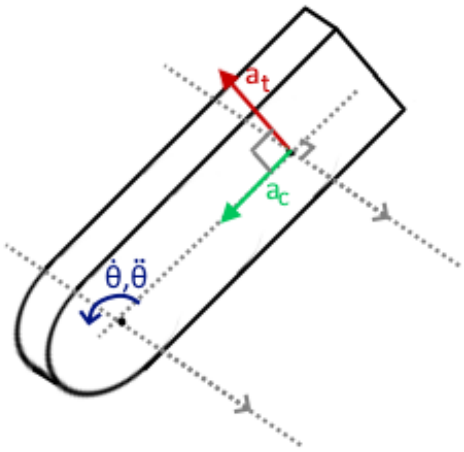

Figure 3.7: The directions of the centripetal and tangential acceleration of a point in a rotating rigid body, relative to the axis of rotation. The centripetal acceleration is denoted a_c and the tangential acceleration is denoted a_t.

To utilize the formula for centripetal acceleration, three feature were created per axial component of aCOM in the anatomical frame. The mathematical justification behind these features can be found in appendix C. For the estimation of x axis aCOM, these features are as follows:

$$
\begin{aligned}
f_{acx,1}(\dot{\beta},\dot{\gamma},\vec{q}) &= \begin{bmatrix}0 & 1 & 0 & 0\end{bmatrix} * \vec{q} \begin{bmatrix}0\\1\\0\\0\end{bmatrix} \vec{q}^{-1} * (\dot{\beta}^2+\dot{\gamma}^2) \\
f_{acx,2}(\dot{\beta},\dot{\gamma},\vec{q}) &= \begin{bmatrix}0 & 1 & 0 & 0\end{bmatrix} * \vec{q} \begin{bmatrix}0\\0\\1\\0\end{bmatrix} \vec{q}^{-1} * (\dot{\beta}^2+\dot{\gamma}^2) \\
f_{acx,3}(\dot{\beta},\dot{\gamma},\vec{q}) &= \begin{bmatrix}0 & 1 & 0 & 0\end{bmatrix} * \vec{q} \begin{bmatrix}0\\0\\0\\1\end{bmatrix} \vec{q}^{-1} * (\dot{\beta}^2+\dot{\gamma}^2)
\end{aligned} \tag{3.9}
$$

Here $\vec{q}$ is the orientation of the body segment, $\vec{q}\left[...\right]\vec{q}^{-1}$ is a quaternion multiplication, and $\begin{bmatrix}0 & 1 & 0 & 0\end{bmatrix} * \left[...\right]$ is a vector multiplication.

The quaternion multiplication and vector multiplication component of each of these three features is an estimation of the contribution of an axial component of the body segment center of mass coordinates in the body segment frame ($\vec{p}_{COM,Sn,Sn}$) to an axial component of the body segment center of mass coordinates in the anatomical frame ($\vec{p}_{COM,Sn,P}$). For the centripetal acceleration parameters, the axial component of $p_{COM,Sn,P}$ corresponds to the axial component of aCOM that is being estimated. To simplify the equation, the contributions will be denoted r_{a-to-b} where a is the axial component of $\vec{p}_{COM,Sn,Sn}$), and b is the axis of the $\vec{p}_{COM,Sn,P}$. The feature names will be similarly adjusted to indicate the contribution that the feature is based on. This results in the following equation for the features for estimating aCOM along the x axis of the anatomical frame:

$$
\begin{aligned}
f_{a_cx,x-to-x}(\dot{\beta},\dot{\gamma},\vec{q}) &= r_{x-to-x} * (\dot{\beta}^2+\dot{\gamma}^2) \\
f_{a_cx,y-to-x}(\dot{\beta},\dot{\gamma},\vec{q}) &= r_{y-to-x} * (\dot{\beta}^2+\dot{\gamma}^2) \\
f_{a_cx,z-to-x}(\dot{\beta},\dot{\gamma},\vec{q}) &= r_{z-to-x} * (\dot{\beta}^2+\dot{\gamma}^2)
\end{aligned} \tag{3.10}
$$

Equations for equivalent features for estimating aCOM along the y and z axis are as follows:

$$
\begin{aligned}
f_{a_cy,x-to-y}(\dot{\alpha},\dot{\gamma},\vec{q}) &= r_{x-to-y} * (\dot{\alpha}^2+\dot{\gamma}^2) \\
f_{a_cy,y-to-y}(\dot{\alpha},\dot{\gamma},\vec{q}) &= r_{y-to-y} * (\dot{\alpha}^2+\dot{\gamma}^2) \\
f_{a_cy,z-to-y}(\dot{\alpha},\dot{\gamma},\vec{q}) &= r_{z-to-y} * (\dot{\alpha}^2+\dot{\gamma}^2)
\end{aligned} \tag{3.11}
$$

$$
\begin{aligned}
f_{a_cz,x-to-z}(\dot{\alpha},\dot{\beta},\vec{q}) &= r_{x-to-z} * (\dot{\alpha}^2+\dot{\beta}^2) \\
f_{a_cz,y-to-z}(\dot{\alpha},\dot{\beta},\vec{q}) &= r_{y-to-z} * (\dot{\alpha}^2+\dot{\beta}^2) \\
f_{a_cz,z-to-z}(\dot{\alpha},\dot{\beta},\vec{q}) &= r_{z-to-z} * (\dot{\alpha}^2+\dot{\beta}^2)
\end{aligned} \tag{3.12}
$$

To utilize the formula for tangential acceleration, six features were created. The mathematical justification for these features can again be seen in appendix C. Like the features based on centripetal acceleration, the features based on tangential acceleration contain quaternion multiplication and vector multiplication components describing the contribution of a component of

$\vec{p}_{COM,Sn,Sn}$ to $\vec{p}_{COM,Sn,Sn}$. These have been simplified in the same manner as the centripetal acceleration contributions.

$$
\begin{aligned}
f_{a_t x,x-to-y}(\ddot{\beta},\vec{q}) &= r_{x-to-y} * \ddot{\beta} \\
f_{a_t x,x-to-z}(\ddot{\gamma},\vec{q}) &= r_{x-to-z} * \ddot{\gamma} \\
f_{a_t x,y-to-y}(\ddot{\beta},\vec{q}) &= r_{y-to-y} * \ddot{\beta} \\
f_{a_t x,y-to-z}(\ddot{\gamma},\vec{q}) &= r_{y-to-z} * \ddot{\gamma} \\
f_{a_t x,z-to-y}(\ddot{\beta},\vec{q}) &= r_{z-to-y} * \ddot{\beta} \\
f_{a_t x,z-to-z}(\ddot{\gamma},\vec{q}) &= r_{z-to-z} * \ddot{\gamma}
\end{aligned}
\tag{3.13}
$$

$$
\begin{aligned}
f_{a_t z,x-to-z}(\ddot{\alpha},\vec{q}) &= r_{x-to-z} * \ddot{\alpha} \\
f_{a_t z,x-to-x}(\ddot{\gamma},\vec{q}) &= r_{x-to-x} * \ddot{\gamma} \\
f_{a_t z,y-to-z}(\ddot{\alpha},\vec{q}) &= r_{y-to-z} * \ddot{\alpha} \\
f_{a_t z,y-to-x}(\ddot{\gamma},\vec{q}) &= r_{y-to-x} * \ddot{\gamma} \\
f_{a_t z,z-to-z}(\ddot{\alpha},\vec{q}) &= r_{z-to-z} * \ddot{\alpha} \\
f_{a_t z,z-to-x}(\ddot{\gamma},\vec{q}) &= r_{z-to-x} * \ddot{\gamma}
\end{aligned}
\tag{3.14}
$$

$$
\begin{aligned}
f_{a_t z,x-to-y}(\ddot{\alpha},\vec{q}) &= r_{x-to-y} * \ddot{\alpha} \\
f_{a_t z,x-to-x}(\ddot{\beta},\vec{q}) &= r_{x-to-x} * \ddot{\beta} \\
f_{a_t z,y-to-y}(\ddot{\alpha},\vec{q}) &= r_{y-to-y} * \ddot{\alpha} \\
f_{a_t z,y-to-x}(\ddot{\beta},\vec{q}) &= r_{y-to-x} * \ddot{\beta} \\
f_{a_t z,z-to-y}(\ddot{\alpha},\vec{q}) &= r_{z-to-y} * \ddot{\alpha} \\
f_{a_t z,z-to-x}(\ddot{\beta},\vec{q}) &= r_{z-to-x} * \ddot{\beta}
\end{aligned}
\tag{3.15}
$$

Using these new features to expand eq.3.6 creates a new equation, which describes the gyroscope based model. Only the features based on axial component of a_c and a_t along the axial component that is being estimated were used in this model, since using all 27 features based on a_c and a_t would add a lot of features and increase the risk of overfitting. This produces the following equation for the model for the x axis component of aCOM:

$$
\begin{aligned}
\vec{a}_{COM,x} = w_{x,0} + \sum_{n=1}^{N} (& w_{x,n} * a_{Sn} \\
& + \sum_{i=1}^{6} w_{x,n,i} * f_{a_t x,i,Sn}(..., \vec{q}) \\
& + \sum_{j=1}^{3} w_{x,n,j} * f_{a_c x,j,Sn}(..., \vec{q}))
\end{aligned}
\tag{3.16}
$$

Here the summations described by $\sum_{i=1}^{6} w_{x,n,i} * f_{a_t x,i,Sn}(..., \vec{q})$ and $\sum_{j=1}^{3} w_{x,n,j} * f_{a_c x,j,Sn}(..., \vec{q})$ happen over all features described in eqs.3.10 and 3.13. The equations for the other two axial components of aCOM are equivalent.

3.4.2 Body segment selection

Due to the high amount of measured body segments, evaluating models for all possible inputs would be time consuming and would clutter the results from the performance evaluation with irrelevant, poorly performing models. As such, the range of considered input body segments was narrowed based on the correlation between the LRM inputs and aCOM.

This was done by calculating the absolute Pearson correlation coefficient between the LRM inputs and aCOM per time series segment. The absolute value of the correlation coefficient was used because a high negative correlation would indicate a variable that would function well with a negative coefficient in the LRM. These Pearson correlation coefficients were aggregated by taking the mean, and the 95% confidence interval and minimum and maximum value of these Pearson correlation coefficients was calculated in order to indicate whether the correlation was consistent across all time series segments or if the correlation varied. All of these values were plotted in a heatmap to give an overview of which body segments were the most promising.

An example of a correlation heatmap for body segment acceleration can be seen in figure 3.8. For the body segment acceleration, correlation heatmaps were made for all three axial components of aCOM along the axes of the anatomical frame. For each of these axial components, the correlation heatmaps were made thrice, once for every axial component of the body segment acceleration within the anatomical frame. This was done to observe cross axis correlation. A variant of this heatmap where the absolute correlation coefficients of the pelvis were subtracted from the absolute Pearson correlation coefficients of the other body segments was also examined in order to test for body segment accelerations that have a lower correlation with aCOM but provide information not found in the pelvis acceleration.

An example of a heatmap for the input parameters based on tangential and centripetal acceleration can be seen in figure 3.9. Individual correlation heatmaps were made for every body segment.

For the models using more than two IMUs, the selection of IMUs was based on the intuition that a human performing a balance task will move their limbs to minimize aCOM movement, and that therefore involving more limbs may provide a better result. As such, inputs using symmetrical inputs from both arms or legs were tested. Afterwards, models using both lower legs, the best performing pair of limb IMUs on the beam walking task, was tested on the other tasks, in addition to two models using four IMU locations: The pelvis, the lower legs and either the head or T8.

3.4.3 Cross validation

In order to test how well the models generalize, cross validation was employed. To test generalisation over subjects, the partition of the cross validation subsets was performed along the lines of the subjects: The subjects were divided into 4 roughly equal groups. The model was evaluated 4 times, with each group acting as a test set once and as part of the training set thrice.

3.4.4 Performance evaluation

To evaluate effectiveness of the different models, the performances of the different models was compared using the r square(r^2) statistic. Models were trained on the training set input data. The r^2 that these models achieved for the test set was calculated per trial and averaged. The

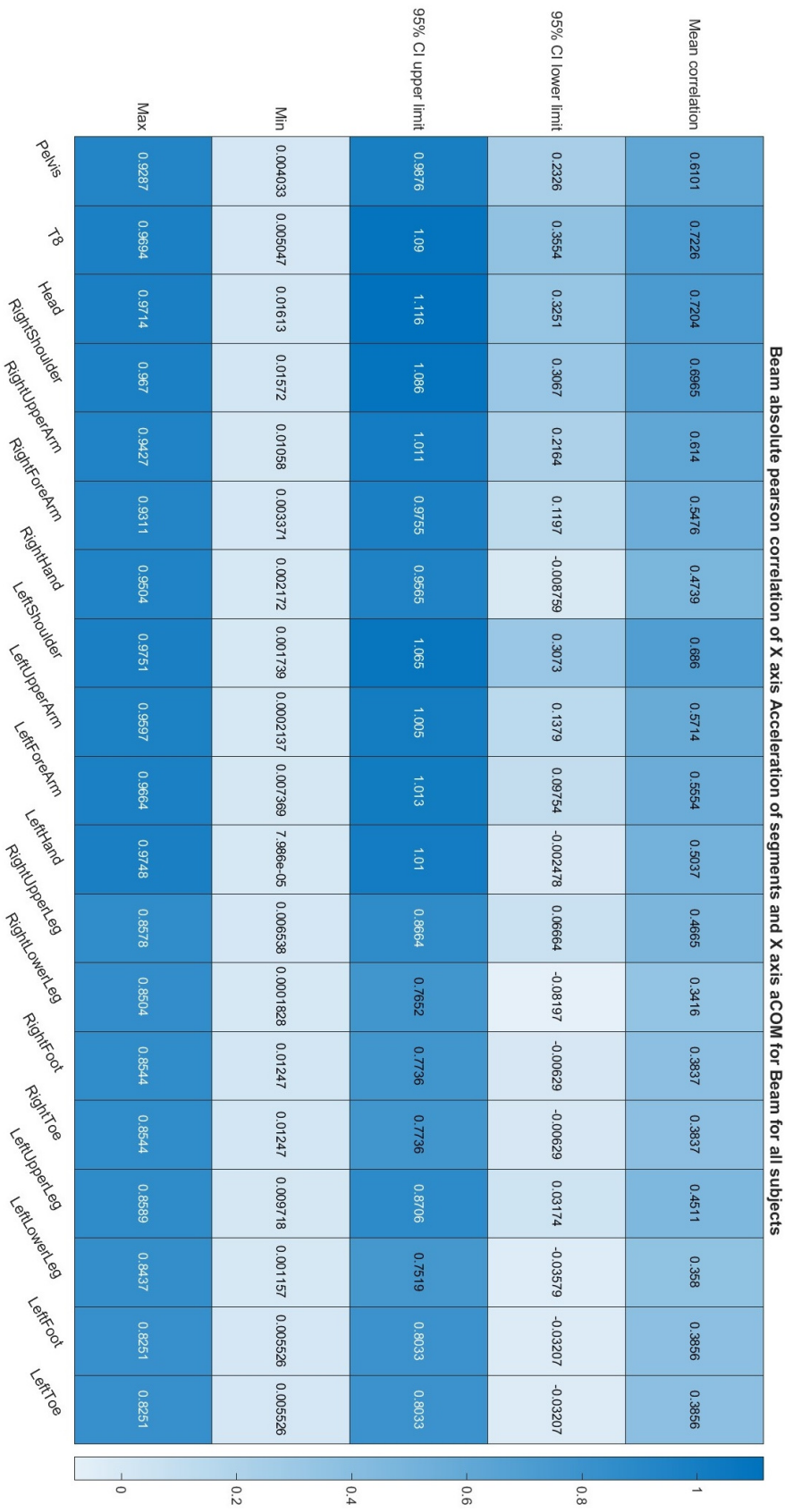

Figure 3.8: An example of a correlation heatmap for body segment acceleration. This heatmap depicts the mean and confidence intervals of the absolute Pearson correlation coefficient between the x axis body segment acceleration and x axis aCOM over all time series segments for the beam walk activity.

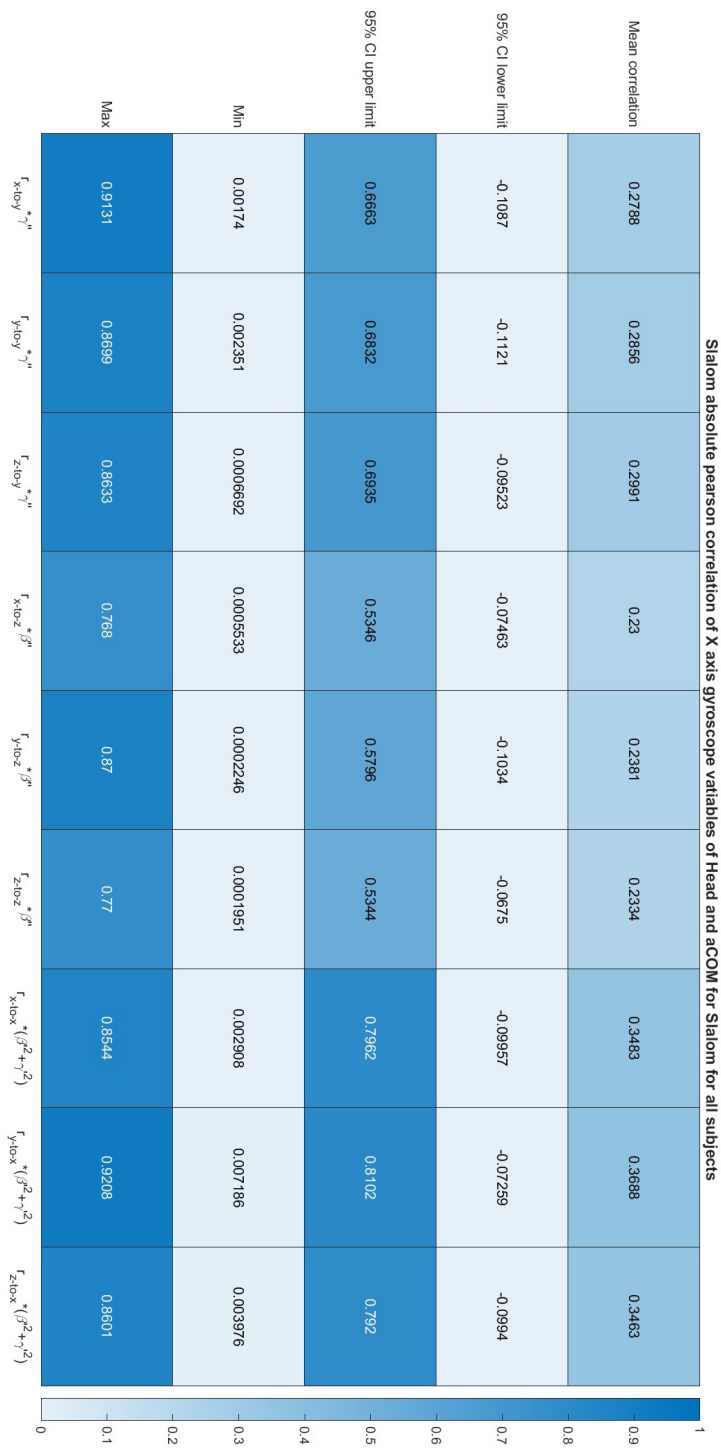

Figure 3.9: An example of a correlation heatmap for gyroscope features. This heatmap depicts the mean and confidence intervals of the absolute Pearson correlation coefficient between the x axis head acceleration and x axis aCOM over all time series segments for the slalom activity.

root mean square error(RMSE) was also examined to contextualize the r^2. These examinations were performed for every axial component of aCOM for models pairing a selected body segment with the pelvis as well as a model that uses only the pelvis. One r^2 and one RMSE heatmap was created for every activity and type of model. An example of an r^2 heatmap can be seen in figure 3.10. These heatmaps were used to create an overview of the r^2 of the different input body segments for the different components of aCOM for that model-activity pairing. In the case of r^2, the average of all three axial components was also calculated. In the case of RMSE, the RMSE over all three axial components was calculated.

The performances of the one direction acceleration models were also compared to the performance of a linear model using coefficients proportional to the segment mass proportions found in literature [34], in order to examine whether the linear regression had any benefits compared to using the contributions of segment accelerations that would be expected from literature. Since differences between the one direction acceleration models and the all direction acceleration models and gyroscope based models are apparent from their respective results, a comparison between the segment mass models and all direction acceleration models and gyroscope based models is not used.

3.4.5 Time series, qq, bland altman and subject r^2 plots

Aside from the performance parameters, several other plots were created to examine different features of the models. Time series plots comparing estimates aCOM to the actual aCOM were created to identify any odd behavior of the estimate or phases of the motion where the estimate underperforms. This investigation was done for models using the head and the sternum segments as these were the best performing segments, and for the gyroscope based models using the upper and lower legs as these segments improved the most compared to the models using only acceleration. Bland Altman plots were created to examine bias and identify any odd groupings within the estimates and errors. qq plots of reference values and the estimates created by the models were used to compare the shapes of the distributions between models. Bar plots of the r^2 for estimates of aCOM for recordings of individual subjects were used to investigate the differences between subjects and the influence of the all direction models and gyroscope models on the variance in performance. These analyses were performed on both body segment acceleration models and the gyroscope based model, but not the models with inputs of more than two IMUs, since the addition of IMUs for the purpose of measuring mediolateral aCOM for balancing tasks did not seem worthwhile enough to warrant further investigation. Since the differences between the all direction acceleration model and one direction acceleration models were minimal, these additional steps of analysis were also not performed for the one direction acceleration model. Since models estimating the vertical component of aCOM performed extremely well for all activities, only the anterioposterior and mediolateral directions were investigated using these analyses.

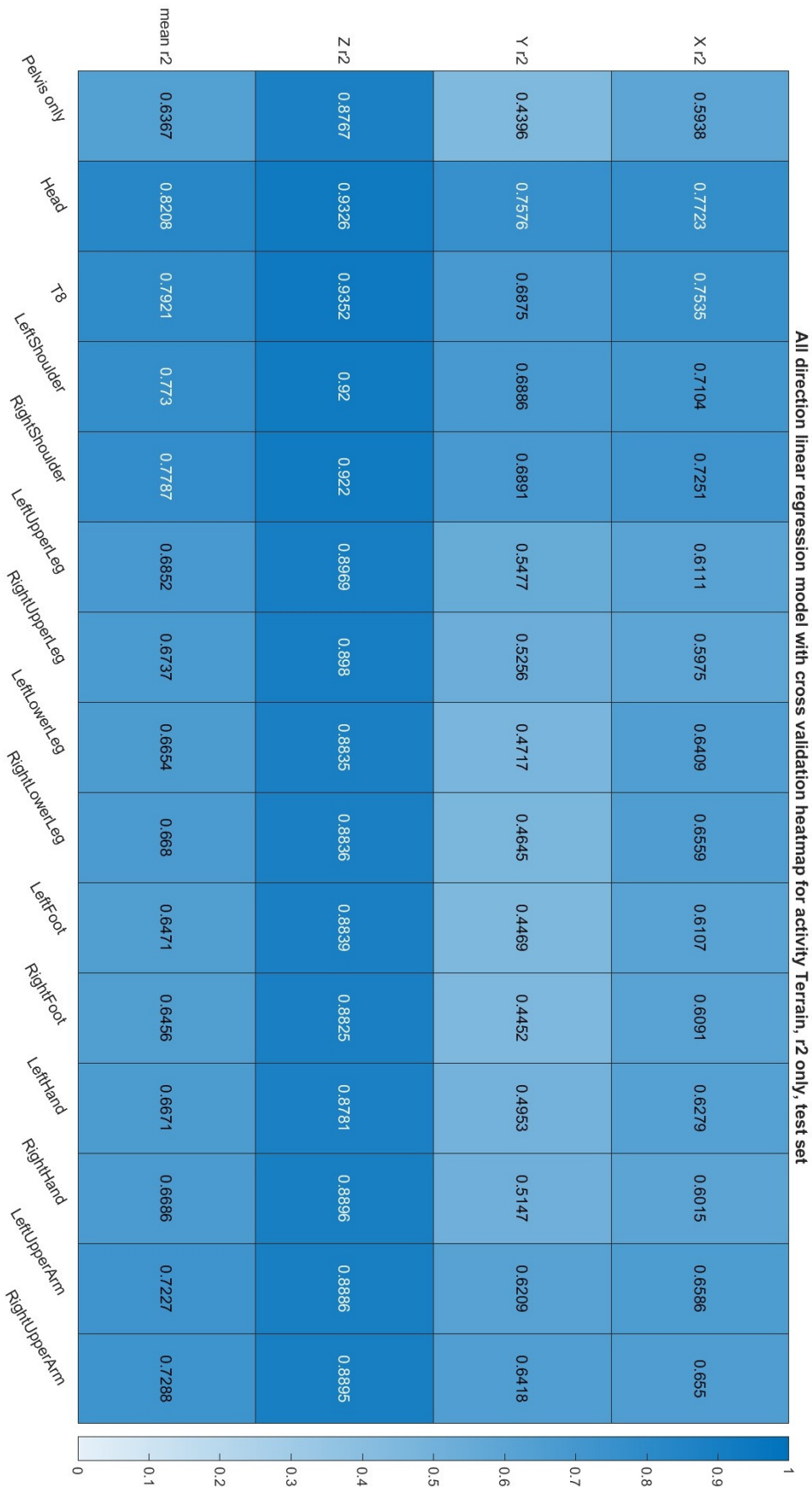

Figure 3.10: An example of an r^2 performance heatmap. This heatmap depicts the r^2 for different models trained and tested on terrain walking acceleration data.

4 RESULTS

This section describes the results of the analysis of the previous section. For each of the separate model types, it will first detail the outcome of the selection of IMUs based on correlation based heatmaps. Then, it will summarize the outcomes of the performance heatmaps for the linear models. To show the best performing input segments for the overall estimation, a compilation of the average r^2 values over the three directional components will be used, and to show the best performing input segments for each directional component, tables of the input segments of the top 3 models with the highest r^2 will be used. Finally, any notable outcomes of the other plots will be described and examples of these outcomes will be provided. A complete collection of all plots made can be found in a zip file on the gitlab page [§] of this project.

4.1 IMU selection

This section describes the outcome of the IMU selection based on the averages of the absolute Pearson correlation coefficient of the different time series segments. It will first describe the results for the correlation between the segment acceleration and aCOM, followed by the results for the correlation between the gyroscope based variables and aCOM.

The outcome for the IMU selection for the linear acceleration models[¶] is as follows: For the same axis correlation, the acceleration of segments that make up or are near the torso, head, sternum(T8), both shoulders, both upper legs and both upper arms were found to have the highest correlation with aCOM. The lower legs and feet were also found to have higher correlation with aCOM for certain activities. In the examination of cross axis correlation, the acceleration of the hands was found to sometimes have a higher correlation than other segments. Inputs from these segments were chosen to be tested in the one direction acceleration model and the all direction acceleration model.

For the correlation with the gyroscope based variables, segments did not have mean correlations that were high across all gyroscope based variables. The variables corresponding to the upper legs, lower legs and shoulders were found to include variables with a higher lower bound for the 95% confidence interval for the absolute Pearson correlation coefficient and therefore had a more consistent correlation over the different time series segments for multiple activities. Based on this, inputs from these segments were chosen to be tested in the gyroscope based model. Segments from which the acceleration performed well in the acceleration based models were also tested to see if the gyroscope based variables would create improvement. The

[§] https://gitlab.utwente.nl/bss_development/students/m_donck/movella-sensors

[¶] The initial correlation heatmaps were accidentally created using a 5Hz lowpass filter in the preprocessing instead of a 10Hz lowpass filter. A sample of the correlation heatmaps was redone and checked and it was determined that there was no significant difference in which segments had the highest correlation. As such, the determinations in this paragraph are based on the correlation of data with a 5Hz lowpass filter applied instead of a 10Hz one.

segments that were added to the examination based on this criteria were the head, T8 and the upper arms. Since the gyroscope based variables derived from the pelvis segment data also had higher lower bounds for the 95% confidence interval, a model using only the segment acceleration and gyroscope based variables from the pelvis was also included in the examination.

Examples of this IMU selection process can be seen in appendix D.

4.2 Performance

This section will summarize the results of the performance heatmaps. Any notable results will be described, and the overall results will be illustrated using a heatmap and a table for each model type. The heatmap will contain the r^2 averaged over all three directional components of aCOM, for each activity and each segment. The table will list the three segments that produce the best performing estimation when used as input for each directional component for each activity.

4.2.1 One direction and all direction acceleration models

Since the one direction acceleration model and the all direction acceleration model perform very similarly, their performances are summarized in a shared subsection. The performance of the one direction acceleration model will be summarized first, and then the performance of the all direction acceleration model will be described in relation to it.

A heatmap showing the overall performance of the one direction acceleration model for all segments for all activities can be seen in figure 4.1, and an overview of the best performing segments per direction of aCOM of the one direction acceleration model can be seen in table 4.1. The one direction acceleration model performs best when using torso segments (head, sternum or shoulders) as input, for most activities. The difference in performance between these torso segments in the anterioposterior direction is often minimal, less than r^2 0.04 . Exceptions to this occur in jumping and downward stairs walking, where the head outperforms the other torso segments significantly, and in turning, where the difference between the head and the right shoulder slightly exceeds this margin. The lower legs and upper arms also provide significant improvement compared to a model using only the pelvis, but models using inputs from these segments perform worse than models using torso segments. Exceptions to this are the natural walking, jump and down stairs walking activities where they perform comparably to models using torso segments.

For the mediolateral direction, the difference in performance between the torso segments is greater than in the anterioposterior direction, with the models using the head generally performing better than the other torso segments. For the beam walk activity in the mediolateral direction, the performance of all models is very poor and only the models using lower legs and sternum provide a significant improvement compared to the model using only the pelvis. For the vertical direction, the models using pelvis input alone perform well for all activities except sit down and stand up, and models using additional semgents do not perform much better than the model using only pelvis inputs. For sit down and stand up, all torso segments and the upper arms provide a similar improvement for the aCOM estimation in the vertical direction.

The heatmap for the overall performance of the all direction acceleration model can be seen in

Activity	aCOM component		
	X	Y	Z
Natural walking	1. Sternum	1. Head	1. Head
	2. Head	2. Shoulder	2. Sternum
	3. Lower leg	3. Sternum	3. Shoulder
Slalom walking	1. Head	1. Head	1. Sternum
	2. Sternum	2. Sternum	2. Head
	3. Shoulder	3. Shoulder	3. Shoulder
Zigzag	1. Head	1. Sternum	1. Sternum
	2. Sternum	2. Head	2. Head
	3. Shoulder	3. Shoulder	3. Shoulder
Turn	1. Head	1. Head	1. Sternum
	2. Sternum	2. Shoulder	2. Head
	3. Shoulder	3. Sternum	3. Shoulder
Sit down and Stand up	1. Shoulder	1. Sternum	1. Sternum
	2. Sternum	2. Head	2. Head
	3. Head	3. Shoulder	3. Shoulder
Jump	1. Head	1. Sternum	1. Upper arm
	2. Shoulder	2. Head	2. Sternum
	3. Lower leg	3. Shoulder	3. Head
Beam walking	1. Head	1. Lower leg	1. Sternum
	2. Shoulder	2. Sternum	2. Shoulder
	3. Sternum	3. Upper arm	3. Head
Terrain walking	1. Head	1. Head	1. Sternum
	2. Shoulder	2. Sternum	2. Shoulder
	3. Sternum	3. Shoulder	3. Head
Stairs walking up	1. Head	1. Head	1. Sternum
	2. Shoulder	2. Shoulder	2. Head
	3. Sternum	3. Sternum	3. Shoulder
Stairs walking down	1. Head	1. Head	1. Sternum
	2. Shoulder	2. Sternum	2. Head
	3. Lower leg	3. Shoulder	3. Shoulder

Table 4.1: Three best performing IMUs per activity per directional component of aCOM for the linear model using only segment acceleration in the same direction as the estimated aCOM component.

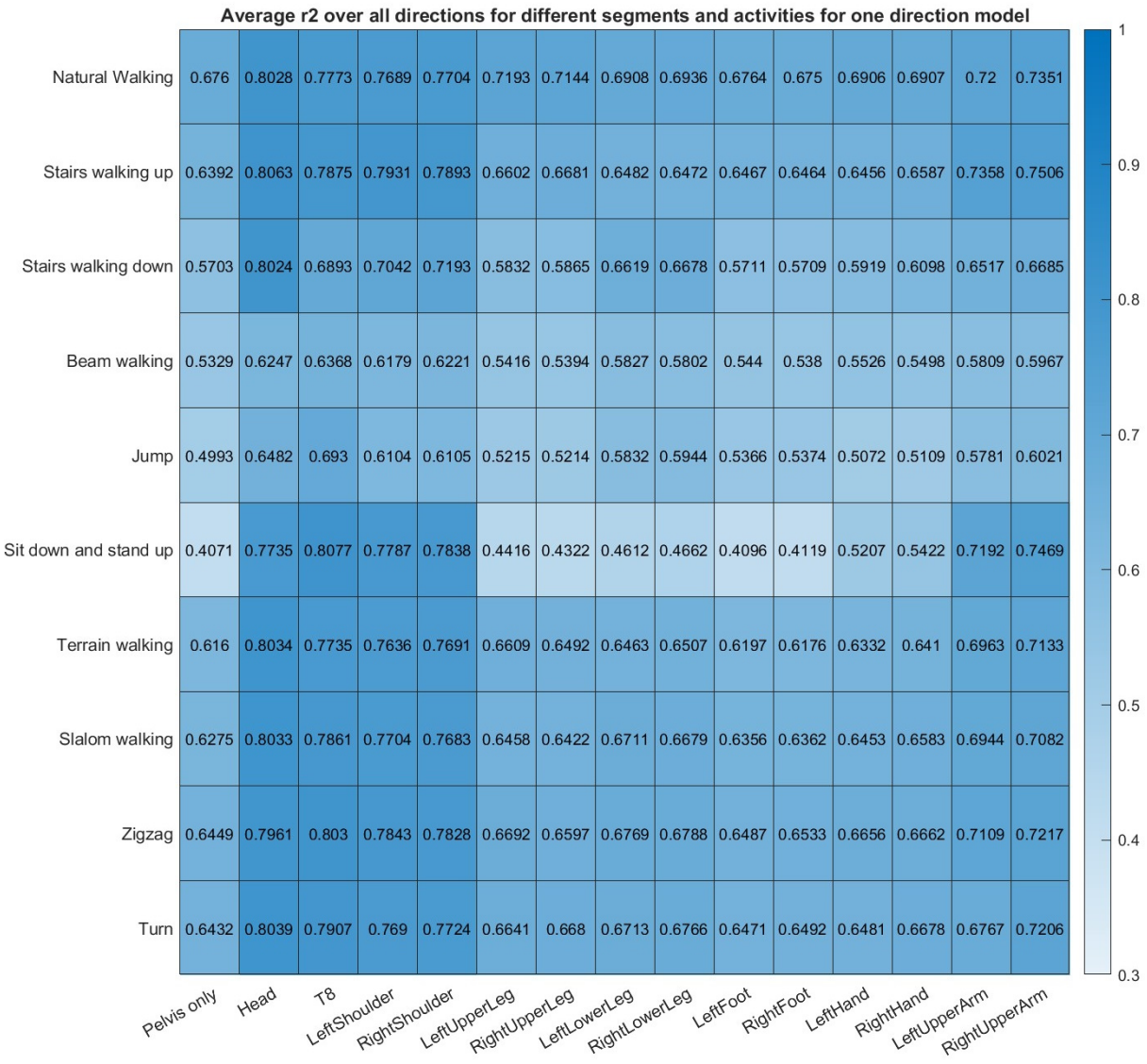

Figure 4.1: A heatmap of the average r^2 of one direction acceleration models using inputs from different segments.

figure 4.2 The IMU location of the best performing model changes for some activities, shown in the bold in table 4.2. Compared to the one direction acceleration model, models using all three directional components of aCOM perform better overall, but the relative performance of the different segments remains largely unchanged. The differences in r^2 that the changes in best performing segment represent are very small. All direction acceleration models which have a lower r^2 than the one direction acceleration model using inputs from the same segment are uncommon and the difference r^2 for these models is very small as well.

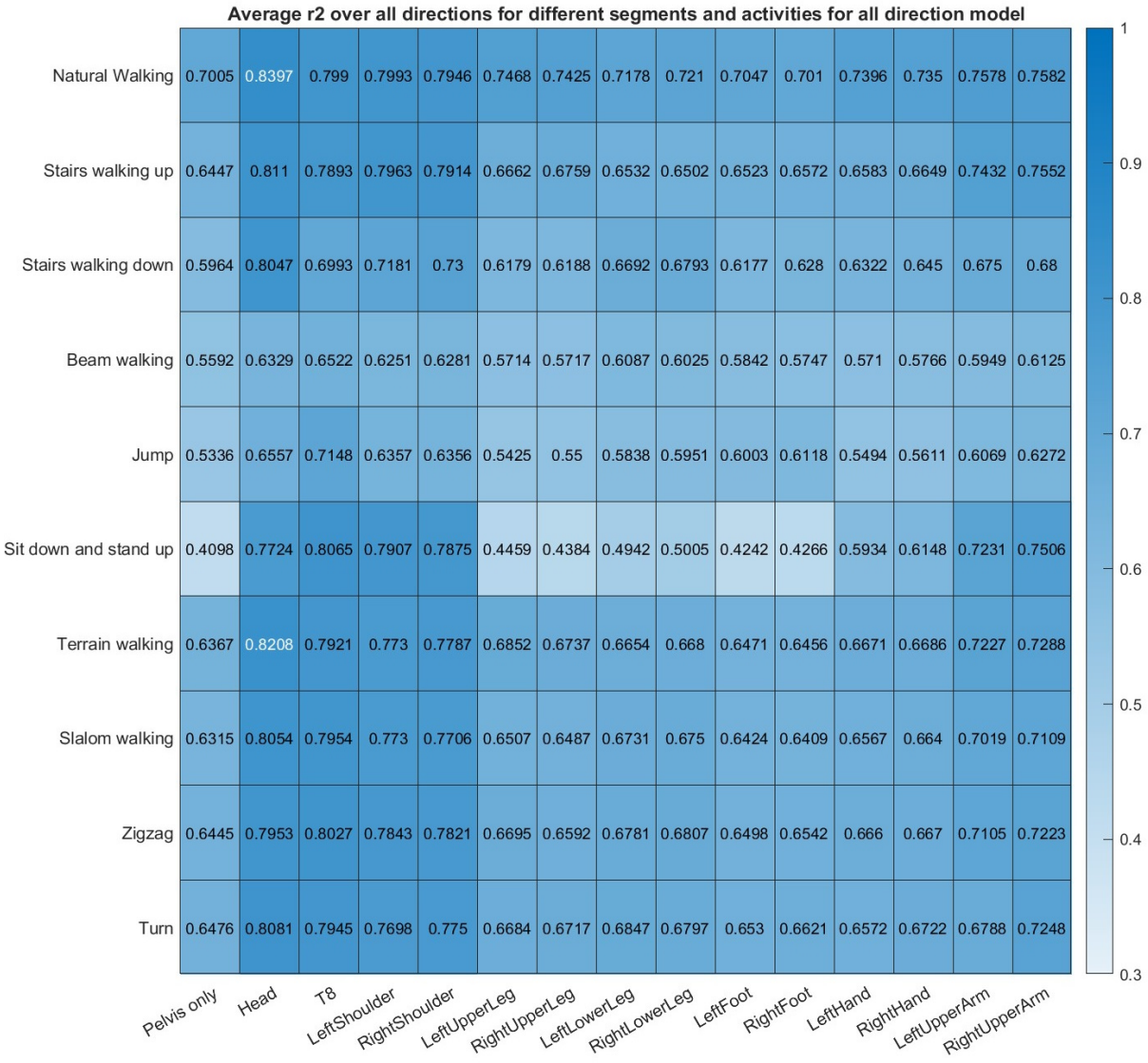

Figure 4.2: A heatmap of the average r^2 of all direction acceleration models using inputs from different segments.

Activity	aCOM component		
	X	Y	Z
Natural walking	1. **Head**	1. Head	1. **Sternum**
	2. **Sternum**	2. Shoulder	2. **Head**
	3. **Shoulder**	3. Sternum	3. Shoulder
Slalom walking	1. Head	1. Head	1. Sternum
	2. Sternum	2. Sternum	2. Head
	3. Shoulder	3. Shoulder	3. Shoulder
Zigzag	1. Head	1. Sternum	1. Sternum
	2. Sternum	2. Head	2. Head
	3. Shoulder	3. Shoulder	3. Shoulder
Turn	1. Head	1. Head	1. Sternum
	2. Sternum	2. Shoulder	2. Head
	3. Shoulder	3. Sternum	3. Shoulder
Sit down and Stand up	1. Shoulder	1. Sternum	1. **Shoulder**
	2. Sternum	2. **Shoulder**	2. **Sternum**
	3. Head	3. **Head**	3. **Head**
Jump	1. Head	1. Sternum	1. **Sternum**
	2. **Foot**	2. Head	2. **Upper arm**
	3. **Shoulder**	3. Shoulder	3. **Shoulder**
Beam walking	1. Head	1. Lower leg	1. Sternum
	2. **Sternum**	2. Sternum	2. Shoulder
	3. **Shoulder**	3. **Foot**	3. Head
Terrain walking	1. Head	1. Head	1. Sternum
	2. **Sternum**	2. **Shoulder**	2. **Head**
	3. **Shoulder**	3. **Sternum**	3. **Shoulder**
Stairs walking up	1. Head	1. Head	1. **Shoulder**
	2. **Sternum**	2. Shoulder	2. **Sternum**
	3. **Shoulder**	3. Sternum	3. **Head**
Stairs walking down	1. Head	1. Head	1. **Head**
	2. Shoulder	2. Sternum	2. **Sternum**
	3. Lower leg	3. Shoulder	3. Shoulder

Table 4.2: Three best performing IMUs per activity per directional component of aCOM for the linear model using only segment acceleration in all three directions. Differences with the best performing IMUs using only one directional component of segment acceleration are shown in bold.

4.2.2 Multi segment model

This subsection shows the performance evaluation of the models using more than two segments. As the three segment model was only evaluated on the beam walk activity, the r^2 calculated for this activity is shown in full in figure 4.3. The results of the lower legs and lower legs and torso segment models will be described and summarized using a heatmap of the average r^2 over all directions of aCOM.

Figure 4.3: A heatmap of the average r^2 of the models using IMU inputs from symmetrical segments.

As can be seen in figure 4.3, only the model using inputs from both lower legs provides improvement in the mediolateral direction compared to a model using only the pelvis, and the lower legs, upper arms and forearms all provide an improvement in the anterioposterior direction compared to a model using only the pelvis.

An heatmap showing an overview of the average r^2 of the multi segment models over all directions of aCOM can be seen in figure 4.4. For the activities besides beam walking, the model using inputs from both lower legs performs significantly worse than the torso segments in both the mediolateral and anterioposterior direction, with the exception of down stairs walking where it provides a better estimate in the anterioposterior direction than the head. The model using inputs from both lower legs also performs worse than the torso segments in the vertical direction when estimating sit down and stand up. For most activities, the combination of pelvis, a torso and both lower legs performs better than just the pelvis and that torso segment in both the mediolateral and anterioposterior direction. Most of these improvements are small, except in the anterioposterior direction for stairs walking down.

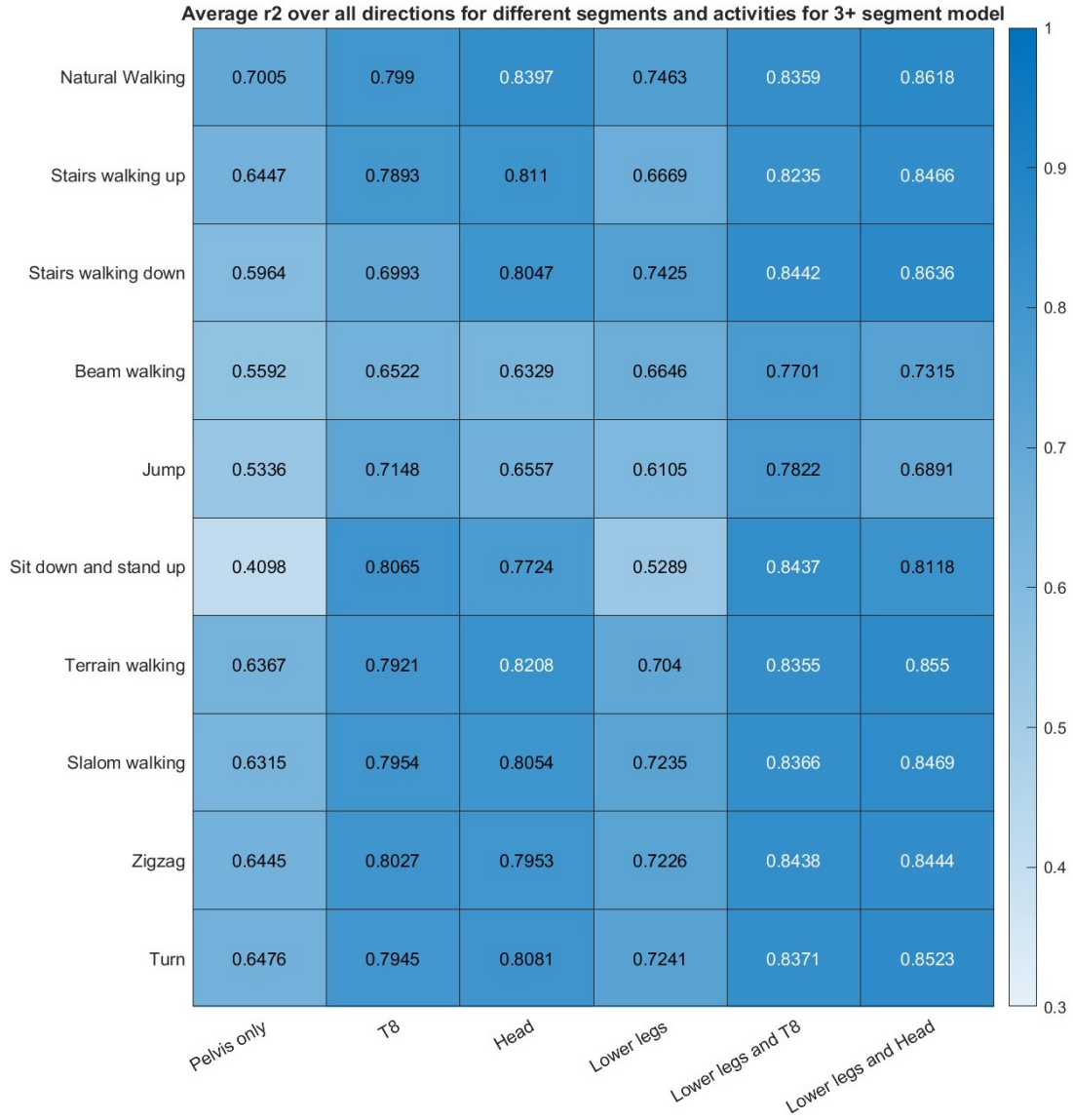

Figure 4.4: A heatmap of the average r^2 of the models using IMU inputs from both lower legs and both lower legs and a either the head or the sternum.

4.2.3 Gyroscope based model

This subsection will summarize the performance of the gyroscope based models. It will describe the major changes relative to the models using only acceleration.

The overall performance of the gyroscope based models can be seen in figure 4.5. The change in best performing IMU that that is produced by changing from the all direction acceleration model to the gyroscope based model is shown in table 4.3. The main difference in performance between the models using only acceleration and the models using the variables based on the tangential and centripetal acceleration is an improvement in the performance of the models using the upper legs. When the gyroscope variables are included, models using the upper legs often perform comparably to the models using the torso segments, though the torso segments generally still perform better. Inputs from the upper legs also provide a significant improvement in the mediolateral estimation of aCOM for the beam activity compared to the pelvis. Aside from the difference that can be seen with the models using inputs from the upper legs, the models using T8 as input also show a significant improvement in the estimation of aCOM in the mediolateral direction for all activities except beam walking, zigzag and jump.

Activity	aCOM component		
	X	Y	Z
Natural walking	1. Head 2. **Upper leg** 3. Shoulder	1. Head 2. Shoulder 3. Sternum	1. Sternum 2. Head 3. Shoulder
Slalom walking	1. **Sternum** 2. **Head** 3. Shoulder	1. **Sternum** 2. **Head** 3. Shoulder	1. Sternum 2. **Shoulder** 3. **Head**
Zigzag	1. **Sternum** 2. **Head** 3. Shoulder	1. Sternum 2. Head 3. Shoulder	1. Sternum 2. Head 3. Shoulder
Turn	1. **Sternum** 2. **Head** 3. Shoulder	1. Head 2. **Sternum** 3. **Shoulder**	1. Sternum 2. Head 3. Shoulder
Sit down and Stand up	1. **Sternum** 2. **Shoulder** 3. **Upper arm**	1. Sternum 2. Shoulder 3. Head	1. **Sternum** 2. **Shoulder** 3. Head
Jump	1. **Lower leg** 2. **Shoulder** 3. **Upper arm**	1. Sternum 2. **Upper leg** 3. Shoulder	1. Sternum 2. **Shoulder** 3. **Upper arm**
Beam walking	1. **Sternum** 2. **Head** 3. Shoulder	1. **Upper leg** 2. **Lower leg** 3. **Sternum**	1. Sternum 2. Shoulder 3. Head
Terrain walking	1. Head 2. Sternum 3. Shoulder	1. **Sternum** 2. **Head** 3. **Shoulder**	1. **Head** 2. **Sternum** 3. Shoulder
Stairs walking up	1. Head 2. Sternum 3. Shoulder	1. **Sternum** 2. Shoulder 3. **Head**	1. Sternum 2. **Head** 3. **Shoulder**
Stairs walking down	1. Head 2. **Upper leg** 3. Lower leg	1. Head 2. Sternum 3. Shoulder	1. Head 2. Sternum 3. Shoulder

Table 4.3: Three best performing IMUs per activity per directional component of aCOM for the linear model using segment acceleration in all three directions as well as the variables based on tangential and centripetal acceleration. Differences with the best performing IMUs using only segment accelleration are shown in bold.

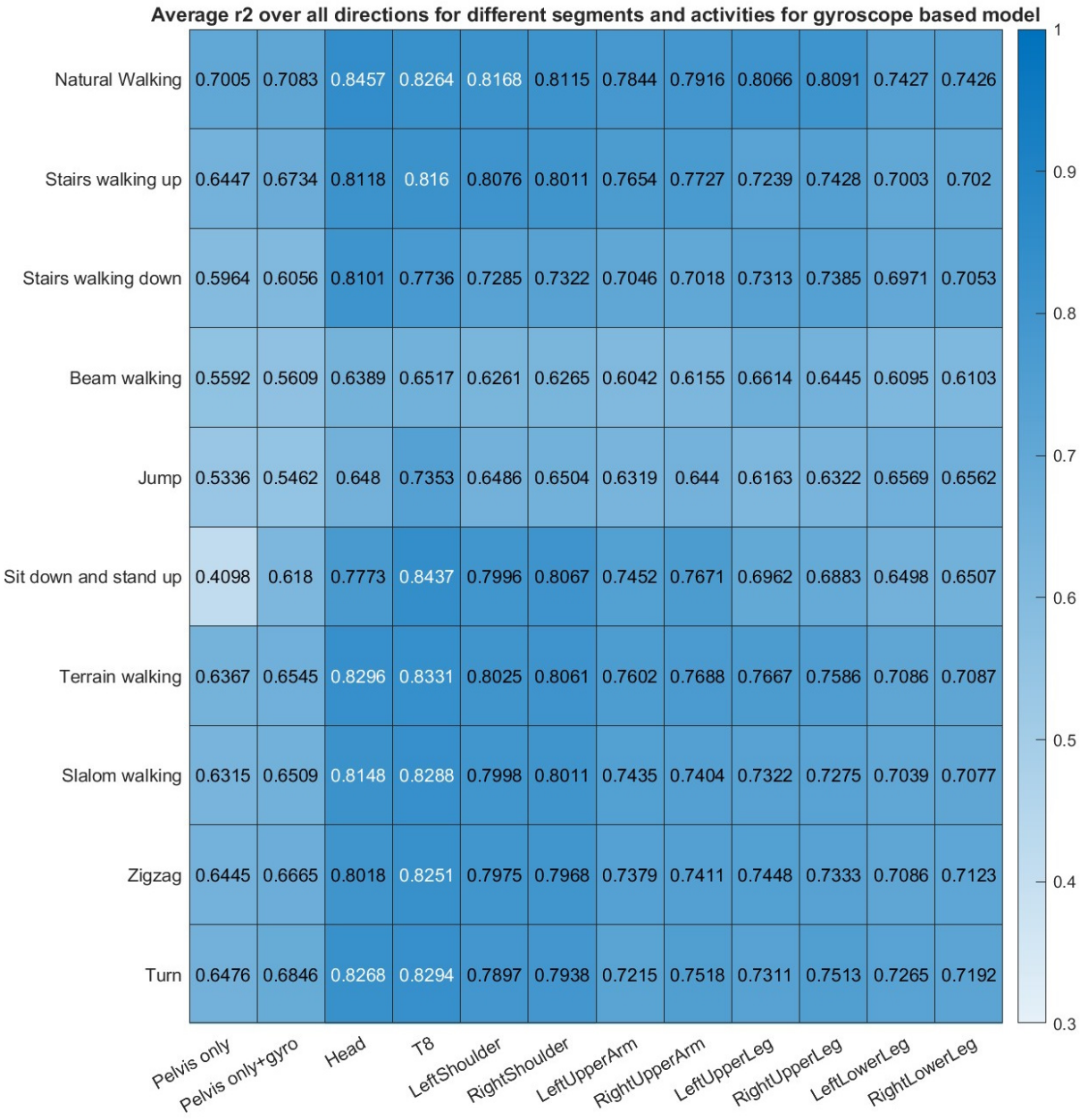

Figure 4.5: A heatmap of the average r^2 of gyroscope based models using inputs from different segments.

4.2.4 Comparison of one direction linear models to mass based linear models

This subsection will summarize the comparison between the performance of the segment mass models and the one direction acceleration models.

A heatmap showing the difference in overall performance between the one direction acceleration model and the segment masses model is shown in figure 4.6. The performance of both models when only the pelvis acceleration is used is identical. The one direction acceleration models using the head and limb segments perform significantly better than the segment mass models using the same segments. No linear regression model performs significantly worse than a segment mass model.

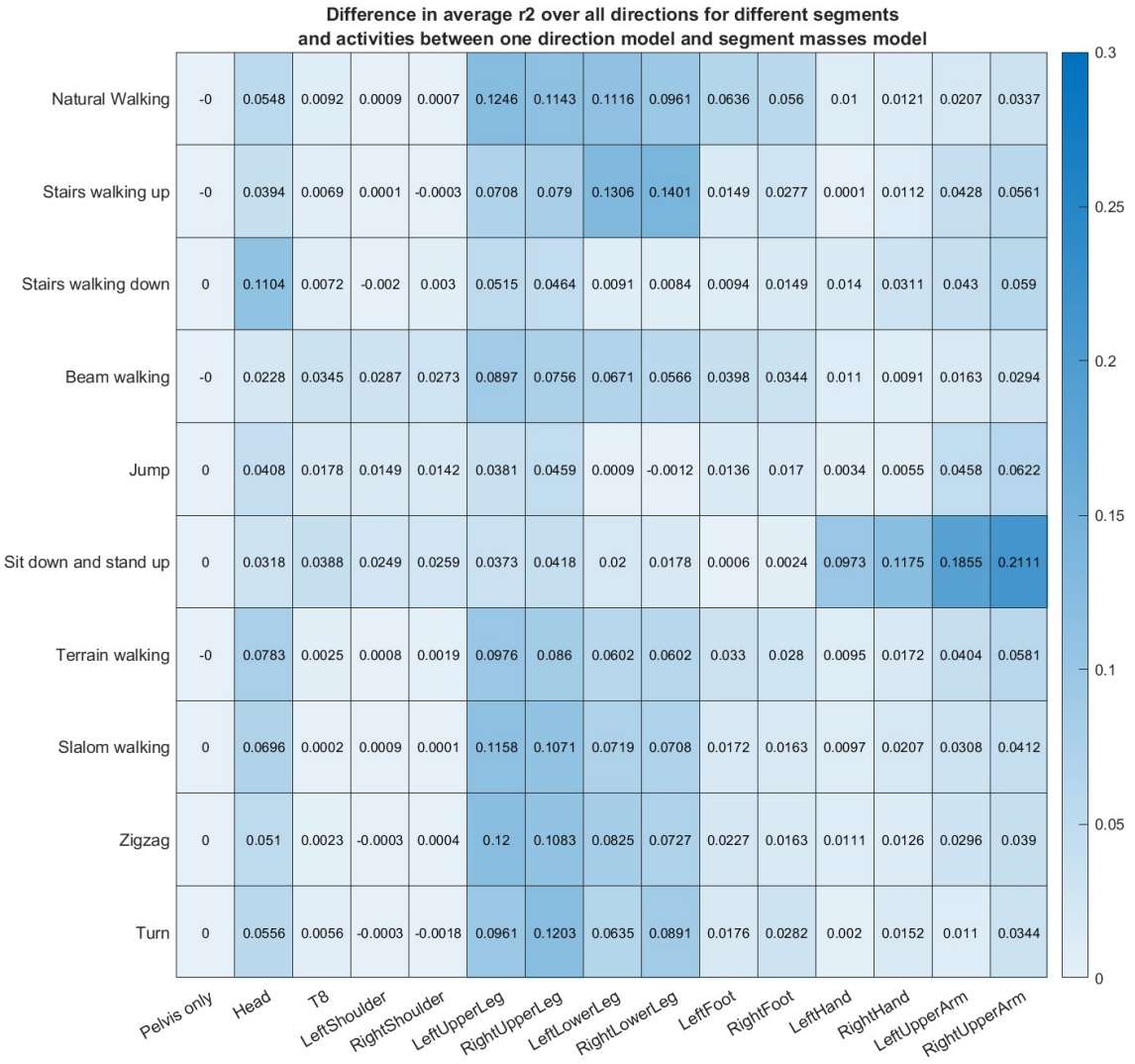

Figure 4.6: A heatmap of the difference in average r^2 between segment mass models and one direction acceleration models using inputs from different segments.

4.3 Time series, bland altman and subject r^2 plots

This section will describe any notable results from the time series plots, bland altman plots and subject r^2 plots. Since the results from the qq plots do not inform any part of the conclusion or discussion of this thesis, their results have been omitted from this section. A brief look at the results of the thesis can instead be found in appendix E.

4.3.1 Time series plots

There are two main observations made from the visual inspection of the time series plots. The first observation is that even for the models with higher r^2, there was often a large distance between the estimate and the reference value at the minima and maxima of the aCOM time series. A series of examples for this are shown in figure 4.7. This distance at minima and maxima was seen in gait and non gait activities.

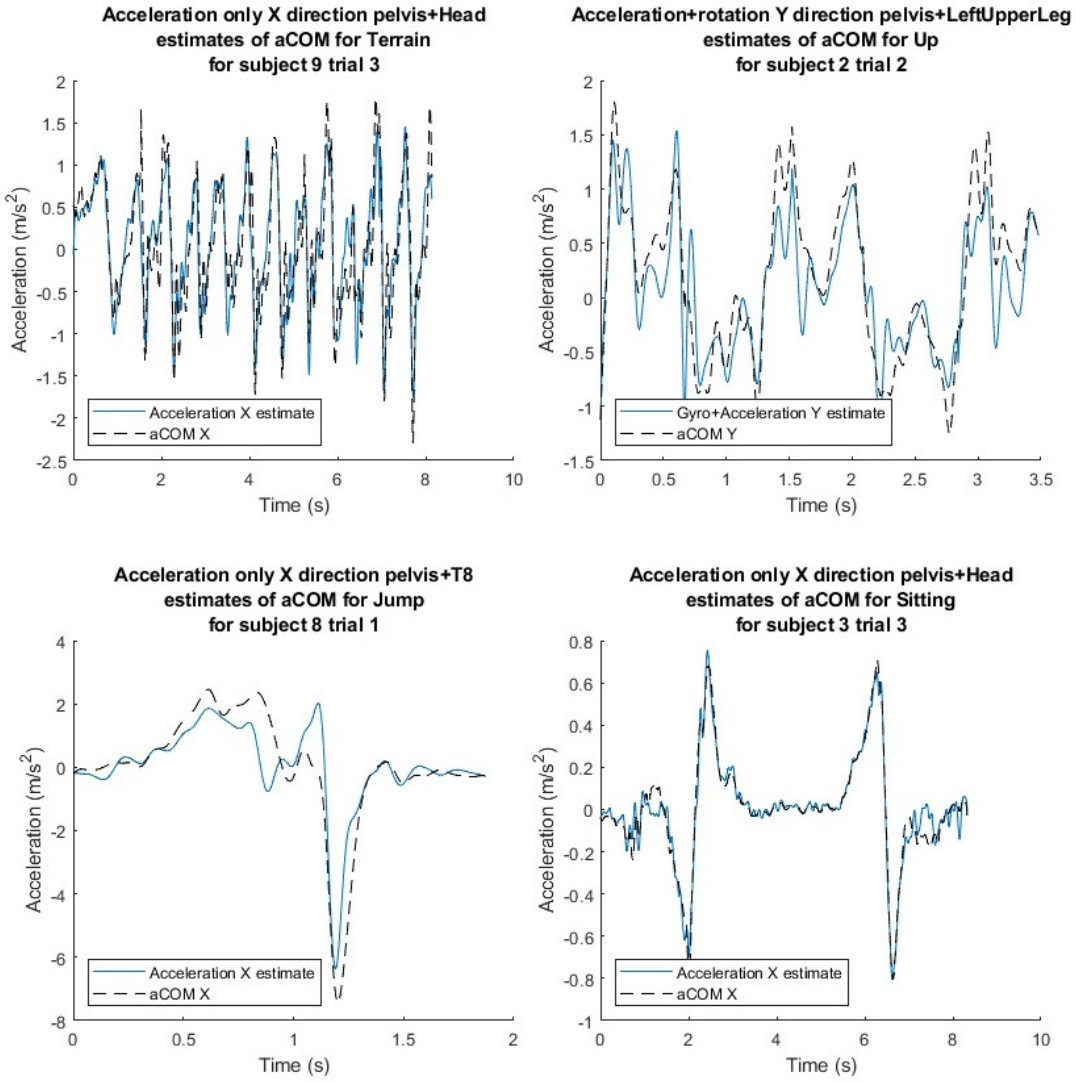

Figure 4.7: Estimates of aCOM from linear regression models for four different activities showing a larger distance between the estimates and reference values for aCOM at the minima and maxima of the time series than at the samples with more moderate values.

The second observation is that there is a lot of variance in the estimates and aCOM movement between subjects, which results in deviations from the reference value that different phases of the gait cycle. An example of two very different time series for the same activity can be seen in figure 4.8.

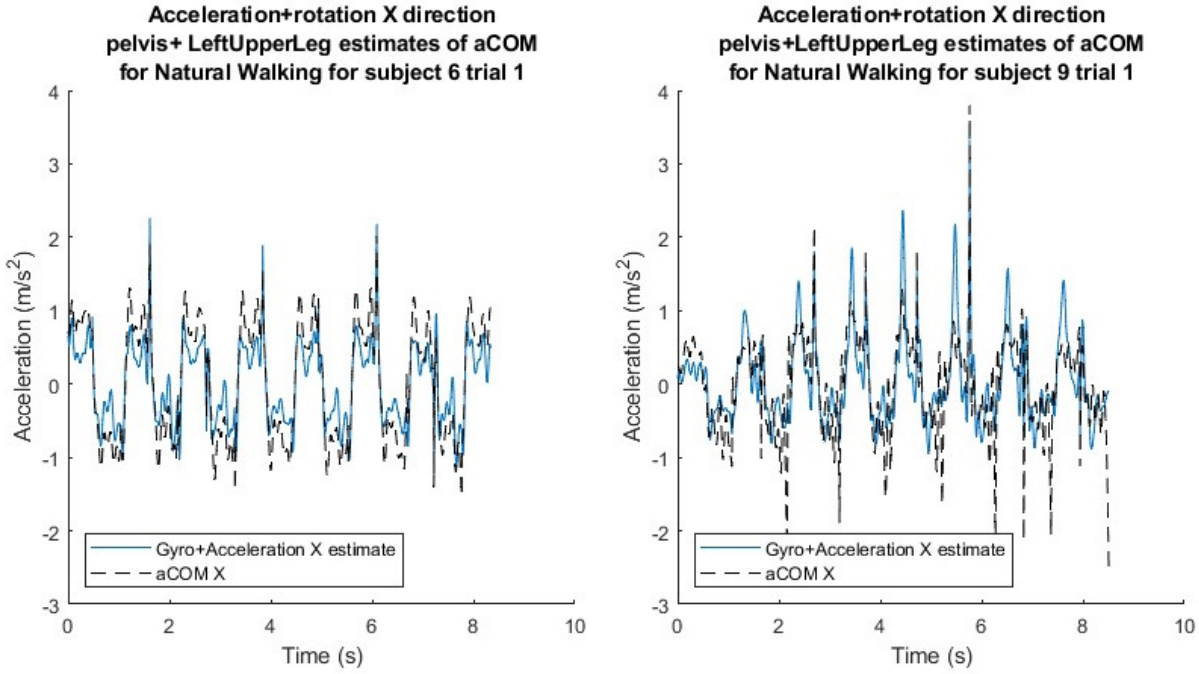

Figure 4.8: Estimates of aCOM from linear regression models for two different subjects for natural walking.

4.3.2 Bland Altman plots

There are two main observations in the Bland Altman plots. One observation in the Bland Altman plots is that all models have a bias that is very close to zero, even when the model performs poorly. An example of a Bland Altman plot showing a bias close to zero can be seen in figure 4.9.

The second observation is that in the Bland Altman plot for the models for estimation of the x-axis component of aCOM for the jump activity, a cross shape was observed. Coloring the start and the end of the jump recordings differently showed that one half of the cross shape could be attributed to the estimates of the start of the jump and the other to the estimates of the end of the jump, generating two separate 'L' shapes. And example of this can be seen in figure 4.10. The cross shape is present in the all direction acceleration models estimating aCOM using inputs from the upper arm, lower leg and upper leg segments, and the gyroscope based models using the upper leg segments. The separate 'L' shapes can be observed in each of the models showing this cross shape except the models using input data from the upper arm segments.

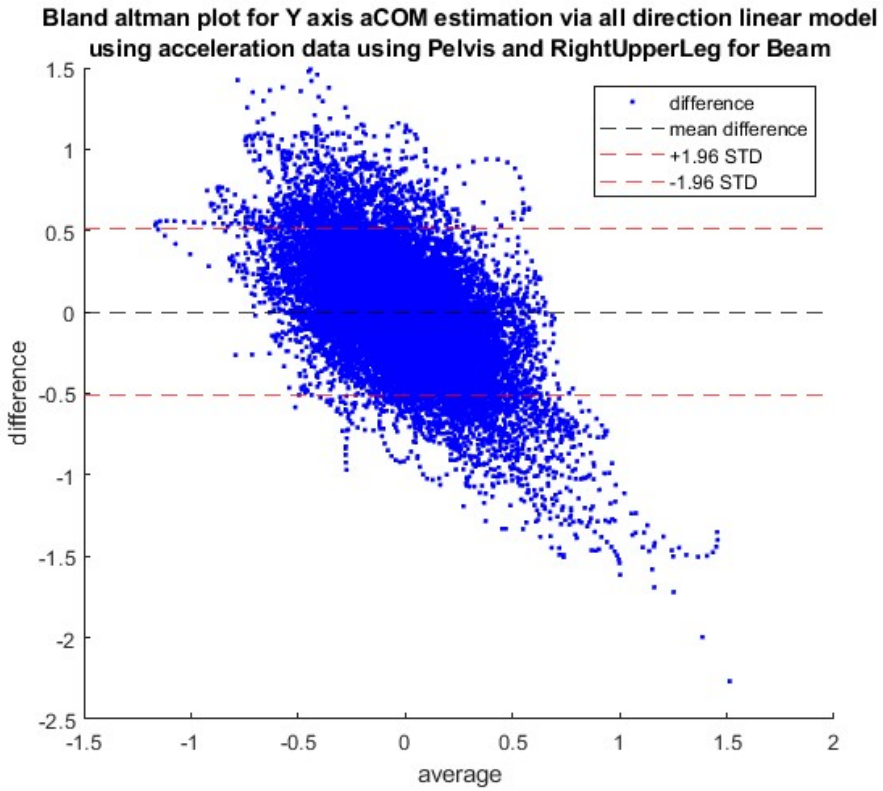

Figure 4.9: A Bland Altman plot of the beam walking activity, showing a bias very close to 0. The bias corresponding to this example is -0.0010.

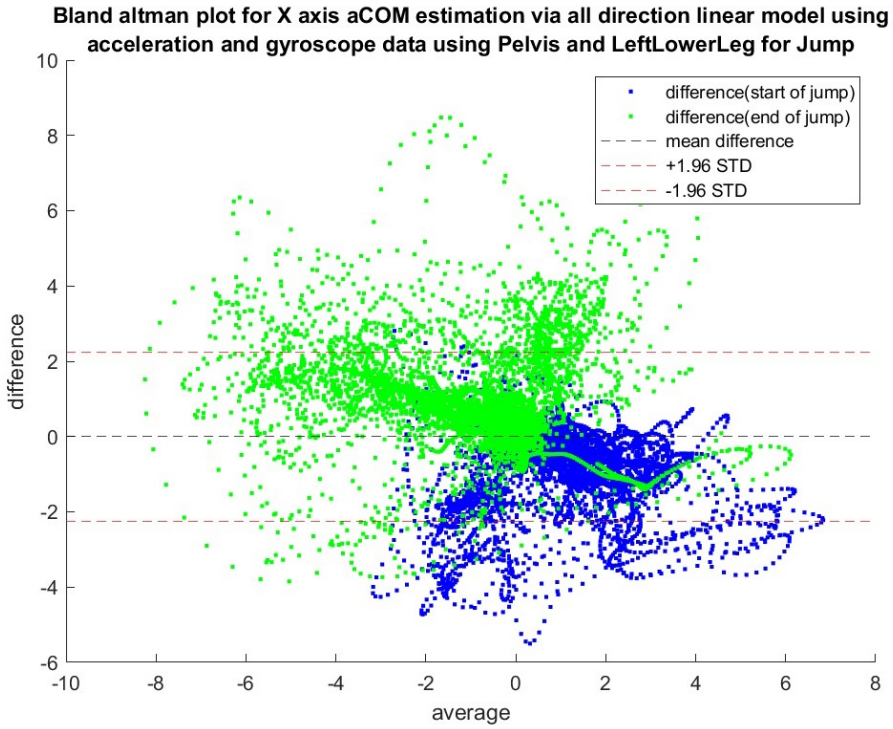

Figure 4.10: A Bland Altman plot of the jump activity divided into the start and end of the jump, showing a cross shape and two 'L' shapes.

4.3.3 Subject-wise r2 bargraphs

The results of the subject-wise r2 bargraphs showed that there was large difference in performance between subjects. Generalization between subjects improved with the gyroscope based model compared to the all direction model in certain cases. An example of this can be seen in figure 4.11. In other cases, the performance difference did not noticeably change, an example can be seen in figure 4.12.

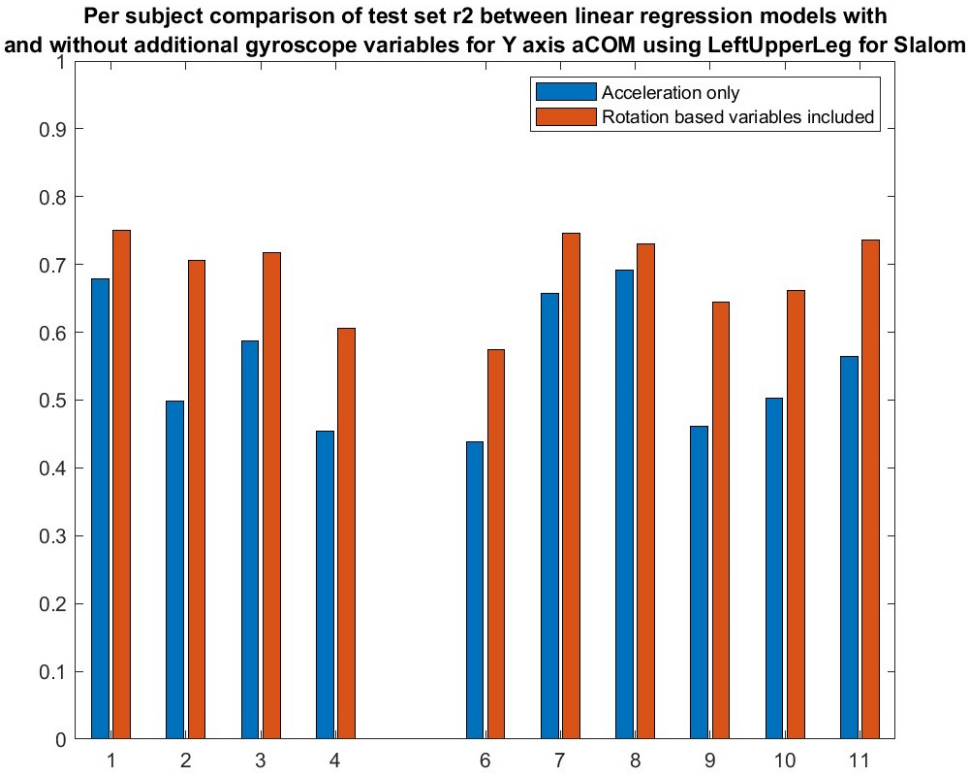

Figure 4.11: A bar graph comparing two different models estimating mediolateral aCOM for slalom walking using inputs from the pelvis and left upper leg segments.

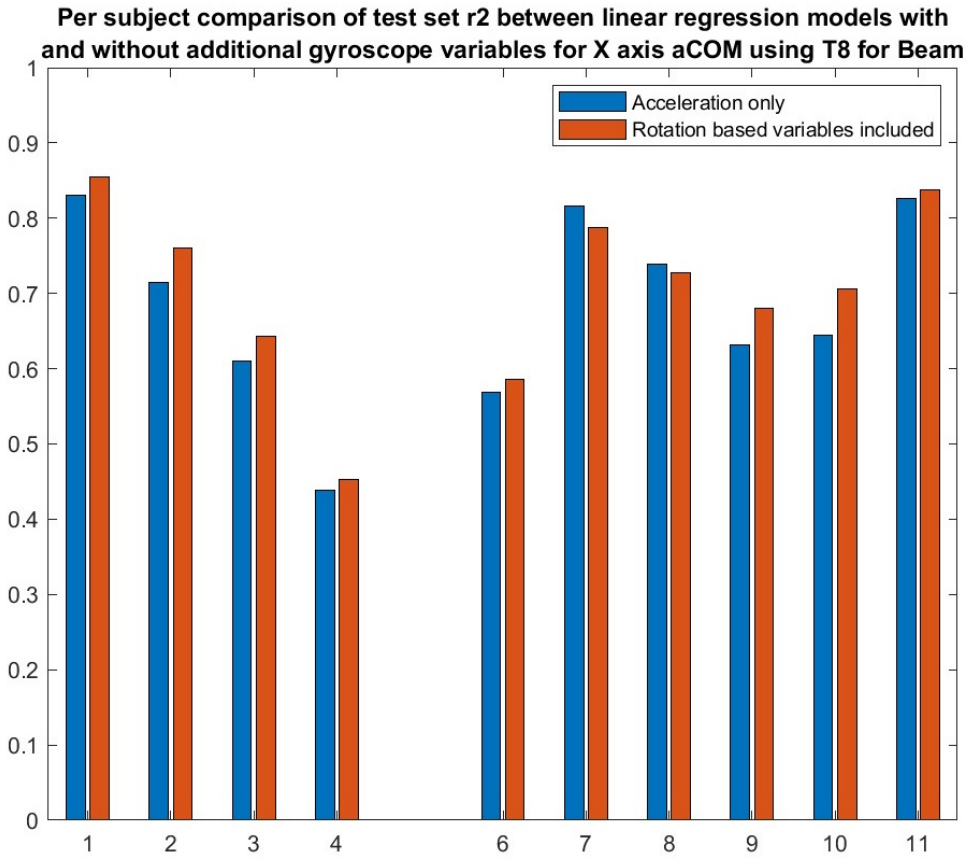

Figure 4.12: A bar graph comparing two different models estimating anterioposterior aCOM for beam walking using inputs from the pelvis and sternum segments.

5 DISCUSSION

This section will discuss the conclusions drawn from the findings from the results, as well as any limitations to the research that was done. It will also compare the results to results found in literature. It will then It will then discuss some possibilities for further investigation.

5.1 Interpretation of results

This section will describe the interpretation of the results. It will first describe the interpretation of the results of the best performing IMU locations from the performance heatmaps. It will then touch on the obtrusiveness of the different well performing IMUs, and then finally describe the interpretation of the results pertaining to the gyroscope based model.

5.1.1 IMU location performance

Activity specific models using inputs from the pelvis and a torso segment were found suitable for modelling walking tasks stairs walking tasks and the sit down and stand up task. Performance of linear regression models using acceleration from the limb and head segments was greater compared to the performance of the model with coefficients determined based on segment mass. This is potentially due to the segment acceleration representing more than just the acceleration of the segment itself: The acceleration of the head might be representative of a larger section of the torso than only the head, and the movement of the left lower leg may also be representative of the movement of the left upper leg and right leg. None of the one direction acceleration models performed significantly worse than the segment mass based models using the same segments, and all gains in performance from the all direction acceleration models and gyroscope based models compared to the one direction acceleration models are most likely due to the capturing of properties other than the contribution to aCOM of the measured segment itself.

Although the comparison with the segment mass model indicates that there may be added value to performing regression, it is not the only model that could be used as an alternative to regression. A hypothetical model where coefficients are determined based on the contributions of the segments to aCOM based on both the mass and the segment acceleration might also be condidered. Such a model might utilize lighter segments such as the hands better than the model based on segment masses. However, such a model would be unable to utilize the segment accelerations along other axes than the estimated aCOM component or the information from the segment rotation that were utilized by the all direction acceleration model and gyroscope based model, evidenced by their performance improvement compared to the one direction ac-

celeration model. Such a model would also likely be unable to utilize the head segment well, as the head is generally is kept stable during the movement of the human body while the models using the head segment and the pelvis segment nevertheless performed well for several tasks. As such, it seems worthwhile to use regression for the purpose of estimating aCOM in setups using a low amount of IMUs, rather than relying on the contributions of the individual segments.

Compared to the findings of Refai, M.I.M. et al. [16]□, the performance of all tested single direction acceleration models in the anterioposterior direction of normal walking perform worse than the findings of Refai, M.I.M. et al. with a single pelvis IMU: The maximum r^2 found in the anterioposterior direction for one direction acceleration models is 0.75 for the model using the sternum and pelvis, whereas Refai, M.I.M. et al. finds r^2 0.79 using only the pelvis. Refai, M.I.M. et al. does find a significantly lower performance in the mediolateral direction(r^2 0.30) than the one direction acceleration model using only the pelvis(r^2 0.47). This also holds true for the slalom activity, where Refai, M.I.M. et al. finds r^2 0.26 in the mediolateral direction, compared to r^2 0.47 from the one direction acceleration model using only the pelvis. In the anterioposterior direction the difference is reduced: Refai, M.I.M. et al. finds r^2 0.52 in the anterioposterior direction whereas the one direction accelleration model using only the pelvis finds a comparable r^2 0.50. Refai, M.I.M. et al. uses a differently defined frame, which might make it easier to estimate anterioposterior aCOM in a straight line while complicating the estimation of aCOM in the anterioposterior direction. The all direction linear regression model does produce a better performance in the natural walking activity than the findings by Refai, M.I.M. et al: The models using the pelvis and head and pelvis and sternum achieve r^2 0.83 and 0.81 respectively, compared to the r^2 0.79 found by Refai, M.I.M. et al.

Compared to the findings by Simonetti, E. et al. [13]□ the one direction acceleration model using only the pelvis performs better in the anterioposterior direction: The one direction acceleration model using only the pelvis achieves r^2 0.67 whereas the estimation by Simonetti, E. et al. finds r^2 0.61. The estimation done by Simonetti, E. et al. in the mediolateral direction outperforms the one direction acceleration model and all direction acceleration model using only the pelvis: Both the one direction acceleration model and all direction acceleration model find r^2 0.47, whereas Simonetti, E. et al. finds r^2 0.58. The one direction models using the pelvis and head, pelvis and sternum and pelvis and shoulder produce better estimations than the single IMU estimation by Simonetti, E. et al., achieving r^2 0.75, 0.64 and 0.69 respectively. Similarly, all direction acceleration models using these segments also perform better than the single IMU estimation by Simonetti, E. et al. Some differences might be caused by the fact that Simonetti, E. et al. is investigating the estimation of aCOM in transfemoral amputee gait, which differs from the gait of individuals who have not undergone amputation.

No models using inputs from one IMU in addition to the pelvis were able to accurately estimate the mediolateral acceleration of the balance task. Assuming balancing tasks and jumping tasks do not constitute a significant portion of a subject's daily living activities, a measurement setup using only an IMU located on the head and an IMU located on the sternum or head may be used to estimate the aCOM via instantaneous linear models combined with activity and step detection. If accurate estimation of mediolateral aCOM during balancing tasks is required, a combination of IMUs, a combination of an IMU on the pelvis, two IMUs on the lower legs and an IMU on the torso may provide higher accuracy than models using just using inputs from the pelvis and a torso segment, although the accuracy achieved by these models is still far below the accuracy that two segment models achieve when estimating mediolateral aCOM in gait. If accuracy in jumping tasks is desired, an IMU placed on the sternum is preferable to an IMU placed on the head.

□Using the property that the r^2 is the square of the pearson correlation coefficient

5.1.2 IMU locations and obtrusiveness

While the IMU location that performs the best can be discovered by comparing performance measures between models using IMUs in different locations for their inputs, the best performing IMU may not be the best IMU to use. Not all locations for IMUs are equally obtrusive, and an important reason for minimizing the amount of IMUs in this manner is to reduce the obtrusiveness of the measurement setup. For instance, the head and the sternum tend to perform well, but attaching an IMU to the sternum of a subject would mean putting on an elastic strap, adhesive tape or even wearing tight shirt for the purpose of keeping the sternum IMU in place. In contrast, an IMU on the head might be attached to a set of glasses or kept in place in a similar fashion to an out of ear hearing aid, both methods which would be less uncomfortable to wear over a long period of time and easier to put on and take off when needed. Similarly, an IMU attached to the upper leg may be approximated by a smartphone which a person is already carrying, which may make the usage of a upper leg IMU an option to consider in spite of the lower accuracy achieved by models using the upper leg IMU in comparison to the models using the torso segments. As for IMUs on the lower legs, these might need to be strapped onto soft tissue on the calf where they would be uncomfortable, or around the ankles where they might resemble ankle bracelets placed on criminals. Since this is undesirable, it may be worthwhile to investigate methods of estimating aCOM that do not require IMUs on the lower leg if the goal is to estimate aCOM in balance tasks in daily living.

5.1.3 Gyroscope based model

The inclusion of the parameters based on tangential and centripetal acceleration is mostly useful for models using inputs from either the upper leg or the sternum. It may also be beneficial for models for estimating aCOM using only a pelvis IMU if the model needs to provide an estimate for a sitting down and standing up task. A concern for the use of these parameters may be that they will only apply to a subset of the subjects and could worsen the outcome for others, but the r2 bargraphs show that the addition of these parameters does not aggravate the differences in performance between subjects and in some cases makes the generalization over subjects more consistent.

5.2 Limitations

There are some limitations on the applicability of the research in this thesis. This section will describe limitations due to the tasks used in the training and testing of the models, and limitations due to issues during the processing. Finally, this section will briefly mention issues with data from one of the subjects.

5.2.1 Representativity of tasks

Since the goal of estimating aCOM in this thesis is to work towards estimating aCOM in daily living, it is worthwhile to consider to what extent the tasks that were tested are representative of daily living. The activities of climbing stairs, sitting down on a seat and getting up from it are significant parts of the daily activities of many people and are relevant activities to consider in

this regard. However, jumping and beam walking may be less relevant for this purpose. Even if a person for some reason makes jumps in their daily routine, which would be uncommon, a jump only lasts for a brief moment in time and will not constitute a large portion of the person's motion in the day. Similarly it may be considered that balancing is not normally a large part of a person's routine. Exceptions may exist here, for instance a person who participates in gardening as a hobby might have to balance along narrow paths in order to reach parts of the garden they maintain. Such activities are also likely to be less common for the elderly, as jumping and balancing are tasks that involve a fall risk.

Aside from the activity type, it may also be considered how representative the activities prescribed by the protocol are of the way they would be performed in daily life. The sit down and stand up task involves the subject sitting straight down after positioning themselves in front of a stool, but in real life a wide variety of sitting strategies are employed. A person may lower themselves to the seat diagonally or pull the seat under themselves in the process of sitting down. People may also lean on arm rests of the chair to raise and lower themselves, or sit down quickly and rely on the back rest of the chair to stop their momentum. None of these strategies are represented in the sit down and stand up task, and the performance of the models created for it may not be representative of the performance of models used to estimate sitting down and standing up in real life. Similarly to using the armrests of a chair, a person may also use the railings of a flight of stairs, which could drastically alter their balancing strategy. As the stairs walking activity did not involve usage of the railing, such strategies are not accounted for by the stairs walking activity.

Finally, certain activities which are common in daily living may not be represented in the investigated activities at all. For instance, daily living activities may involve kneeling down to pick or clean something up, pushing a shopping cart at the grocery store, or kitchen tasks where a person is walking or standing while doing something with their hands. None of these activities are investigated in this thesis and may need to be investigated in order to create a model that captures enough a person's potential daily life activities.

5.2.2 Processing issues

HD processing normally provides the best estimates of the motion captured by the Link suit. However, the data gathered in the experiment would exhibit spikes in the vertical component of the acceleration data of certain segments after HD reprocessing. In order to avoid these artefacts, Normal processing was used instead. Although the relation between the segments and the COM should be similar regardless of the reprocessing quality, this still means that the estimation was performed for a less accurate reference value for aCOM. The accuracy of the estimate may change if models are tested and trained using the more accurate values for aCOM that would be provided via HD processed data.

5.2.3 Subject 5

The recordings of subject 5 were found to significantly deviate from the recordings of other subjects and as such were not used in the training and evaluation of the model. The specifics of how this was investigated can be found in appendix F.

5.3 Future work

Based on the results found in this thesis, some recommendations can be given. In this section, two potential avenues for improving the performance of the model will be provided: Classification of different movement strategies, nonlinear modelling and use of time domain information, and the use of demographic information. The possibility of using models with multiple activities will also be discussed. Finally, it will be discussed whether the current results could be put to practical use.

5.3.1 Classification of different movement strategies

This thesis assumed the models used would be paired with working activity detection, and to this end the data was manually labeled as belonging to some activity. However, in the time series plots it is apparent that there is a lot of variance in the type of motion between the different subjects, and the performance of the models varied significantly between subjects. If working activity detection is assumed, it may be possible to distinguish between these different types of motion. A form of unsupervised learning may be able to distinguish different movement strategies which could be easier to model individually. Such an investigation may also benefit from a dataset which includes different walking paces.

5.3.2 Use of demographic information

Another way to reduce the difference in performance between subjects may be to adjust the models based on demographic information The models were tested and trained on both male and female subjects of different heights. This information would be easy for a physician to gather, and differences in demographic between subjects may explain some of the differences in motion within the same activity.

5.3.3 Nonlinear modelling

The time series plots also showed that the estimates provided by the models were less accurate when the reference values for aCOM had more extreme values. This indicates that the relationship between aCOM and the input variables may be different for very high absolute values of aCOM. A nonlinear model may be able to represent this behavior. Linear splines can easily be added to a linear regression model as an extra basis function and would allow the model to provide different estimates for more extreme input values, and may therefore be a worthwhile addition to investigate.

5.3.4 Time domain modelling

This thesis only investigated instantaneous models, but aCOM and the parameters used to investigate it are time domain signal and useful data may be contained in the time domain of the input parameters. It can already be seen that models for the jump activity may benefit from time domain parameters, as the start of the jump and the end of the jump create different shapes

within the Bland Altman plots which indicates that different relations between the parameters and aCOM may apply for different parts of the jump. Models for other activities may also benefit from this, but this is not indicated in the Bland Altman plots.

5.3.5 Multi-activity models

This thesis assumes working activity detection, and to implement the findings of the thesis in any kind of practical application would require activity detection to be developed. It is however unclear how necessary this activity detection is. It may be possible to create models that perform well for multiple activities, or at least well enough for activities that have lower requirements for the accuracy of the estimate. It may be worthwhile to investigate how much performance is impacted by combining different activities into the same group, as well as investigating which, if any, activities need to be distinguished in order for the model to function.

5.3.6 Potential applications

As mentioned in the previous paragraph, the models investigated in this thesis cannot be put to use in measurement applications directly without the use of activity detection. Nevertheless, the outcome of this research may provide a starting point for the IMUs used in monitoring applications. Since the models using the IMUs on the head and sternum provide the overall best performance, it is reasonable to investigate these first when aiming to create a minimally obtrusive monitoring application. The improvement in performance of the models using the upper leg IMUs and pelvis IMUs when the rotation based variables were included also indicates that it may be worthwhile to attempt to utilize the rotation of the sensor when estimating aCOM with only a pelvis IMU or a smartphone.

6 CONCLUSION

For the estimating the reference value of aCOM provided by the 17 segment model used by the MVN software in the natural walking activity in the anterioposterior direction, the best performing linear regression models using only acceleration out of the examined group are the models using the head sternum or shoulder segment in combination with the pelvis segment, at r^2 0.83, 0.81 and 0.78 respectively. Models using these segments also perform best for the zigzag activity at r^2 0.78, 0.78 and 0.76, for the turn activity at r^2 0.79, 0.77 and 0.76, for the sit down and stand up activity at r^2 0.84, 0.87 and 0.87, for the beam walking activity at r^2 0.72, 0.71 and 0.70, for the terrain walking activity at r^2 0.77, 0.75 and 0.73, and for the stairs walking up activity at r^2 0.71, 0.69 and 0.69. For the jump activity, the models using head foot or shoulder segment in combination with the pelvis segment perform the best, at r^2 0.72, 0.7 and 0.67 respectively. For the stairs walking down activty, the models using the head shoulder or lower leg segment in combination with the pelvis perform best at r^2 0.64, 0.54 and 0.54 respectively.

For the mediolateral direction, the best performing models using segment acceleration to estimate the reference value of aCOM provided by the 17 segment model used by the MVN software in the natural walking activity in the mediolateral direction are also the models using the head, sternum or shoulder segments in combination with the pelvis, at r^2 0.75, 0.64 and 0.69 respecively. Models using these segments also perform best for slalom walking at r^2 0.80, 0.75 and 0.75, for zigzag at r^2 0.72, 0.73 and 0.71, for turn at r^2 0.73, 0.69 and 0.70, for sit down and stand up at r^2 0.51, 0.57 and 0.52, for jump at r^2 0.29, 0.53 and 0.29, for terrain walking at r^2 0.76, 0.79 and 0.69, for stairs walking up at r^2 0.80, 0.75 and 0.77, and for stairs walking down at r^2 0.79, 0.70 and 0.68. For the beam walking activity in the mediolateral direction, all models perform poorly, the best performing models using the pelvis in addition to the lower leg, sternum or foot, achieving r^2 0.35, 0.32 and 0.31 respectively.

In the vertical direction, all linear regression models estimating the reference value of aCOM provided by the 17 segment model used by the MVN software using acceleration perform well for all activities except the sit down and stand up activity, achieving > 0.8 r^2 for any model using any segment in combination with the pelvis. The models combining the pelvis with the head, sternum or shoulder segments achieve r^2 > 0.9 for all activities except slalom, zigzag and turn, where they achieve r^2 > 0.85.

A linear regression model using the segment acceleration to estimate the mediolateral component of the reference value of aCOM provided by the 17 segment model used by the MVN software using acceleration for the beam activity using both lower leg segments and the pelvis achieved a better performance than the models using segment accelerations from two segments, achieving r^2 0.43. A model using both lower legs, the pelvis and the head achieved r^2 0.47 and a model using the pelvis, both lower legs and the sternum achieved r^2 0.56.

The best performing models estimating the anterioposterior component of the reference value of aCOM provided by the 17 segment model used by the MVN software using acceleration and

the 9 parameters informed by the rotation of the segments use the pelvis in addition to the head, sternum or shoulder in the case of the slalom walking activity at r^2 0.74, 0.76 and 0.72, the zigzag activity at r^2 0.78, 0.81 and 0.78, the turn activity at r^2 0.82, 0.82 and 0.79, the beam walking activity at r^2 0.73, 0.74, 0.71, the terrain walking activity at r^2 0.79, 0.77 and 0.76, and stairs walking up 0.71, 0.70, 0.70. For the natural walking activity, the best performing models use the pelvis in addition to the head, upper leg or shoulder segment at r^2 0.84, 0.83 and 0.81, for the sit down and stand up activity the best performing models use the pelvis in addition to the sternum, shoulder or upper arm segment at r^2 0.90, 0.88, 0.85, for the jump activity, the best performing models use the pelvis in addition to the lower leg, shoulder or upper arm segment at r^2 0.81, 0.75 and 0.75, and for the stairs walking down activity the best performing models use the pelvis in addition to the head, upper leg and lower leg segment, at r^2 0.68, 0.59 and 0.57.

The best performing models estimating the mediolateral component of the reference value of aCOM provided by the 17 segment model used by the MVN software using acceleration and the 9 parameters informed by the rotation of the segments for natural walking use the pelvis in addition to the head, sternum or shoulder, achieving r^2 0.75, 0.72 and 0.73 respectively. Models using these segments also perform best in the mediolateral direction for slalom walking at r^2 0.82, 0.82 and 0.79, for zigzag at r^2 0.73, 0.77 and 0.73, for sit down and stand up at r^2 0.52, 0.65 and 0.55, for terrain walking at r^2 0.76, 0.79 and 0.74, for stairs walking up at r^2 0.79, 0.81, 0.79, and stairs walking down at r^2 0.80, 0.78, 0.72. For the jump activity, the best performing models use the pelvis segment in addition to the sternum, upper leg or shoulder, achieving r^2 0.52, 0.24 and 0.25, and for the beam walking activity the best performing models use the pelvis in addition to the upper leg, lower leg or sternum, achieving r^2 0.41, 0.34 and 0.30, respectively.

The best overall performance for all investigated activities for a linear regression model using 2 segments including the pelvis, from the group of models that was investigated in this study, is achieved by the models using the pelvis segment and either the sternum segment or head segment.

REFERENCES

[1] Matthew N Cramer and Ollie Jay. Biophysical aspects of human thermoregulation during heat stress. *Autonomic Neuroscience*, 196:3–13, 2016.

[2] Hanneke Pierre Franciscus Xaverius Moonen, Karin Josephina Hubertina Beckers, and Arthur Raymond Hubert van Zanten. Energy expenditure and indirect calorimetry in critical illness and convalescence: current evidence and practical considerations. *Journal of Intensive Care*, 9:1–13, 2021.

[3] Lachlan Mitchell, Luke Wilson, Grant Duthie, Kate Pumpa, Jonathon Weakley, Christopher Scott, and Gary Slater. Methods to assess energy expenditure of resistance exercise: A systematic scoping review. *Sports Medicine*, pages 1–16, 2024.

[4] Cara B Ebbeling, Janis F Swain, Henry A Feldman, William W Wong, David L Hachey, Erica Garcia-Lago, and David S Ludwig. Effects of dietary composition on energy expenditure during weight-loss maintenance. *Jama*, 307(24):2627–2634, 2012.

[5] Meo Vincent C Caya, Analyn N Yumang, Jhayvee V Arai, John Daryll A Niñofranco, and Kenneth Aaron S Yap. Human activity recognition based on accelerometer vibrations using artificial neural network. In *2019 IEEE 11th international conference on humanoid, nanotechnology, information technology, communication and control, environment, and management (HNICEM)*, pages 1–5. IEEE, 2019.

[6] Stylianos Paraschiakos, Cláudio Rebelo de Sá, Jeremiah Okai, P Eline Slagboom, Marian Beekman, and Arno Knobbe. A recurrent neural network architecture to model physical activity energy expenditure in older people. *Data Mining and Knowledge Discovery*, 36(1):477–512, 2022.

[7] T Matsumura, VT Chemmalil, ML Gray, JE Keating, RL Kieselbach, SB Latta, N Occhialini, E Kinnal, S O'Toole, and RA Peura. Device for measuring real-time energy expenditure by heart rate and acceleration for diabetic patients. In *2009 IEEE 35th Annual Northeast Bioengineering Conference*, pages 1–2. IEEE, 2009.

[8] Ann M Swartz, Scott J Strath, DAVID R BASSETT, WILLIAM L O'BRIEN, George A King, and Barbara E Ainsworth. Estimation of energy expenditure using csa accelerometers at hip and wrist sites. *Medicine & Science in Sports & Exercise*, 32(9):S450–S456, 2000.

[9] Panagiota Anastasopoulou, Sascha Härtel, Mirnes Tubic, and Stefan Hey. Using support vector regression for assessing human energy expenditure using a triaxial accelerometer and a barometer. In *Wireless Mobile Communication and Healthcare: Third International Conference, MobiHealth 2012, Paris, France, November 21-23, 2012, Revised Selected Papers 3*, pages 106–113. Springer, 2013.

[10] Marta Delsoglio, Najate Achamrah, Mette M Berger, and Claude Pichard. Indirect calorimetry in clinical practice. *Journal of clinical medicine*, 8(9):1387, 2019.

[11] Alberto E Minetti. The biomechanics of skipping gaits: a third locomotion paradigm? *Proceedings of the Royal Society of London. Series B: Biological Sciences*, 265(1402):1227–1233, 1998.

[12] Stephanie K Herndon, Bradford C Bennett, Adam Wolovick, Andrew Filachek, Glenn A Gaesser, Arthur Weltman, and Mark F Abel. Center of mass motion and the effects of ankle bracing on metabolic cost during submaximal walking trials. *Journal of orthopaedic research*, 24(12):2170–2175, 2006.

[13] Emeline Simonetti, Elena Bergamini, Giuseppe Vannozzi, Joseph Bascou, and Hélène Pillet. Estimation of 3d body center of mass acceleration and instantaneous velocity from a wearable inertial sensor network in transfemoral amputee gait: a case study. *Sensors*, 21(9):3129, 2021.

[14] Elena M Gutierrez-Farewik, Åsa Bartonek, and Helena Saraste. Comparison and evaluation of two common methods to measure center of mass displacement in three dimensions during gait. *Human movement science*, 25(2):238–256, 2006.

[15] Christian Liedtke, Steven AW Fokkenrood, Jasper T Menger, Herman van der Kooij, and Peter H Veltink. Evaluation of instrumented shoes for ambulatory assessment of ground reaction forces. *Gait & posture*, 26(1):39–47, 2007.

[16] Mohamed Irfan Mohamed Refai, Bert-Jan F Van Beijnum, Jaap H Buurke, and Peter H Veltink. Portable gait lab: estimating 3d grf using a pelvis imu in a foot imu defined frame. *IEEE transactions on neural systems and rehabilitation engineering*, 28(6):1308–1316, 2020.

[17] Paul D. Groves. *4.3 Inertial Measurement Unit*, pages 149–151. Artech House, 2013.

[18] Gaspare Pavei, Francesca Salis, Andrea Cereatti, and Elena Bergamini. Body center of mass trajectory and mechanical energy using inertial sensors: A feasible stride? *Gait & posture*, 80:199–205, 2020.

[19] Weijun Tao, Tao Liu, Rencheng Zheng, and Hutian Feng. Gait analysis using wearable sensors. *Sensors*, 12(2):2255–2283, 2012.

[20] Chang June Lee and Jung Keun Lee. A cnn-lstm model for imu-based energy expenditure estimation under various walking conditions. In *2024 IEEE International Symposium on Inertial Sensors and Systems (INERTIAL)*, pages 1–2. IEEE, 2024.

[21] Patrick Slade, Mykel J Kochenderfer, Scott L Delp, and Steven H Collins. Sensing leg movement enhances wearable monitoring of energy expenditure. *Nature Communications*, 12(1):4312, 2021.

[22] H. Martin Schepers*, Edwin H. F. van Asseldonk, Jaap H. Buurke, and Peter H. Veltink. Ambulatory estimation of center of mass displacement during walking. *IEEE Transactions on Biomedical Engineering*, 56(4):1189–1195, 2009.

[23] Marianne J Floor-Westerdijk, H Martin Schepers, Peter H Veltink, Edwin HF van Asseldonk, and Jaap H Buurke. Use of inertial sensors for ambulatory assessment of center-of-mass displacements during walking. *IEEE transactions on biomedical engineering*, 59(7):2080–2084, 2012.

[24] Lotte L Lintmeijer, Gert S Faber, Hessel R Kruk, AJ “Knoek” van Soest, and Mathijs J Hofmijster. An accurate estimation of the horizontal acceleration of a rower’s centre of mass using inertial sensors: a validation. *European Journal of Sport Science*, 18(7):940–946, 2018.

[25] Håvard Myklebust, Øyvind Gløersen, and Jostein Hallén. Validity of ski skating center-of-mass displacement measured by a single inertial measurement unit. *Journal of applied biomechanics*, 31(6):492–498, 2015.

[26] Mackenzie Collins, Iris C. Levine, Philippa C. Gosine, Roger E. Montgomery, Konika Nirmalanathan, and Alison C. Novak. A comparison of minimum segment models for the estimation of centre of mass position and velocity for slip recovery during a bathtub transfer task. *Gait & Posture*, 109:153–157, 2024.

[27] Christopher M. Bishop, editor. *Pattern Recognition and Machine Learning*. Springer New York, New York, NY, 2006.

[28] Nadia Magnenat-Thalmann, Osman Ratib, and Hon Fai Choi. *3D multiscale physiological human*. Springer, 2013.

[29] Movella Technologies B.V, "MVN User Manual", `https://www.movella.com/hubfs/MVN_User_Manual.pdf`, Accessed: 17-04-2024.

[30] Jeff Sanny William Moebs, Samuel J. Ling. *University Physics Volume 1*. OpenStax, 09 2016.

[31] f Xsens Technologies B.V., "Xsens MVN quick setup sheet", `https://www.beamsystems.nl/media/2386/xsense-mvn_quick_setup_sheet.pdf`, Accessed: 24-05-2024.

[32] Evandro Bernardes and Stéphane Viollet. Quaternion to euler angles conversion: A direct, general and computationally efficient method. *Plos one*, 17(11):e0276302, 2022.

[33] J. B. Kuipers. *Quaternions and Rotation Sequences: A Primer with Applications to Orbits, Aerospace and Virtual Reality*. Princeton University Press, Princeton, 2006.

[34] R. Dumas, L. Chèze, and J.-P. Verriest. Adjustments to mcconville et al. and young et al. body segment inertial parameters. *Journal of Biomechanics*, 40(3):543–553, 2007.

[35] Paolo de Leva. Adjustments to zatsiorsky-seluyanov's segment inertia parameters. *Journal of Biomechanics*, 29(9):1223–1230, 1996.

[36] J. B. Kuipers. *Quaternions and Rotation Sequences: A Primer with Applications to Orbits, Aerospace and Virtual Reality*. Princeton University Press, Princeton, 2006.

A TABLE OF START AND END REQUIREMENTS FOR DATA EXTRACTED FROM RECORDINGS

The following are the criteria set for the start and end of a recording for each activity: For natural walking, the start and end were chosen to be the first and last step, or the last step before the person started turning. For slalom walking, zigzag and walk and turn, the start and end were chosen to be when the person first starts turning and when they first stop turning. For the sit down and stand up For the beam walking activity, only steps that started and ended on the beam were considered, and as such the recordings were cut off so that the last step onto the beam and the first step off the beam were not included.

Activity	Start criteria	End criteria
Natural walking	Before the first step	During any step where the subject starts to turn, or towards the very end of the recording
Slalom, Zigzag, Turn	Before the subject starts to turn	After last the step in which the subject turns
Sit down and Stand up	Before the subject starts to bend	After the subject finishes standing up
Jump	Before the subject prepares to jump	After the subject has resumed normal posture
Beam	During last step onto the beam	During first step off the beam
Terrain walking	Before the first step	Towards the very end of the recording
Stairs walking up/down	Before the first step onto the stairs	After the last step off the stairs

Table A.1: Start and end criteria for different activities.

B DURATION BASED RECORDING SEGMENT EXCLUSION

As part of the processing of the data prior to the creation of the models, the duration of the different step segments was checked for abnormalities. Based on this examination, a number of recording segments were excluded from the training and evaluation data.

The examination of the lengths of recording segments was performed via a scatterplot of the duration of the step segments of the gait-based activities, which is shown in figure B.1. From this scatterplot it was determined that certain cycles within the dataset were extraordinarily long or short in duration. Noticeably long recording segments were present in the stairs walking, turning and beam walking activities. A noticably short outlier was present in the terrain walking. Recording segments with such an abnormal duration represent steps that were taken extremely quickly or extremely slowly. Including these steps might negatively impact the evaluation of the model, since the experiment was not designed to record training data with a wide variety of walking paces. In order to homogenize the activity datasets, thresholds for exclusion were determined from a visual inspection of the scatter plot and visual comparison of the cycles with extreme lengths within certain thresholds. The cycles with lengths outside of these thresholds were excluded from the dataset. The thresholds are listed in table B.1.

Activity	Threshold
Up	Above 210 frames (0.88 s)
Down	Above 210 frames (0.88 s)
Terrain	Below 90 frames (0.38 s)
Turn	Above 250 frames (1.04 s)

Table B.1: Cycle length exclusion criteria for different activities.

None of the cyclic units of the beam walking activity were excluded despite the high variance of the step duration within the dataset, since the variation of step duration is a feature of human balance control. As consequence of this feature, the duration of the cyclic units within the activity will naturally be erratic and this should be reflected in the dataset.

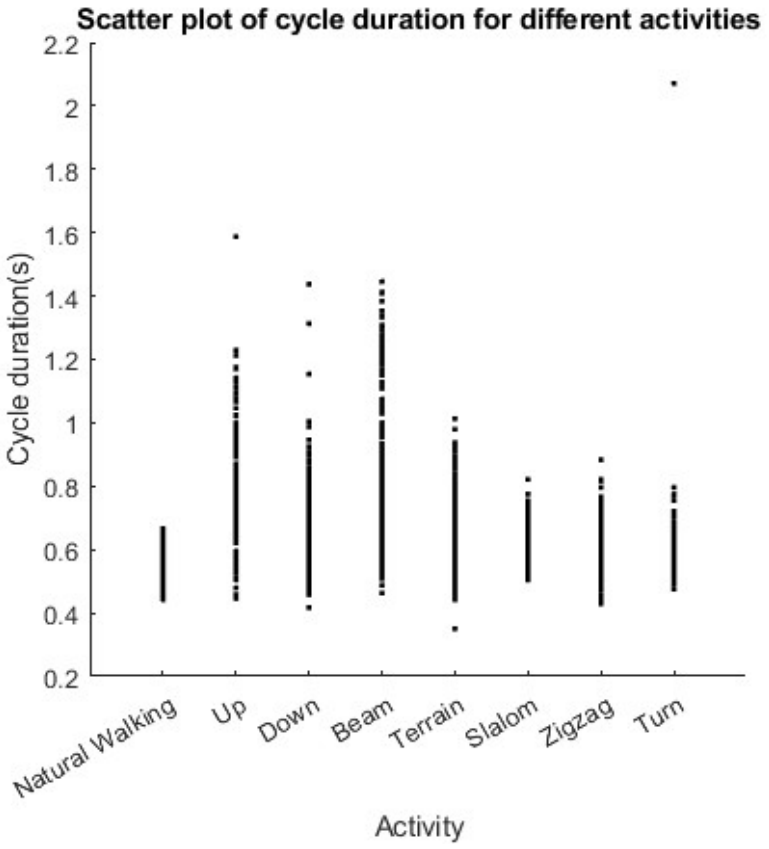

Figure B.1: A scatterplot of cycle duration present in the different gait activities.

C MATHEMATICAL JUSTIFICATION OF INPUT PARAMETERS OF LINEAR MODELS

This appendix contains the kinematic justification behind the input parameters used in the three model types.

As per eq.2.12, any variable that contributes to the segment center of mass acceleration can be said to contribute to the whole body center of mass acceleration.

For every input parameter used, it will be shown that an LRM can be used to estimate the unknowns in the relationship between the input parameters and aCOM. First this will be done for a model that uses only the segment acceleration, then it will be done for a model using a set of parameters derived from the segment angular velocity and angular acceleration.

C.1 Acceleration as input parameter

Acceleration is an input parameter that relates to the simplest case where the basis functions from 2.1 leave the input unaltered.

$$\bar{u} = w_0 + \sum_{n=1}^{N} w_n * v_n \tag{C.1}$$

A model that comforms to this simplest case would require inputs that are kinematically related to aCOM via some constant. By making the assumption that only the linear segment acceleration(a^{Sn}) measured by an IMU contributes significantly to the acceleration of a segment center of mass, eq.2.12 can be rewritten to a form that uses accleration as input and is compatible with eq.C.1.

$$\bar{\vec{a}}_{COM} = \sum_{n=1}^{N} \frac{m_n}{M} * \vec{a}_{Sn} \tag{C.2}$$

Since segment masses and the total body mass are assumed to be constant, $\frac{m_n}{M}$ can be estimated by the linear model as a coefficient when $alin^{seg_n}$ is the input.

$$\bar{\vec{a}}_{COM} = w_0 + \sum_{n=1}^{N} w_n * \vec{a}_{Sn} \tag{C.3}$$

Since the relationship between segment acceleration as an estimate for segment center of mass acceleration and aCOM can be formulated as a set of input-coefficient pair within a linear regression model, segment acceleration is a biomechanically valid input parameter to use in a linear regression model estimating aCOM.

Linear regression model using tangential acceleration, centripetal acceleration and segment acceleration

The basic linear regression model from the previous section only uses the segment acceleration data, which represents the accelerometer data from the IMU as input. Segment orientation data, representing the IMU's gyroscope data, is used to rotate the direction of this acceleration into anatomical frame, but data corresponding to the gyroscope measurements is otherwise not utilized in the basic linear regression model. However, the gyroscope data may contain additional information about aCOM. Simply using the segment angular velocity or angular acceleration as an extra linear acceleration variable in the input for the basic linear regression model would not be biomechanically justified, as the simple linear regression model relies on a linear relation between a_{Sn} and aCOM. This relation is not present for angular velocity. Since a direct linear relation is not present, a feature that does have a linear relation with aCOM would need to be created from the angular velocity in order to utilize gyroscope measurements as input. In this section, such a feature will be created using the kinematic equations for centripetal acceleration(a_c) and tangential acceleration(a_t). These equations are as follows [30]:

Given a reference frame that does not move in relation to the segment origin, the contributions of linear acceleration, tangential acceleration and in the segment center of mass position in fact fully describe $\vec{a}_{COM,Sn}$.

$$\vec{a}_{COM,Sn} = \vec{a}_{Sn} + \vec{a}_c + \vec{a}_t \tag{C.4}$$

$\vec{a}_c$ and $\vec{a}_t$ can be written out when eq.C.4 is divided into its directional components within the segment coordinate system:

$$\begin{aligned} a_{COM,Sn,x} &= a_{Sn,x} - r_{x,Sn} * (\dot{\beta}^2 + \dot{\gamma}^2) + r_{y,Sn} * \ddot{\gamma} + r_{z,Sn} * \ddot{\beta} \\ a_{COM,Sn,y} &= a_{Sn,y} - r_{y,Sn} * (\dot{\alpha}^2 + \dot{\gamma}^2) + r_{x,Sn} * \ddot{\gamma} + r_{z,Sn} * \ddot{\alpha} \\ a_{COM,Sn,z} &= a_{Sn,z} - r_{z,Sn} * (\dot{\alpha}^2 + \dot{\beta}^2) + r_{x,Sn} * \ddot{\beta} + r_{y,Sn} * \ddot{\alpha} \end{aligned} \tag{C.5}$$

Here $r_{x,Sn}$,$r_{y,Sn}$,$r_{z,Sn}$ are the x, y and z coordinates of the segment center of mass within the segment frame. These equations shows that the assumption made for the simple linear regression model is only valid when the linear acceleration is measured very close to the segment center of mass(so that r is very small), or when the angular velocity and acceleration are close to zero.

To include the gyroscope measurements in the estimation of aCOM, eqs.C.2 and C.3 can be expanded using eq.C.4 to describe a linear model with the assumption that both the measured linear acceleration as well as a_c and a_t caused by the measured rotation of the segment contribute to $\vec{a}_{COM,Sn}$..

$$\overline{\vec{a}}_{COM} = \sum_{n=1}^{N} \frac{m_n}{M} * (\overrightarrow{a_{Sn}} + \overrightarrow{a_c} + \overrightarrow{a_t}) \tag{C.6}$$

a_{Sn} is already included in the basic regression model, but a_c and a_t are not. If a_c and a_t are known, they could easily be added to eq.C.3, resulting in eq.C.7 for the x axis aCOM. The accelerations along the other axes have been excluded from this equation for space but this does not indicate their exclusion from the actual model.

$$\overline{a}_{COM,x} = \sum_{n} w_{x,n,p} * a_{Sn,x} + w_{x,n,c} * a_{c,Sn,x} + w_{x,n,t} * a_{t,Sn,x} \tag{C.7}$$

However, a_c and a_t can only be known if the coordinates of the segment center of mass are known. Although estimates for the segment center of mass coordinates exist in literature[35], using these would limit the use of the rotational variables to only estimate the contributions of their respective segments. This is not ideal because the rotation of a segment can potentially provide information about multiple segments. For instance, the rotation of the right upper arm might coincide with rotation in the right lower arm, resulting in an effective center of mass with different coordinates from the actual right upper arm center of mass. As such, it would be useful to have the LRM estimate the center of mass coordinates instead of providing them to it. In order to do this, the coordinates of the segment center of mass have to be written in such a way that the segment center of mass coordinates can be used as part of $w_{x,n,c}$ and $w_{x,n,t}$ in eq. C.7. To do this, the model will first be formulated for a case where the coordinates of the segment center of mass are constant in the anatomical frame, and then the formula will be expanded to cover a case where the coordinates are based on a rotation from the segment frame to the anatomical frame.

If the coordinates of the segment center of mass are constant in the anatomical frame, it can be shown that it would be trivial to formulate the LRM up in way where it would estimate the center of mass coordinates. If the two angular components of eq C.7 are written out, it can be seen that each of the center of mass coordinates in that equation are multiplied with a coefficient.

$$w_{x,n,c} * a_{c,Sn,x} = w_{x,n,c} * -r_x * (\dot{\beta}^2 + \dot{\gamma}^2) \tag{C.8}$$

$$w_{x,n,t} * a_{t,Sn,x} = w_{x,n,t,y} * r_y * \ddot{\gamma} + w_{x,n,t,z} * r_z * \ddot{\beta} \tag{C.9}$$

Two coefficients that are multiplied can be simplified to a single coefficient, so if the segment center of mass coordinates are treated as coefficients, they can be merged with an existing coefficient in eq.C.8 in the following manner:

$$w_{x,n,c} * -r_x = w_{x,n,1} \tag{C.10}$$

$$w_{x,n,t} * r_y = w_{x,n,2} \tag{C.11}$$

$$w_{x,n,t} * r_z = w_{x,n,3} \tag{C.12}$$

These can be filled in to eq.C.9 to create a linear model with coefficients that represent estimates each of the center of mass coordinates. Of course, the segment center of mass coordinates are not constant in the anatomical frame, they are only constant within the segment frame.

While this does mean that the magnitude of $\vec{r}$ remains constant, its direction will depend on the segment orientation within the anatomical frame. This can be described using a quaternion rotation.

$$\vec{r}_P = q\vec{r}_{Sn}q^{-1} \tag{C.13}$$

Here $\vec{r}_P$ is the segment center of mass coordinates within the anatomical frame, $\vec{q}$ is a unit quaternion describing the orientation of the segment in the anatomical frame, and $\vec{q}^{-1}$ is the inverse of $\vec{q}$. Writing out the quaternion vectors of the center of mass coordinates produces the following equation:

$$\begin{bmatrix} 0 \\ r_{x,P} \\ r_{y,P} \\ r_{z,P} \end{bmatrix} = \vec{q} \begin{bmatrix} 0 \\ r_{x,Sn} \\ r_{y,Sn} \\ r_{z,Sn} \end{bmatrix} \vec{q}^{-1} \tag{C.14}$$

While the segment center of mass coordinates within the segment frame are still constant within this equation, and the quaternion is known, the quaternion rotation in this equation creates a situation where the axial components of $\vec{r}_P$ are each a function of three of the segment center of mass coordinates within the segment frame. In order to estimate the coordinates using an LRM, each of the individual contributions of the axial components of $\vec{r}_{Sn}$ to the axial components of $\vec{r}_P$ would need to be known. It is possible to seperate out these individual contributions using the distributive property of quaternion rotation [36], which allows eq C.14 to be written out as a sum of the rotations of the directional components.

$$\begin{bmatrix} 0 \\ r_{x,P} \\ r_{y,P} \\ r_{z,P} \end{bmatrix} = q \begin{bmatrix} 0 \\ r_{x,Sn} \\ 0 \\ 0 \end{bmatrix} q^{-1} + q \begin{bmatrix} 0 \\ 0 \\ r_{y,Sn} \\ 0 \end{bmatrix} q^{-1} + q \begin{bmatrix} 0 \\ 0 \\ 0 \\ r_{z,Sn} \end{bmatrix} q^{-1} \tag{C.15}$$

Since quaternion rotation does not change the magnitude of a vector, the magnitude can be taken outside of the matrix.

$$\begin{bmatrix} 0 \\ r_{x,P} \\ r_{y,P} \\ r_{z,P} \end{bmatrix} = r_{x,Sn} * q \begin{bmatrix} 0 \\ 1 \\ 0 \\ 0 \end{bmatrix} q^{-1} + r_{y,Sn} * q \begin{bmatrix} 0 \\ 0 \\ 1 \\ 0 \end{bmatrix} q^{-1} + r_{z,Sn} * q \begin{bmatrix} 0 \\ 0 \\ 0 \\ 1 \end{bmatrix} q^{-1} \tag{C.16}$$

If the axial components of the rotated axial unit vectors can be separated, the individual contributions of the directional components of $\vec{r}_{Sn}$ will be known. These can be found using the fact that the quaternion rotation of the axial unit vectors depends only on $\vec{q}$, which means that each of the directional components of the rotated vector can be written as a function of $\vec{q}$.

$$
\begin{aligned}
q \begin{bmatrix} 0 \\ 1 \\ 0 \\ 0 \end{bmatrix} q^{-1} &= \begin{bmatrix} 0 \\ f_{x,1}(q) \\ f_{y,1}(q) \\ f_{z,1}(q) \end{bmatrix} \\
q \begin{bmatrix} 0 \\ 0 \\ 1 \\ 0 \end{bmatrix} q^{-1} &= \begin{bmatrix} 0 \\ f_{x,2}(q) \\ f_{y,2}(q) \\ f_{z,2}(q) \end{bmatrix} \\
q \begin{bmatrix} 0 \\ 0 \\ 0 \\ 1 \end{bmatrix} q^{-1} &= \begin{bmatrix} 0 \\ f_{x,3}(q) \\ f_{y,3}(q) \\ f_{z,3}(q) \end{bmatrix}
\end{aligned} \tag{C.17}
$$

These directional components can be inserted into eq.C.16 to produce an equation that details the contributions of the axial components of $\vec{r}_{Sn}$ to the axial components of $\vec{r}_P$.

$$
\begin{bmatrix} 0 \\ r_{x,P} \\ r_{y,P} \\ r_{z,P} \end{bmatrix} = r_{x,seg} * \begin{bmatrix} 0 \\ f_{x,1}(\vec{q}) \\ f_{y,1}(\vec{q}) \\ f_{z,1}(\vec{q}) \end{bmatrix} + r_{y,seg} * \begin{bmatrix} 0 \\ f_{x,2}(\vec{q}) \\ f_{y,2}(\vec{q}) \\ f_{z,2}(\vec{q}) \end{bmatrix} + r_{z,seg} * \begin{bmatrix} 0 \\ f_{x,3}(\vec{q}) \\ f_{y,3}(\vec{q}) \\ f_{z,3}(\vec{q}) \end{bmatrix} \tag{C.18}
$$

Which can be condensed to

$$
\begin{bmatrix} 0 \\ r_{x,P} \\ r_{y,P} \\ r_{z,P} \end{bmatrix} = \begin{bmatrix} 0 \\ r_{x,Sn} * f_{x,1}(\vec{q}) + r_{y,Sn} * f_{x,2}(\vec{q}) + r_{z,Sn} * f_{x,3}(\vec{q}) \\ r_{x,Sn} * f_{y,1}(\vec{q}) + r_{y,Sn} * f_{y,2}(\vec{q}) + r_{z,Sn} * f_{y,3}(\vec{q}) \\ r_{x,Sn} * f_{z,1}(\vec{q}) + r_{y,Sn} * f_{z,2}(\vec{q}) + r_{z,Sn} * f_{z,3}(\vec{q}) \end{bmatrix} \tag{C.19}
$$

This equation can be inserted into eqs.C.8 and C.9 to merge the components of $\vec{r}_{Sn}$ with the coefficients of the LRM. Inserting eq. C.19 into eq. C.8 creates the following equation

$$
w_{x,n,c} * a_{c,Sn,x} = w_{x,n,c} * -(r_{x,Sn} * f_{x,1}(\vec{q}) + r_{y,Sn} * f_{x,2}(\vec{q}) + r_{z,Sn} * f_{x,3}(\vec{q})) * (\dot{\beta}^2 + \dot{\gamma}^2) \tag{C.20}
$$

Since the segment center of mass coordinates are multiplied directly with the coefficient of the linear model, the coordinates and the coefficients can be merged into three coefficients.

$$
\begin{aligned}
w_{x,n,c} * -r_{x,Sn} &= w_{x,n,c,1} \\
w_{x,n,c} * -r_{y,Sn} &= w_{x,n,c,2} \\
w_{x,n,c} * -r_{z,Sn} &= w_{x,n,c,3}
\end{aligned} \tag{C.21}
$$

These coefficients can be inserted into eq.C.20

$$
\begin{aligned}
w_{x,n,c} * a_{c,seg_n,x} = & w_{x,n,c,1} * f_{x,1}(\vec{q}) * (\dot{\beta}^2 + \dot{\gamma}^2) + \\
& w_{x,n,c,2} * f_{x,2}(\vec{q}) * (\dot{\beta}^2 + \dot{\gamma}^2) + \\
& w_{x,n,c,3} * f_{x,3}(\vec{q}) * (\dot{\beta}^2 + \dot{\gamma}^2)
\end{aligned} \tag{C.22}
$$

Inserting eq.C.19 into eq.C.9 works similarly and produces the following equation

$$\begin{aligned} w_{x,n,t} * a_{t,Sn,x} =& w_{x,n,t,y} * (r_{x,Sn} * f_{y,1}(\vec{q}) + r_{y,Sn} * f_{y,2}(\vec{q}) + r_{z,Sn} * f_{y,3}(\vec{q})) * \ddot{\theta}_z + \\ & w_{x,n,t,z} * (r_{x,Sn} * f_{z,1}(\vec{q}) + r_{y,Sn} * f_{z,2}(\vec{q}) + r_{z,Sn} * f_{z,3}(\vec{q})) * \ddot{\theta}_y \end{aligned} \tag{C.23}$$

Like with eq.C.20, coefficients can again be merged.

$$\begin{aligned} w_{x,n,t,y} * r_{x,Sn} &= w_{x,n,t,1} \\ w_{x,n,t,y} * r_{y,Sn} &= w_{x,n,t,2} \\ w_{x,n,t,y} * r_{z,Sn} &= w_{x,n,t,3} \\ w_{x,n,t,z} * r_{x,Sn} &= w_{x,n,t,4} \\ w_{x,n,t,z} * r_{y,Sn} &= w_{x,n,t,5} \\ w_{x,n,t,z} * r_{z,Sn} &= w_{x,n,t,6} \end{aligned} \tag{C.24}$$

And again these coefficients can be inserted into eq.C.23

$$\begin{aligned} w_{x,n,t} * a_{t,seg_n,x} =& w_{x,n,t,1} * f_{y,1}(\vec{q}) * \ddot{\gamma} + w_{x,n,t,2} * f_{y,2}(\vec{q}) * \ddot{\gamma} + \\ & w_{x,n,t,3} * f_{y,3}(\vec{q})) + * \ddot{\gamma} + w_{x,n,t,4} * f_{z,1}(\vec{q}) * \ddot{\beta} + \\ & w_{x,n,t,5} * f_{z,2}(\vec{q}) * \ddot{\beta} + w_{x,n,t,6} * f_{z,3}(\vec{q}) * \ddot{\beta} \end{aligned} \tag{C.25}$$

Similar equations can be calculated for the y and z components of a_c and a_t. Since $f_{x,n}(\vec{q}) * (\dot{\beta}^2 + \dot{\gamma}^2)$, $f_{y,n}(\vec{q}) * \ddot{\gamma}$ and $f_{z,n}(\vec{q}) * \ddot{\beta}$ are all functions of the inputs from the IMU, they can all be used as basis functions for the linear model. These basis functions can be used to incorporate the information from the angular velocity and angular acceleration into the estimation of aCOM, while allowing the linear model to estimate the location of the segment center of mass itself. Basis functions which can do the same for the y and z axes can be created in an equivalent manner.

For the sake of completeness, each of the basis functions derived from eqs.C.16, C.17, C.22 and C.25 will be listed below. The seperation of axial components that was previosusly performed by writing the components of unit vectors down as functions of $\vec{q}$ is here represented as a vector multiplication. For a_c the derived features are as follows:

$$\begin{aligned} f_{acx,1}(\dot{\beta}, \dot{\gamma}, \vec{q}) &= \begin{bmatrix} 0 & 1 & 0 & 0 \end{bmatrix} * \vec{q} \begin{bmatrix} 0 \\ 1 \\ 0 \\ 0 \end{bmatrix} \vec{q}^{-1} * (\dot{\beta}^2 + \dot{\gamma}^2) \\ f_{acx,2}(\dot{\beta}, \dot{\gamma}, \vec{q}) &= \begin{bmatrix} 0 & 1 & 0 & 0 \end{bmatrix} * \vec{q} \begin{bmatrix} 0 \\ 0 \\ 1 \\ 0 \end{bmatrix} \vec{q}^{-1} * (\dot{\beta}^2 + \dot{\gamma}^2) \\ f_{acx,3}(\dot{\beta}, \dot{\gamma}, \vec{q}) &= \begin{bmatrix} 0 & 1 & 0 & 0 \end{bmatrix} * \vec{q} \begin{bmatrix} 0 \\ 0 \\ 0 \\ 1 \end{bmatrix} \vec{q}^{-1} * (\dot{\beta}^2 + \dot{\gamma}^2) \end{aligned} \tag{C.26}$$

$$
\begin{aligned}
f_{acy,1}(\dot{\alpha},\dot{\gamma},\vec{q}) &= \begin{bmatrix}0 & 0 & 1 & 0\end{bmatrix} * \vec{q} \begin{bmatrix}0\\1\\0\\0\end{bmatrix} \vec{q}^{-1} * (\dot{\alpha}^2 + \dot{\gamma}^2) \\
f_{acy,2}(\dot{\alpha},\dot{\gamma},\vec{q}) &= \begin{bmatrix}0 & 0 & 1 & 0\end{bmatrix} * \vec{q} \begin{bmatrix}0\\0\\1\\0\end{bmatrix} \vec{q}^{-1} * (\dot{\alpha}^2 + \dot{\gamma}^2) \\
f_{acy,3}(\dot{\alpha},\dot{\gamma},\vec{q}) &= \begin{bmatrix}0 & 0 & 1 & 0\end{bmatrix} * \vec{q} \begin{bmatrix}0\\0\\0\\1\end{bmatrix} \vec{q}^{-1} * (\dot{\alpha}^2 + \dot{\gamma}^2)
\end{aligned}
\tag{C.27}
$$

$$
\begin{aligned}
f_{acz,1}(\dot{\beta},\dot{\gamma},\vec{q}) &= \begin{bmatrix}0 & 0 & 0 & 1\end{bmatrix} * \vec{q} \begin{bmatrix}0\\1\\0\\0\end{bmatrix} \vec{q}^{-1} * (\dot{\alpha}^2 + \dot{\beta}^2) \\
f_{acz,2}(\dot{\alpha},\dot{\beta},\vec{q}) &= \begin{bmatrix}0 & 0 & 0 & 1\end{bmatrix} * \vec{q} \begin{bmatrix}0\\0\\1\\0\end{bmatrix} \vec{q}^{-1} * (\dot{\alpha}^2 + \dot{\beta}^2) \\
f_{acz,3}(\dot{\alpha},\dot{\beta},\vec{q}) &= \begin{bmatrix}0 & 0 & 0 & 1\end{bmatrix} * \vec{q} \begin{bmatrix}0\\0\\0\\1\end{bmatrix} \vec{q}^{-1} * (\dot{\alpha}^2 + \dot{\beta}^2)
\end{aligned}
\tag{C.28}
$$

And for a_t the derived features are as follows:

$$
\begin{aligned}
f_{atx,1}(\ddot{\beta},\vec{q}) &= \begin{bmatrix}0 & 0 & 1 & 0\end{bmatrix} * \vec{q} \begin{bmatrix}0\\1\\0\\0\end{bmatrix} \vec{q}^{-1} * \ddot{\beta} \\
f_{atx,2}(\ddot{\gamma},\vec{q}) &= \begin{bmatrix}0 & 0 & 0 & 1\end{bmatrix} * \vec{q} \begin{bmatrix}0\\1\\0\\0\end{bmatrix} \vec{q}^{-1} * \ddot{\gamma} \\
f_{atx,3}(\ddot{\beta},\vec{q}) &= \begin{bmatrix}0 & 0 & 1 & 0\end{bmatrix} * \vec{q} \begin{bmatrix}0\\0\\1\\0\end{bmatrix} \vec{q}^{-1} * \ddot{\beta} \\
f_{atx,4}(\ddot{\gamma},\vec{q}) &= \begin{bmatrix}0 & 0 & 0 & 1\end{bmatrix} * \vec{q} \begin{bmatrix}0\\0\\1\\0\end{bmatrix} \vec{q}^{-1} * \ddot{\gamma} \\
f_{atx,5}(\ddot{\beta},\vec{q}) &= \begin{bmatrix}0 & 0 & 1 & 0\end{bmatrix} * \vec{q} \begin{bmatrix}0\\0\\0\\1\end{bmatrix} \vec{q}^{-1} * \ddot{\beta} \\
f_{atx,6}(\ddot{\gamma},\vec{q}) &= \begin{bmatrix}0 & 0 & 0 & 1\end{bmatrix} * \vec{q} \begin{bmatrix}0\\0\\0\\1\end{bmatrix} \vec{q}^{-1} * \ddot{\gamma}
\end{aligned}
\tag{C.29}
$$

$$
\begin{aligned}
f_{atz,1}(\ddot{\alpha},\vec{q}) &= \begin{bmatrix}0 & 0 & 0 & 1\end{bmatrix} * \vec{q} \begin{bmatrix}0\\1\\0\\0\end{bmatrix} \vec{q}^{-1} * \ddot{\alpha} \\
f_{atz,2}(\ddot{\gamma},\vec{q}) &= \begin{bmatrix}0 & 1 & 0 & 0\end{bmatrix} * \vec{q} \begin{bmatrix}0\\1\\0\\0\end{bmatrix} \vec{q}^{-1} * \ddot{\gamma} \\
f_{atz,3}(\ddot{\alpha},\vec{q}) &= \begin{bmatrix}0 & 0 & 0 & 1\end{bmatrix} * \vec{q} \begin{bmatrix}0\\0\\1\\0\end{bmatrix} \vec{q}^{-1} * \ddot{\alpha} \\
f_{atz,4}(\ddot{\gamma},\vec{q}) &= \begin{bmatrix}0 & 1 & 0 & 0\end{bmatrix} * \vec{q} \begin{bmatrix}0\\0\\1\\0\end{bmatrix} \vec{q}^{-1} * \ddot{\gamma} \\
f_{atz,5}(\ddot{\alpha},\vec{q}) &= \begin{bmatrix}0 & 0 & 0 & 1\end{bmatrix} * \vec{q} \begin{bmatrix}0\\0\\0\\1\end{bmatrix} \vec{q}^{-1} * \ddot{\alpha} \\
f_{atz,6}(\ddot{\gamma},\vec{q}) &= \begin{bmatrix}0 & 1 & 0 & 0\end{bmatrix} * \vec{q} \begin{bmatrix}0\\0\\0\\1\end{bmatrix} \vec{q}^{-1} * \ddot{\gamma}
\end{aligned}
\tag{C.30}
$$

$$
\begin{aligned}
f_{atz,1}(\ddot{\alpha},\vec{q}) &= \begin{bmatrix}0 & 0 & 1 & 0\end{bmatrix} * \vec{q} \begin{bmatrix}0\\1\\0\\0\end{bmatrix} \vec{q}^{-1} * \ddot{\alpha} \\
f_{atz,2}(\ddot{\beta},\vec{q}) &= \begin{bmatrix}0 & 1 & 0 & 0\end{bmatrix} * \vec{q} \begin{bmatrix}0\\1\\0\\0\end{bmatrix} \vec{q}^{-1} * \ddot{\beta} \\
f_{atz,3}(\ddot{\alpha},\vec{q}) &= \begin{bmatrix}0 & 0 & 1 & 0\end{bmatrix} * \vec{q} \begin{bmatrix}0\\0\\1\\0\end{bmatrix} \vec{q}^{-1} * \ddot{\alpha} \\
f_{atz,4}(\ddot{\beta},\vec{q}) &= \begin{bmatrix}0 & 1 & 0 & 0\end{bmatrix} * \vec{q} \begin{bmatrix}0\\0\\1\\0\end{bmatrix} \vec{q}^{-1} * \ddot{\beta} \\
f_{atz,5}(\ddot{\alpha},\vec{q}) &= \begin{bmatrix}0 & 0 & 1 & 0\end{bmatrix} * \vec{q} \begin{bmatrix}0\\0\\0\\1\end{bmatrix} \vec{q}^{-1} * \ddot{\alpha} \\
f_{atz,6}(\ddot{\beta},\vec{q}) &= \begin{bmatrix}0 & 1 & 0 & 0\end{bmatrix} * \vec{q} \begin{bmatrix}0\\0\\0\\1\end{bmatrix} \vec{q}^{-1} * \ddot{\beta}
\end{aligned}
\tag{C.31}
$$

D EXAMPLES OF IMU SELECTION

This section will provide examples of the correlation heatmaps that were examined and the descisions that were made based on them. It will be shown that every segment that was selected to be tested in the models was shown to be potentially useful in at least one heatmap. The full set of correlation heatmaps can be found in a zip file on the gitlab page [§] of this project.

D.1 Same direction correlation heatmaps

This section will show examples of descisions made via heatmaps of the average correlation of segment accelerations in a given direction with the aCOM component of that same direction.

In figure D.1, a correlation heatmap for the X axis component of segment accelerations and the X axis component of aCOM for the natural walking activity is shown. The correlation between aCOM and the segment acceleration of T8 and the pelvs is the highest of the displayed group, and the lower bound of the confidence interval of the correlation between the segment acceleration of the upper legs is also fairly high. As such, these segments were identified as potentially useful based on this heatmap.

In figure D.2, a correlation heatmap for the X axis component of segment accelerations and the X axis component of aCOM for the sit down and stand up activity is shown. The segment accelerations of T8, the head the shoulders and the upper arms have relatively high correlations and lower bounds for the confidence intervals of their correlations. Due to this correlation and confidence interval, these segments were therefore identified as potentially useful based on this heatmap.

In figure D.3, a correlation heatmap for the X axis component of segment accelerations and the X axis component of aCOM for the jump activity is shown. The segment accelerations of T8, the upper legs and the lower legs had relatively high correlations with aCOM and were therefore identified as potentially useful. Although the correlation between the feet and aCOM is relatively low, lower bound of the correlation between the acceleration of the feet and aCOM is relatively high. This was used to also identify the feet segments as potentially useful.

[§] https://gitlab.utwente.nl/bss_development/students/m_donck/movella-sensors

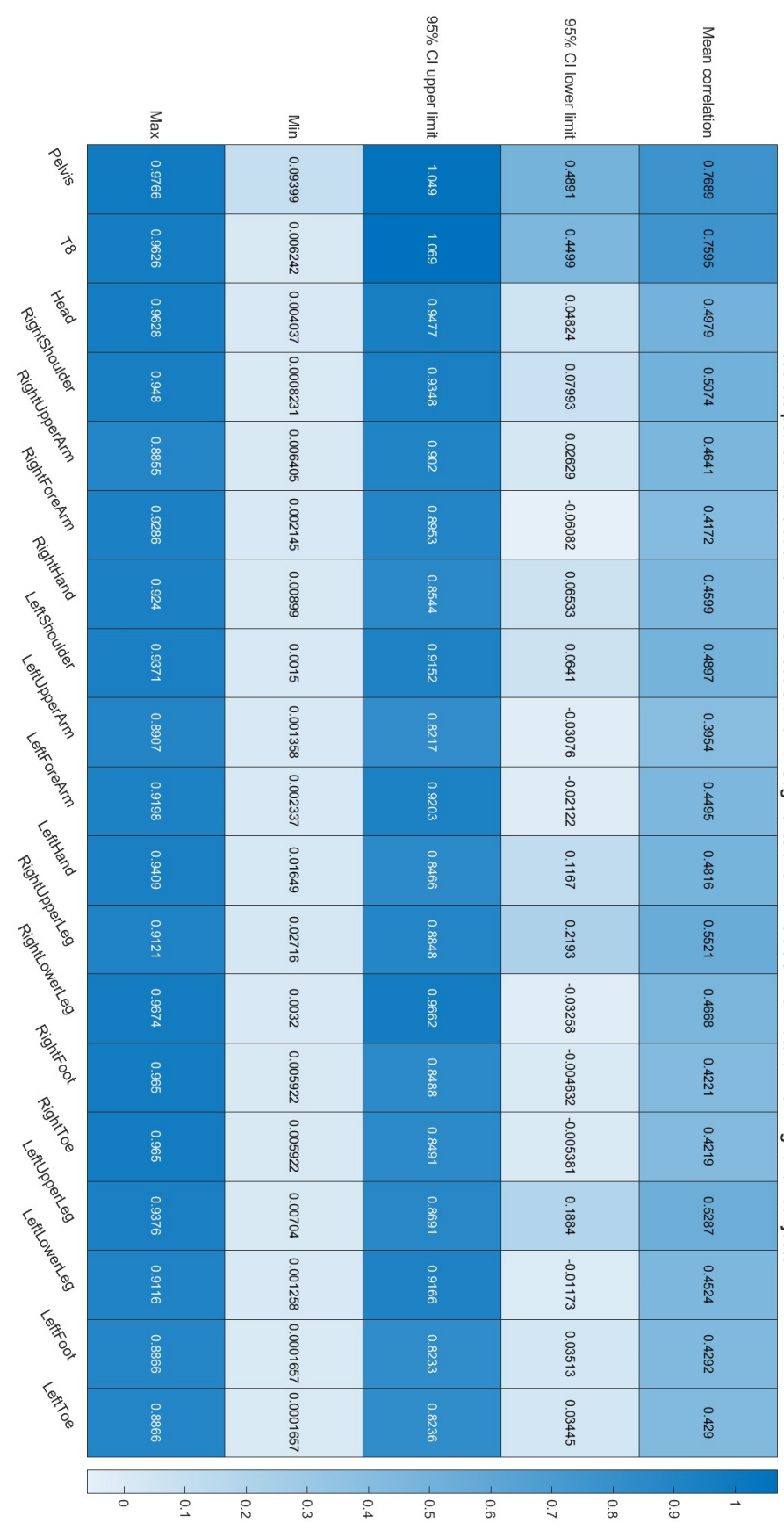

Figure D.1: A correlation heatmap for the X axis component of segment accelerations and the X axis component of aCOM for the natural walking activity.

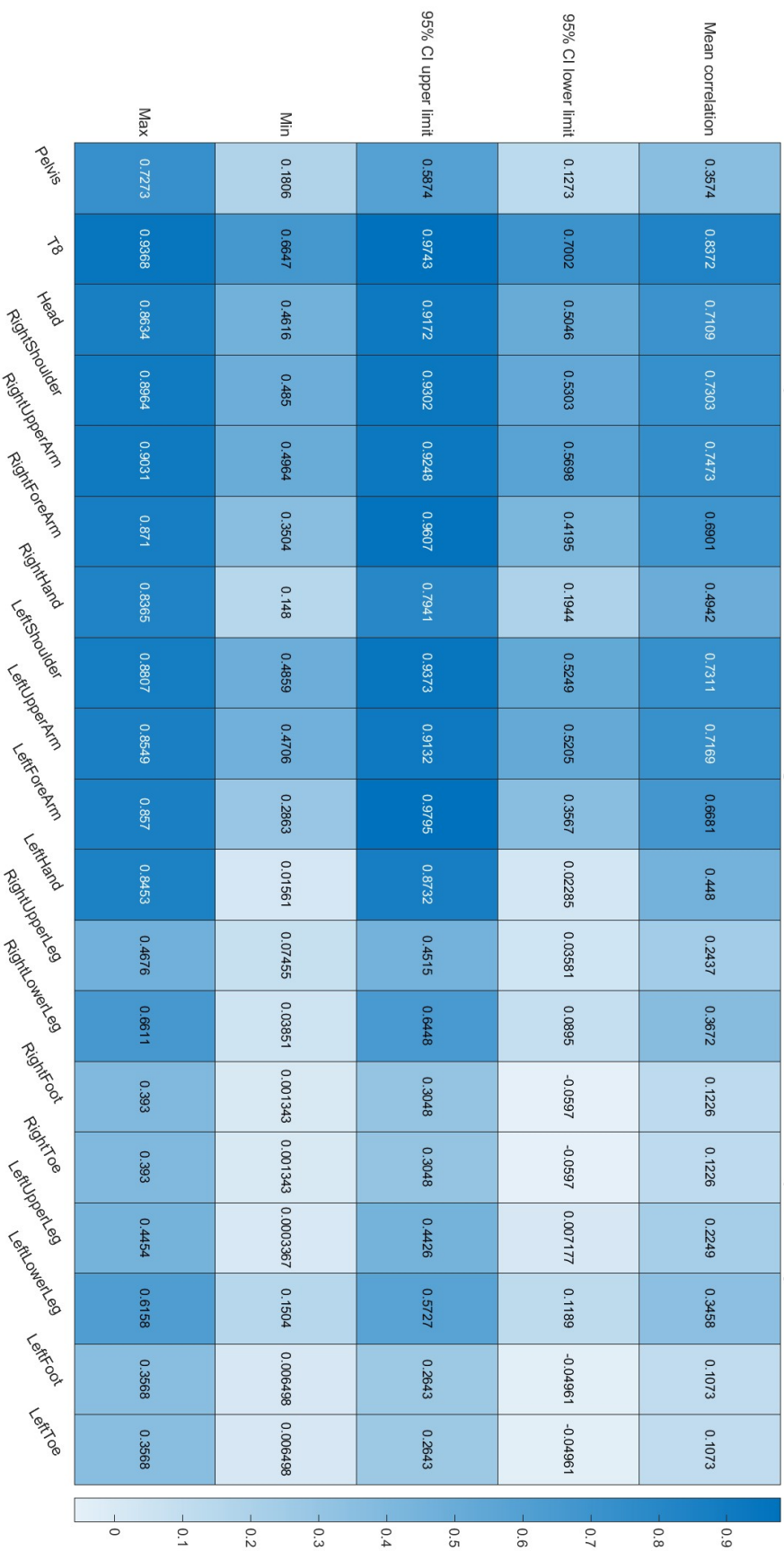

Figure D.2: A correlation heatmap for the X axis component of segment accelerations and the X axis component of aCOM for the sit down and stand up activity.

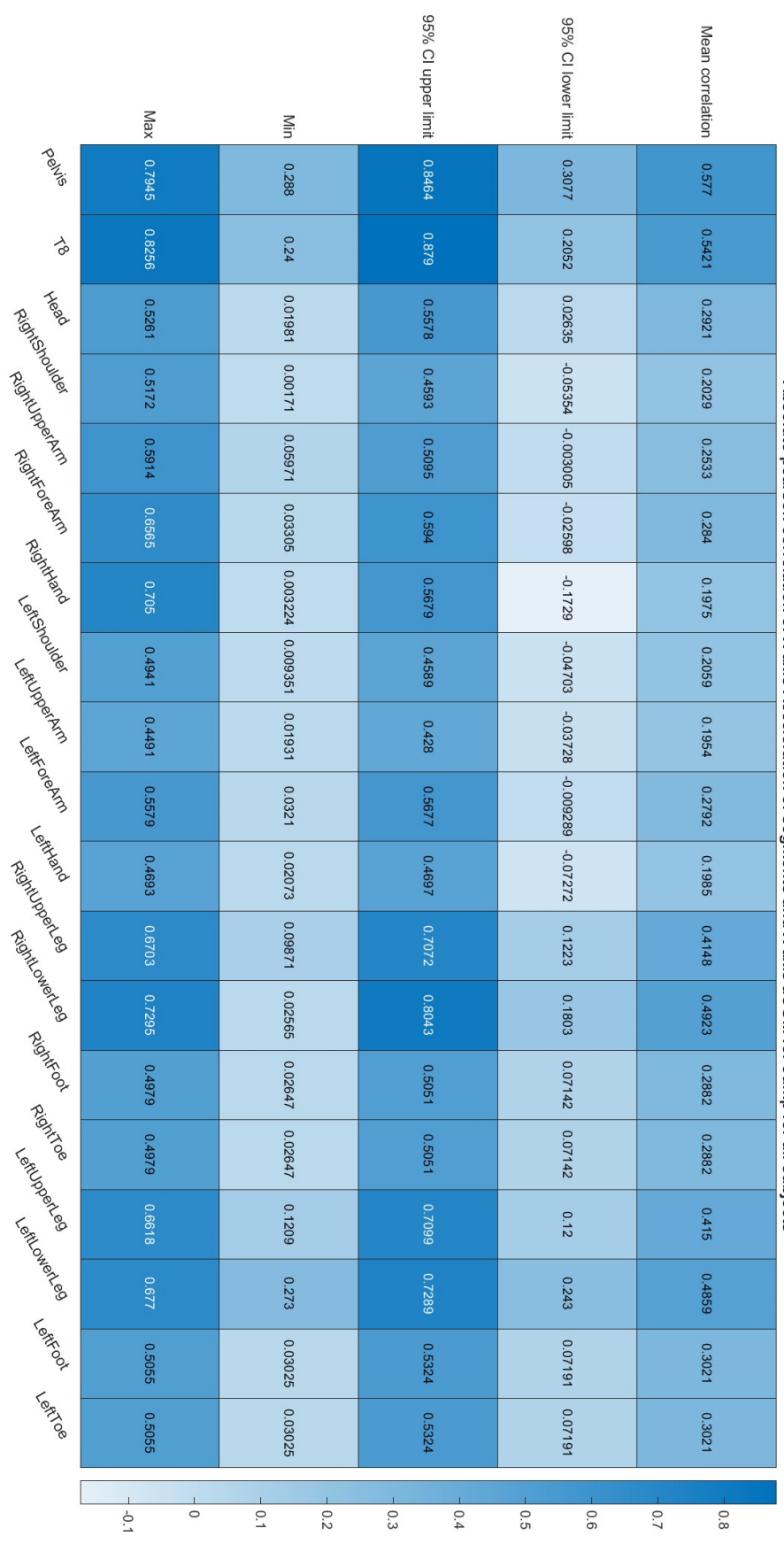

Figure D.3: A correlation heatmap for the X axis component of segment accelerations and the X axis component of aCOM for the jump activity.

D.2 Cross axis correlation heatmaps

This section will show an example of a descision made via the heatmaps of the average correlation of segment accelerations in a given direction with the aCOM component of a different direction. While other cases of noticable cross axis correlation exist, the example provided here is the only case where cross axis correlation was used to select a segment for use in the linear regression models.

In figure D.4, a correlation heatmap for the X axis component of segment accelerations and the Z axis component of aCOM for the stairs walking down activity is shown. The correlatations for the acceleration of the hands segments and the upper bounds of their confidence interval are slightly higher than that of the other segments, and this was used to identify the hands as potentially useful segments.

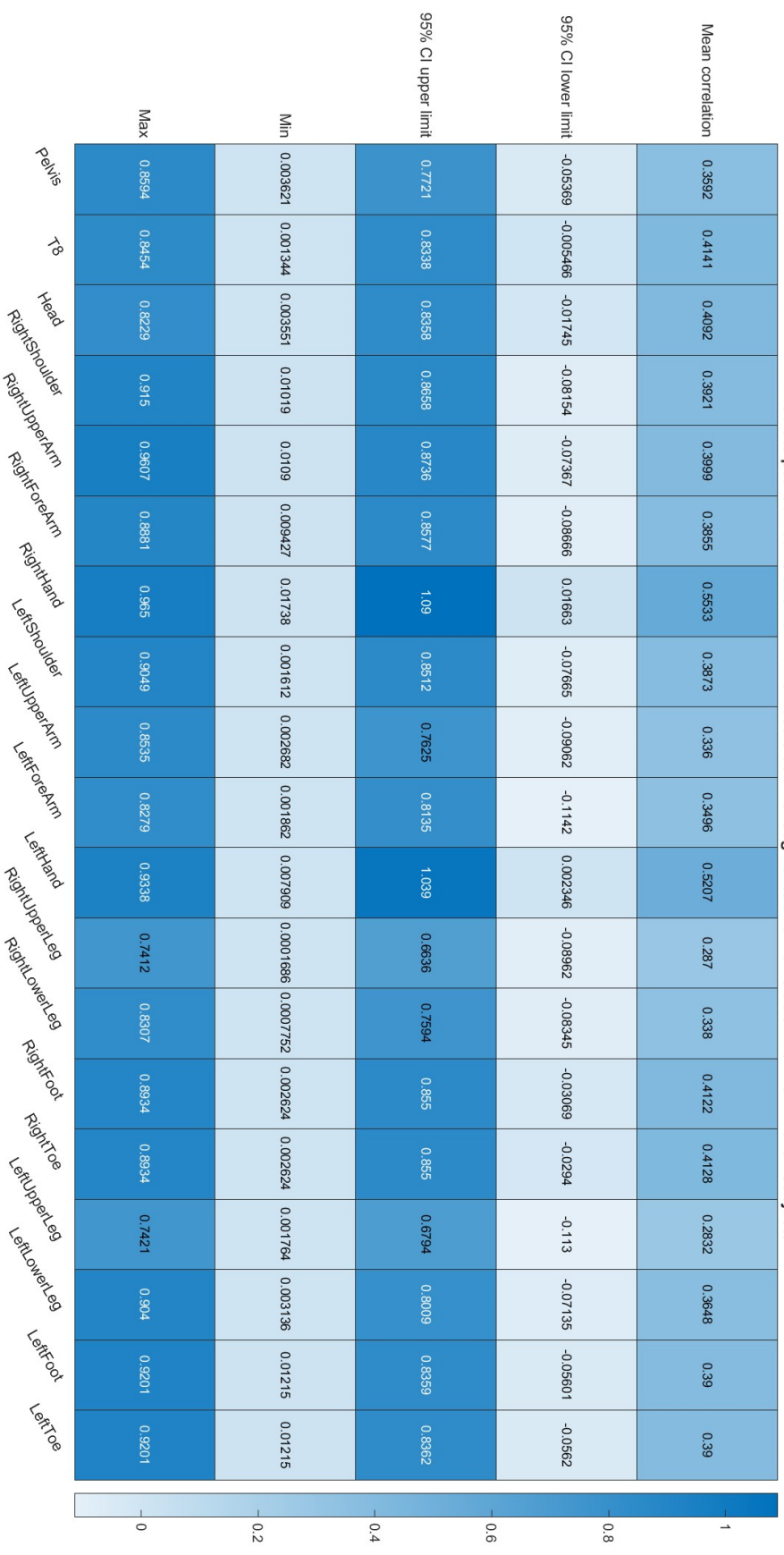

Figure D.4: A correlation heatmap for the Z axis component of segment accelerations and the X axis component of aCOM for the stairs walking down activity.

D.3 Rotation based variables heatmap

This section will show examples of a descision made via the heatmaps of the average correlation of the gyroscope based variables calculated from the rotation of a certain segment corresponding to a given direction with the aCOM component of the same direction.

In figures D.5, D.6 ,D.7 and D.8, heatmaps of the average correlation of the rotation based variables corresponding to acceleration along the X axis of the pelvis, shoulder, lower leg and upper leg with the X axis component aCOM for the sit down and stand up, natural walking, stairs walking down and terrain activities are shown. Each of these heatmaps shows at least one lower bound of of the confidence interval of the average correlation which is significantly higher than 0. Based on this the shoulder, lower leg and upper leg have been selected as potentially useful segments and a model using both the rotation based variables and the accelerations of only the pelvis to estimate aCOM was tested seperately.

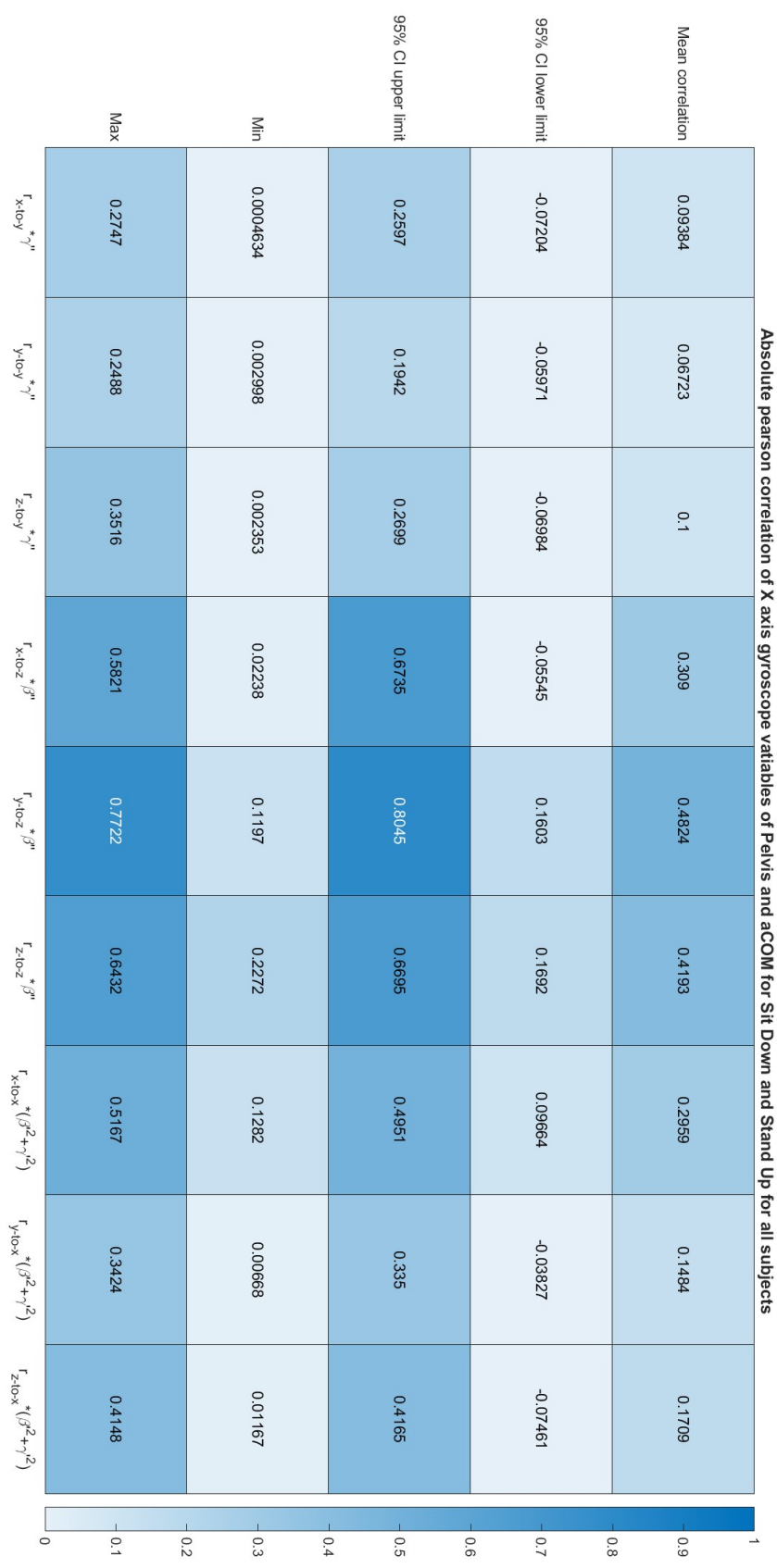

Figure D.5: A correlation heatmap of the average correlation of the rotation based variables corresponding to acceleration along the X axis of the pelvis with the X axis component aCOM for the sit down and stand up activity.

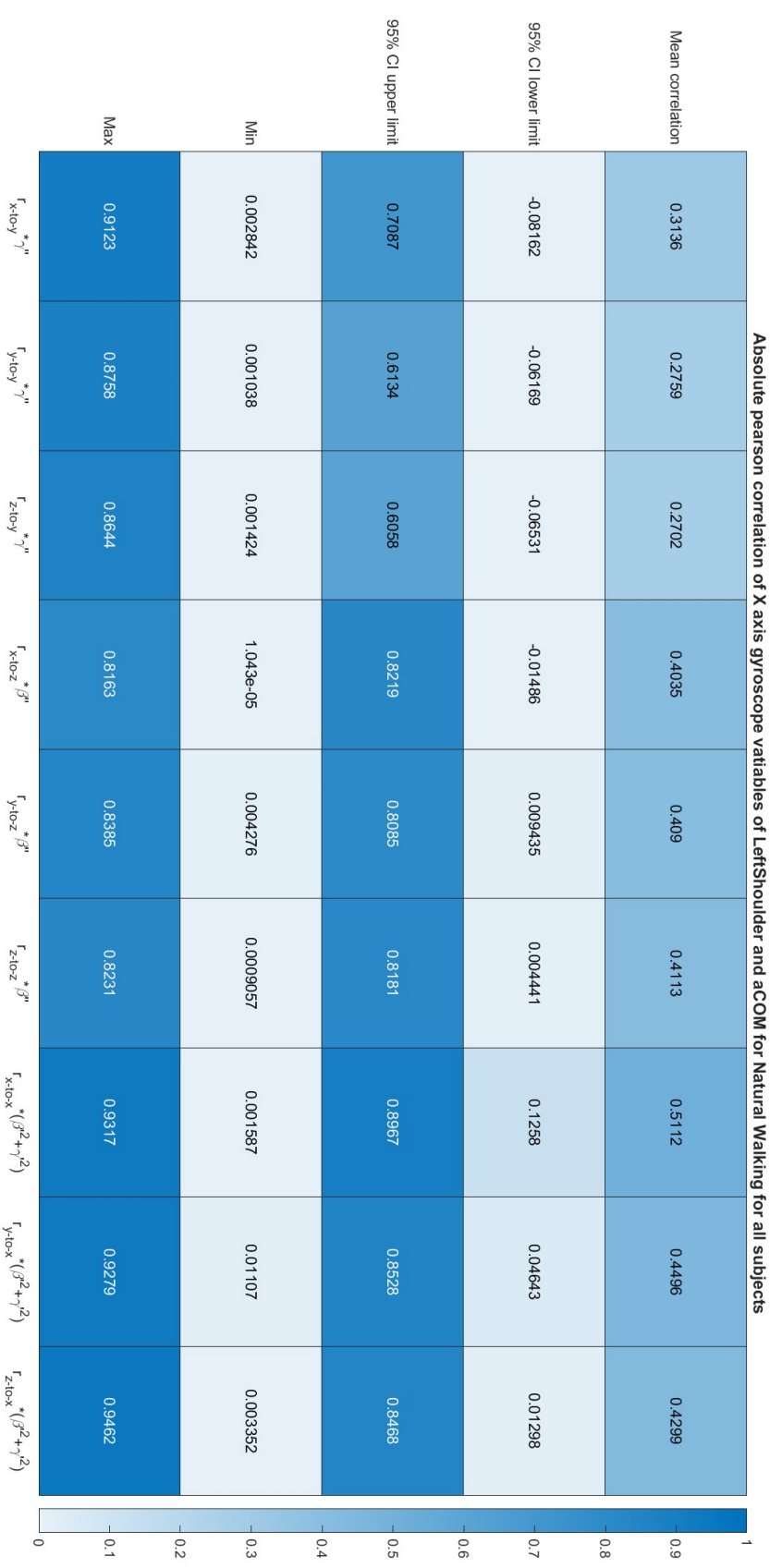

Figure D.6: A correlation heatmap of the average correlation of the rotation based variables corresponding to acceleration along the X axis of the left shoulder with the X axis component aCOM for the natural walking activity.

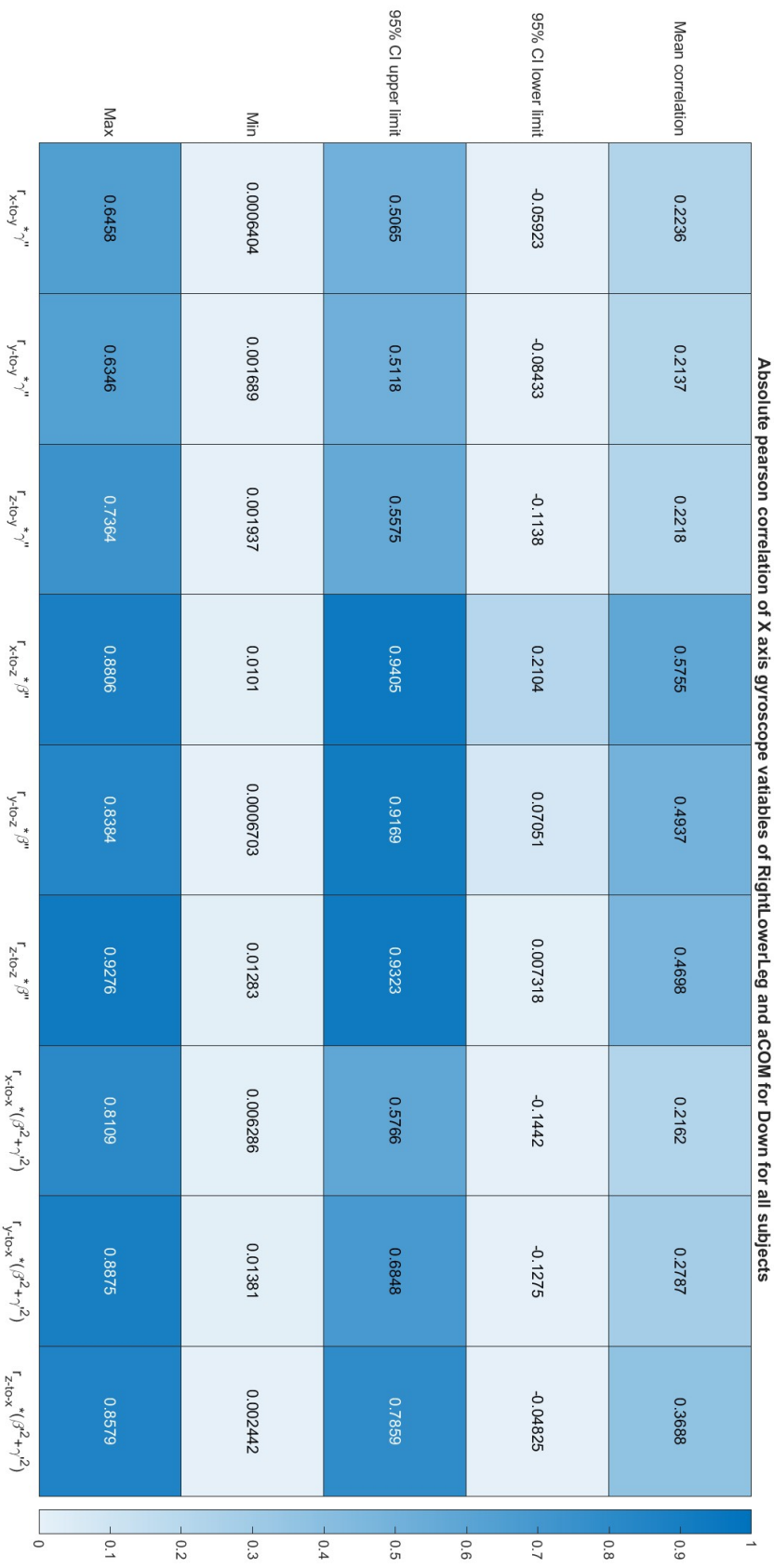

Figure D.7: A correlation heatmap of the average correlation of the rotation based variables corresponding to acceleration along the X axis of the right lower leg with the X axis component aCOM for the stairs walking down activity.

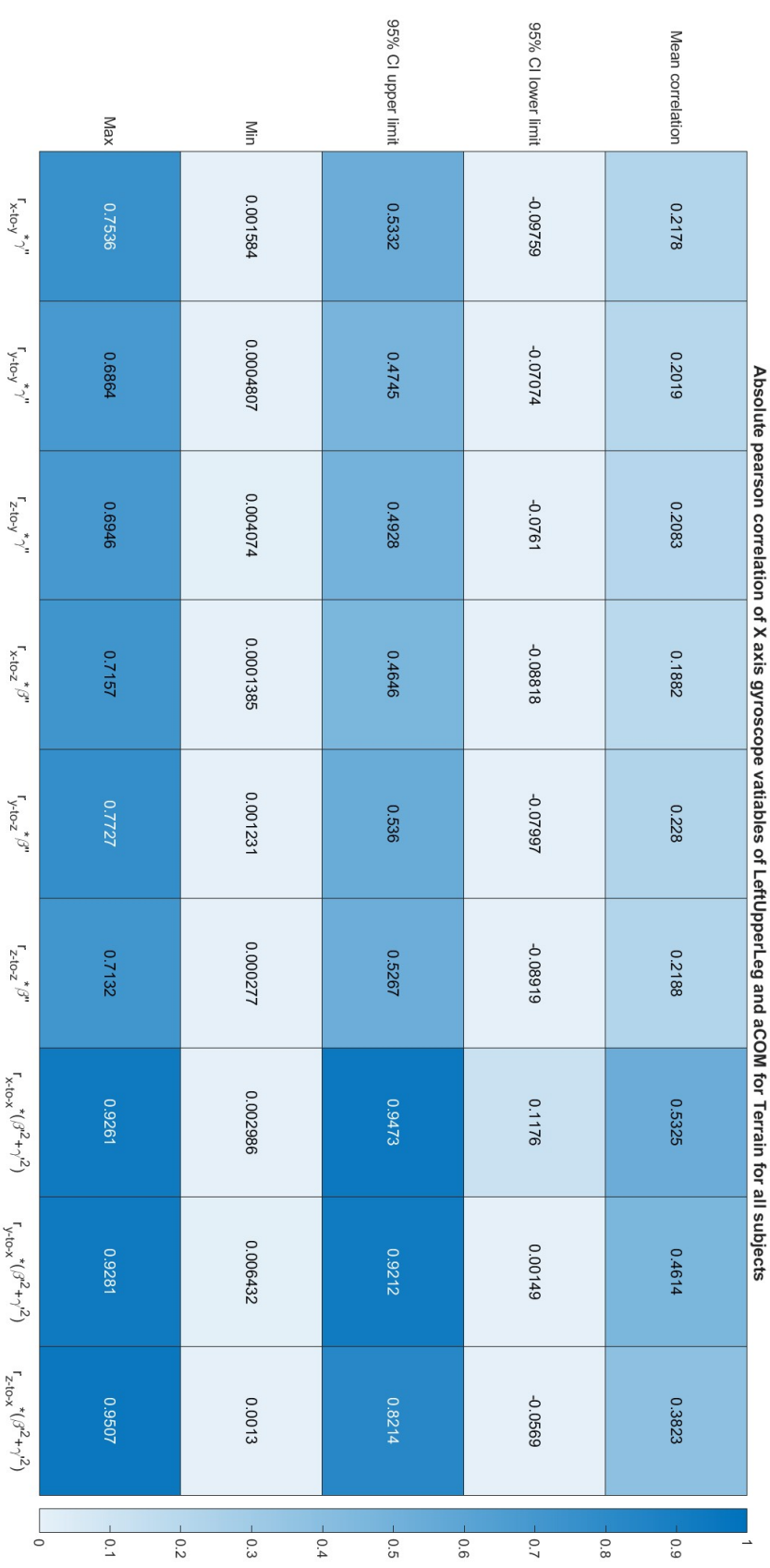

Figure D.8: A correlation heatmap of the average correlation of the rotation based variables corresponding to acceleration along the X axis of the left upper leg with the X axis component aCOM for the terrain walking activity.

E QQ PLOT RESULTS

This appendix will briefly discuss the main observation found in the qq plots.

E.0.1 qq plots

The vast majority of the qq plots that were created showed a significant deviation from a linear relation at the tails, indicating that the distributions of the model and the reference values differ from each other. These deviations were present for both the all direction acceleration model and the gyroscope based model. These distributions did not change drastically in shape for the gyroscope based model compared to the all direction acceleration model using the same segments, even when the performance of the model improved. An example of this can be seen in figure E.1.

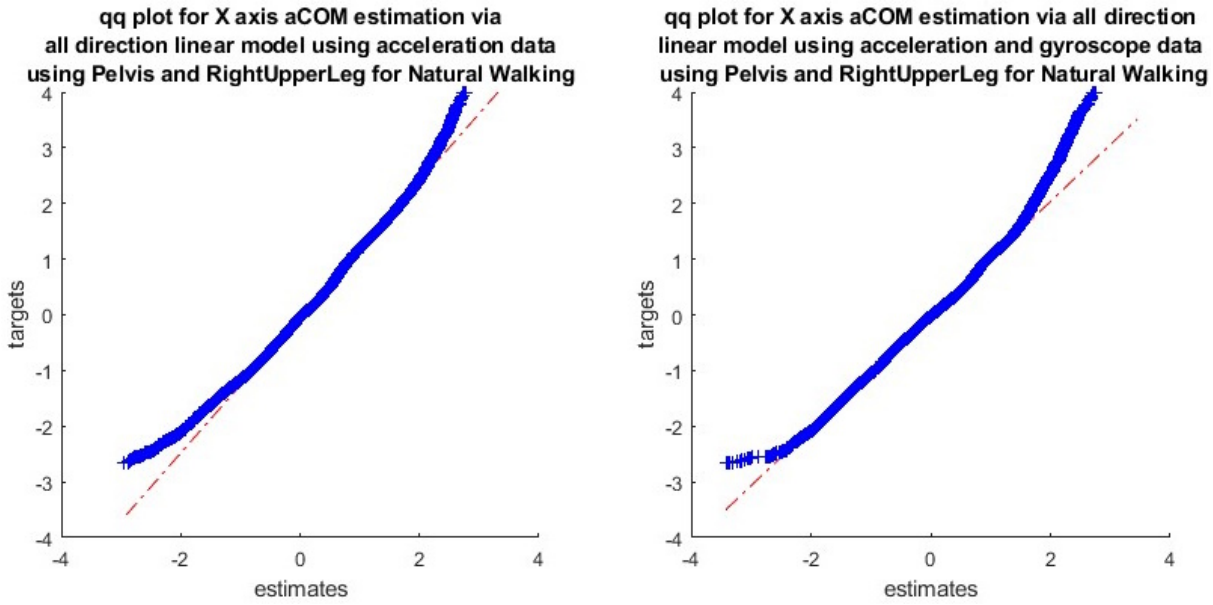

Figure E.1: qq plots corresponding to models for estimating aCOM in the natural walking activity using the right upper leg, with and without using the gyroscope variables..

F INVESTIGATION OF ABNORMAL DATA FROM SUBJECT 5

This appendx details the investigation of abnormal data found in the recordings corresponding to subject. This appendix will first explain how the abnormalities were found, the examinations that were performed on these initially found abnormalities. It will then detail how the determination was made that they were present outside of just the natural walking activity and finally why the decision was made to exclude the data from subject 5 due to these abnormalities.

F.1 Discovery

The abnormalities were discovered during the examination of the initial Bland Altman plots. A streak-like shape was detected in the Bland Altman plots for the models for the natural walking activity. Examining which samples belonged to which subject showed that the streak-like shape was formed by data from subject 5. Two instances of Bland Altman plots displaying this streak with data from subject 5 highlighted can be seen in figures F.1 and F.2.

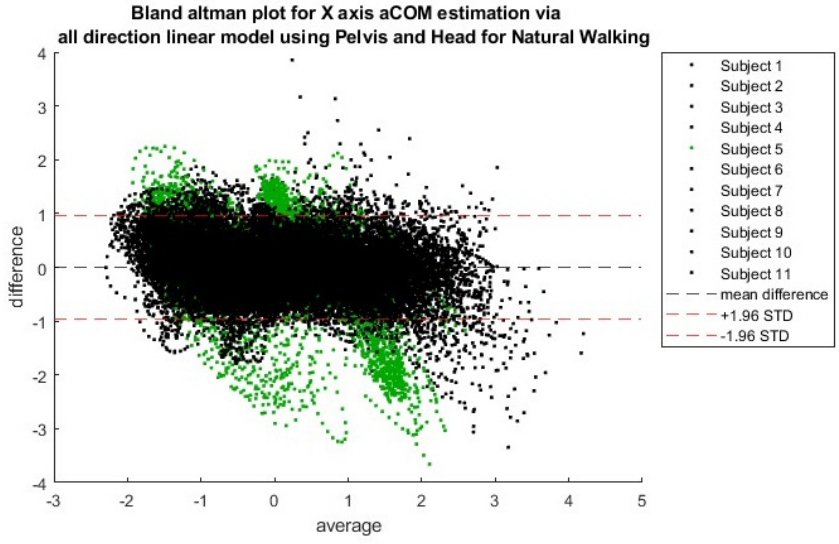

Figure F.1: An example of 'streaks' in the Bland Altman plots for models estimating aCOM in natural walking using the head segment, with the data from subject 5 highlighted.

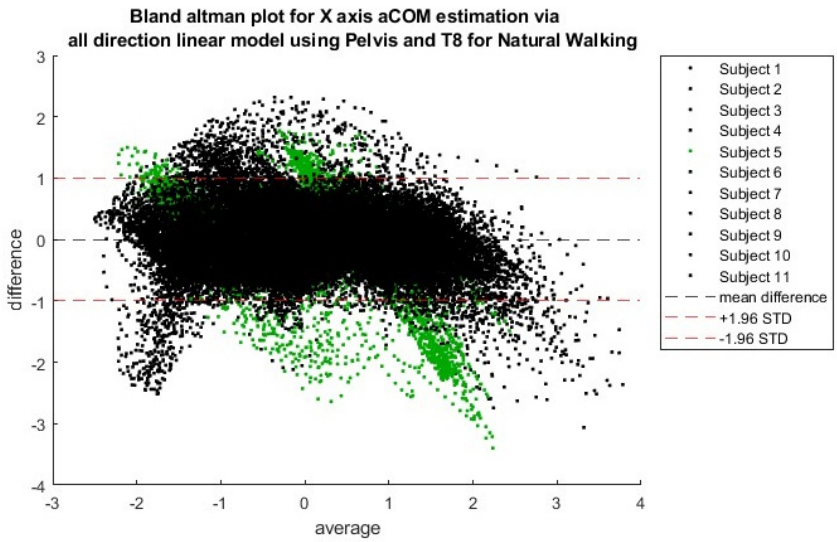

Figure F.2: An example of 'streaks' in the Bland Altman plots for models estimating aCOM in natural walking using the sternum segment, with the data from subject 5 highlighted.

As it was shown that these 'streaks' came from data from subject 5, it was further investigated whether the 'streaks' were formed from all data from subject 5 or a single recording. It was found that all recordings of subject 5 contributed to this streak, as can be seen in figures F.3 and F.4.

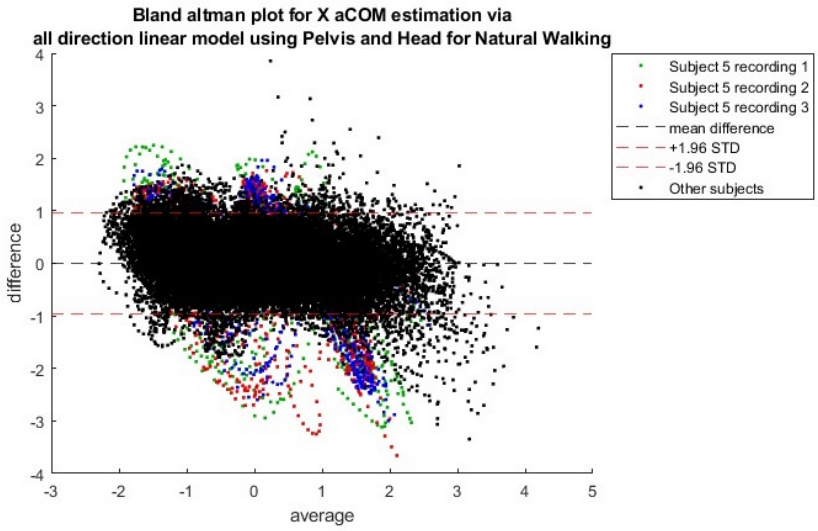

Figure F.3: An example of 'streaks' in the Bland Altman plots for models estimating aCOM in natural walking using the head segment, with individual subject 5 recordings in seperate colors.

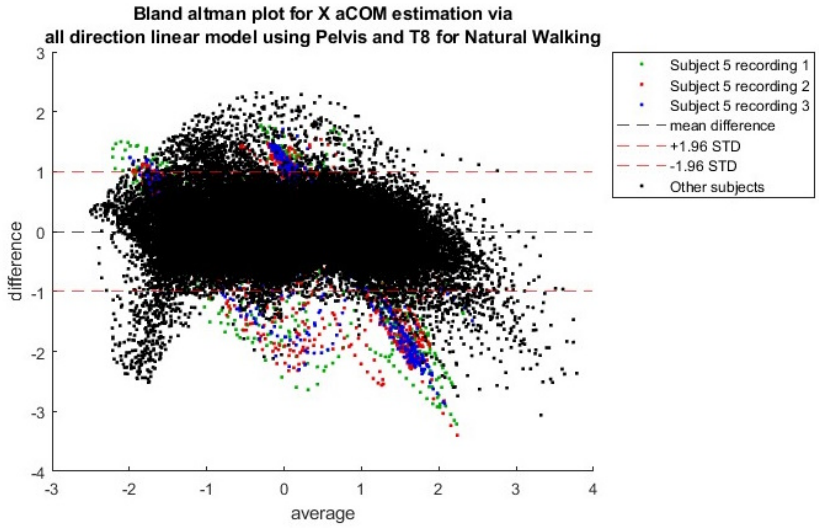

Figure F.4: An example of 'streaks' in the Bland Altman plots for models estimating aCOM in natural walking using the sternum segment, with the individual recordings subject 5 given seperate colors.

To further investigate the nature of these odd shapes within the Bland Altman plot, time series plots from subject 5 for natural walking were compared to time series plots from other subjects. It was found that the natural walking activity recordings for subject 5 contained oscillations in the anterioposterior acceleration of the pelvis that were not present in the recordings of the other subjects, which can be seen in figure F.5. To examine whether these oscillations persisted, time series from the slalom activity, which was recorded after the natural walking activity, were examined. These did not contain this oscillation, as can be seen in figure F.6.

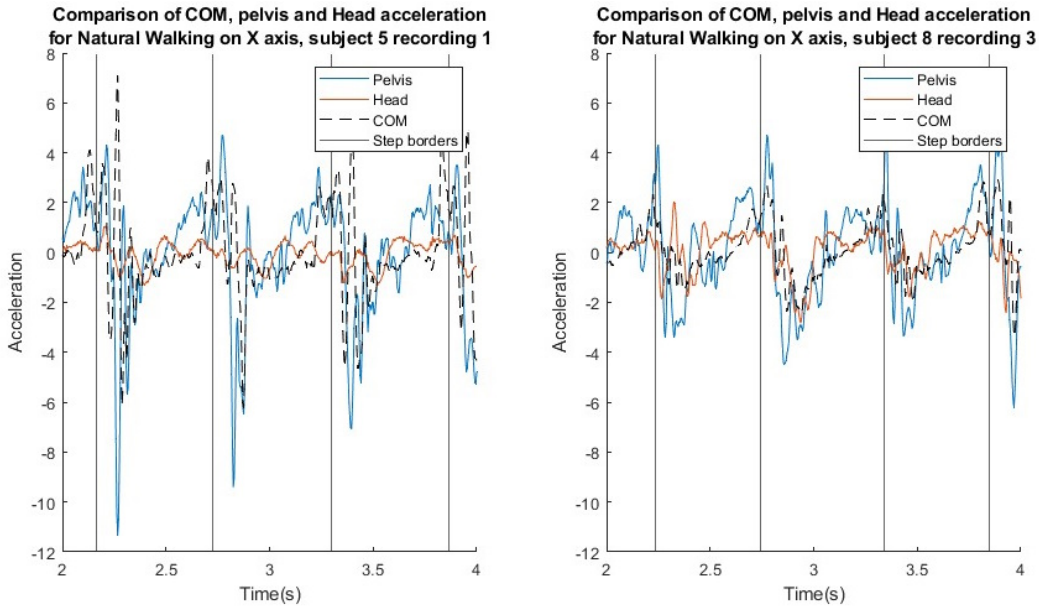

Figure F.5: A section of a time series plot of the anterioposterior acceleration of the head, pelvis and aCOM for subjects 5 and 8 for the natural walking activity.

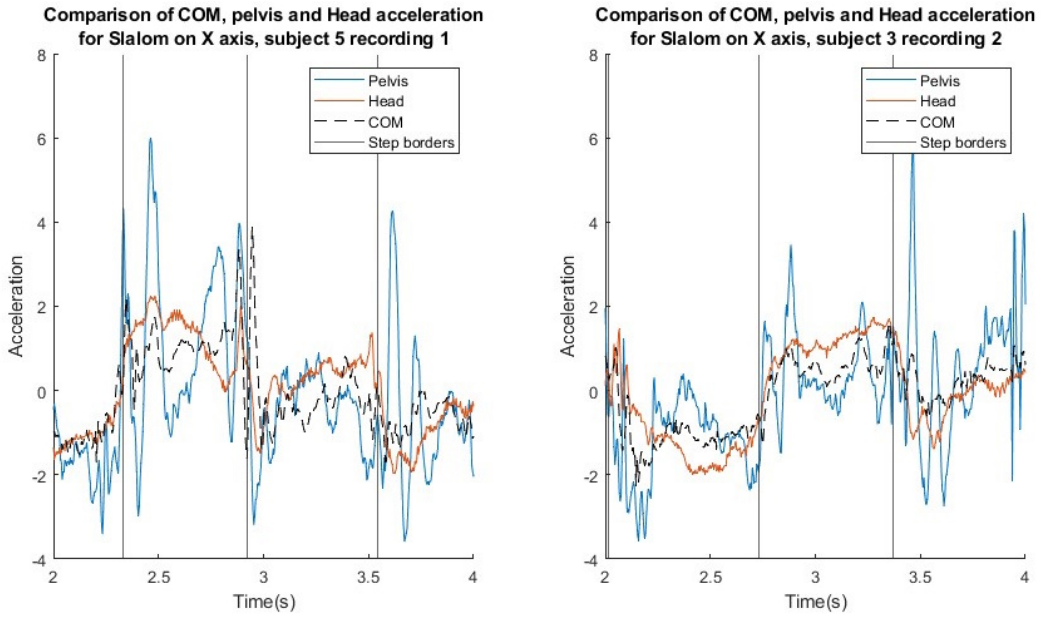

Figure F.6: A section of a time series plot of the anterioposterior acceleration of the head, pelvis and aCOM for subjects 5 and 3 for the slalom activity.

F.2 Further investigation of the abnormalities

The abnormalities were further examined by examining the average coefficients of the model trained with and without the data of subject 5, as shown in figure F.7. The coefficients of models trained on data from only one subject were also examined, and it was found that the coefficients from subject 5 in natural were outliers in certain cases, producing very low coefficients for acceleration from the pelvis segment in comparison to other subjects, as can be seen in figure F.8. The difference in coefficients between subject 5 and the other subjects was not high for models using the shoulder or head segments. Removing subject 5 also produced a large difference in performance in the anterioposterior direction for the natural walking activity. A heatmap of the differences in the trial average of r^2 that the addition of subject 5 makes is shown in figure F.9.

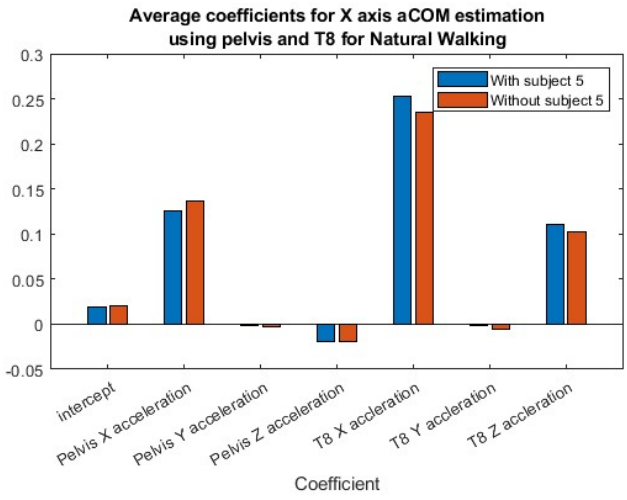

Figure F.7: The average coefficients of the models that estimate aCOM using sternum acceleration, with and without subject 5 in the training set.

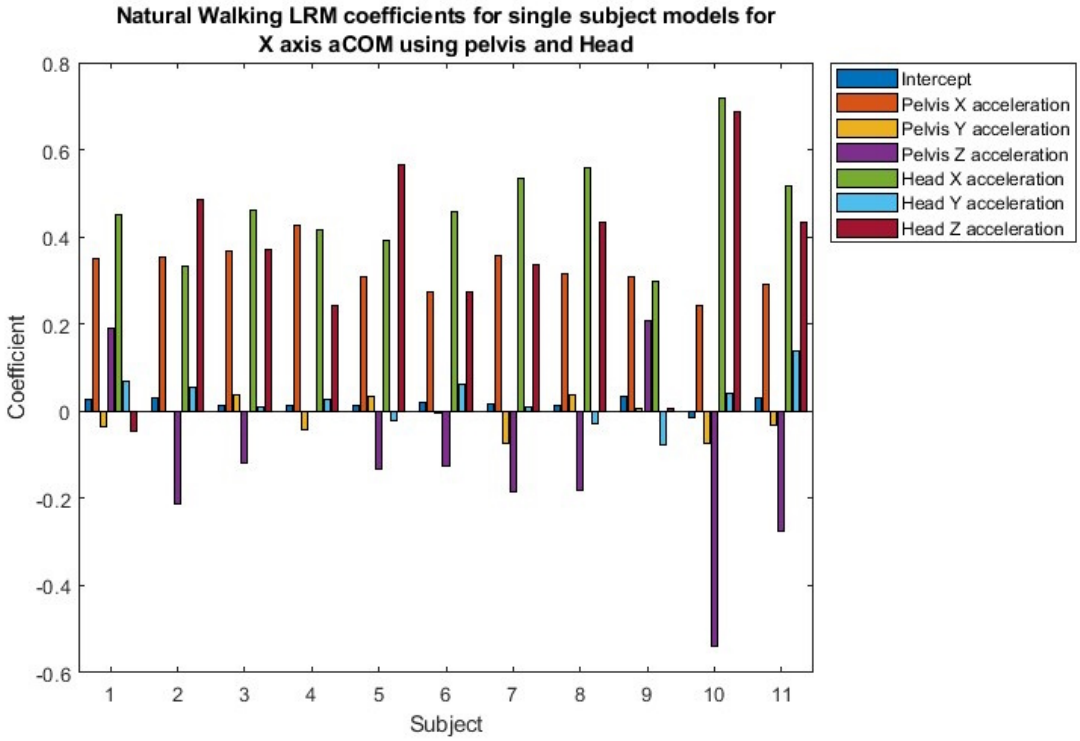

Figure F.8: A bar graph of the coefficients for subject specific models for the beam walking activity using the lower legs and pelvis.

F.3 Discovery of abnormalities outside the natural walking activity

Although subject 5 does not seem to be an outlier in the slalom activity, it did present itself as an outlier when examining the coefficients on models trained on individual subjects for the beam walk activity, in the case of models using three segments. This can be seen in figure F.10. Subject 5 does not appear to be an outlier when examining two segment models for the beam activity, however. It was suspected that subject 5 may have been more or less trained in walking across a narrow surface than the other subjects, and that this created the difference in coefficients for the single subject models. This was examined by examining the variances of the mediolateral aCOM of each of the subjects. A subject who keeps their COM steady is more trained and may produce different motion from the other subjects. As is shown in figure F.11, subject 5 does have more variance in aCOM than most other subjects, but the same is the case for subject 8 whose recordings do not lead to linear regression models with deviating coefficients. As such, it appears that subject 5 is an outlier in more activities than just natural walking. Investigating coefficients of subject specific models for the estimation of mediolateral aCOM in the terrain walk activity also showed that the recordings from subject 5 produced an abnormally low coefficient for the mediolateral pelvis acceleration for the majority of segments. An example of this can be seen in figure F.12. Since the beam walk activity was performed after the slalom activity, there does not appear to be a clearly defined point in time where the abnormalities stop.

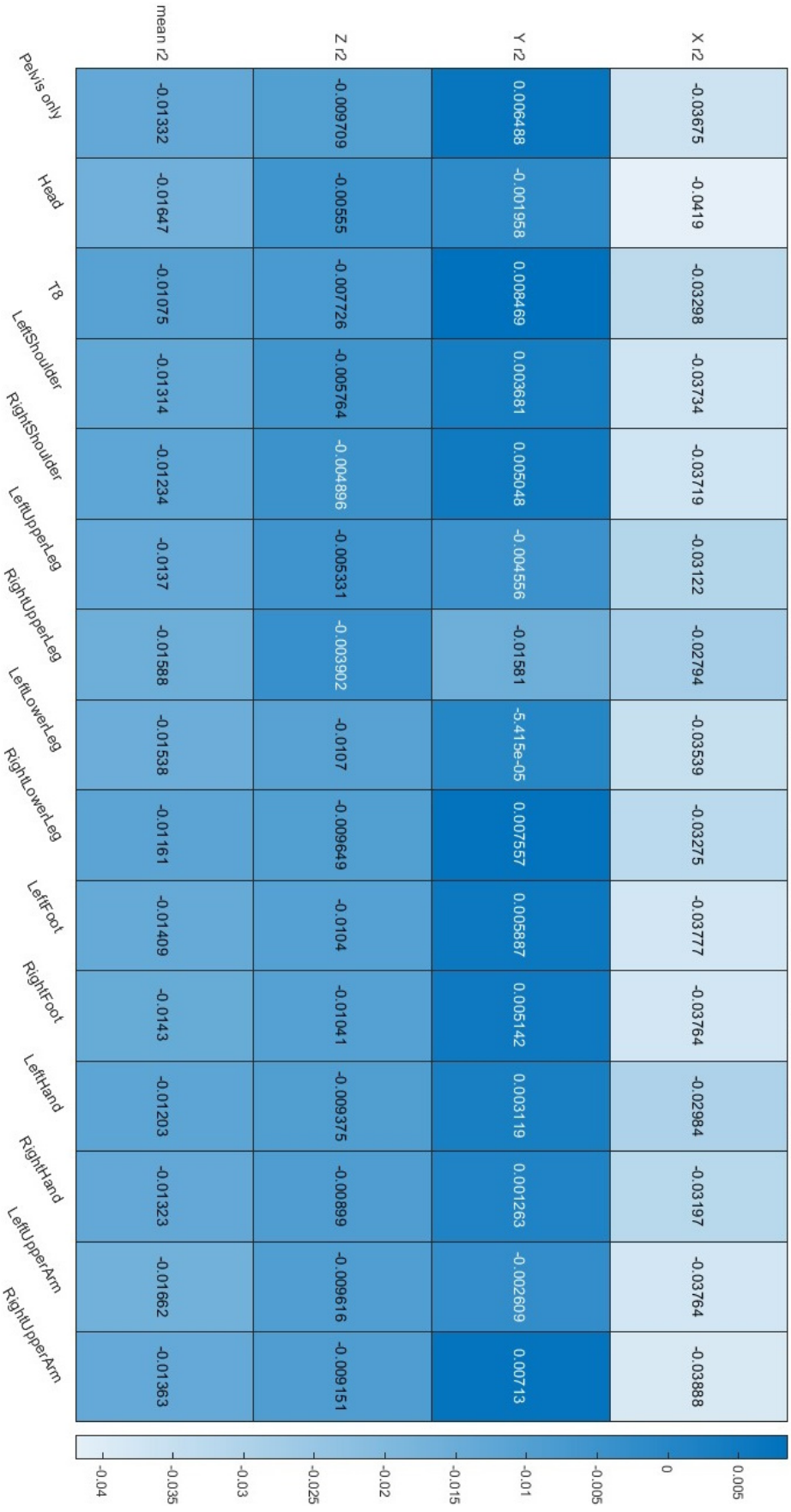

Figure F.9: The difference in r^2 between the tests sets for models with and without subject 5 in the dataset. A negative value means that r^2 is lower when subject 5 is included in the dataset.

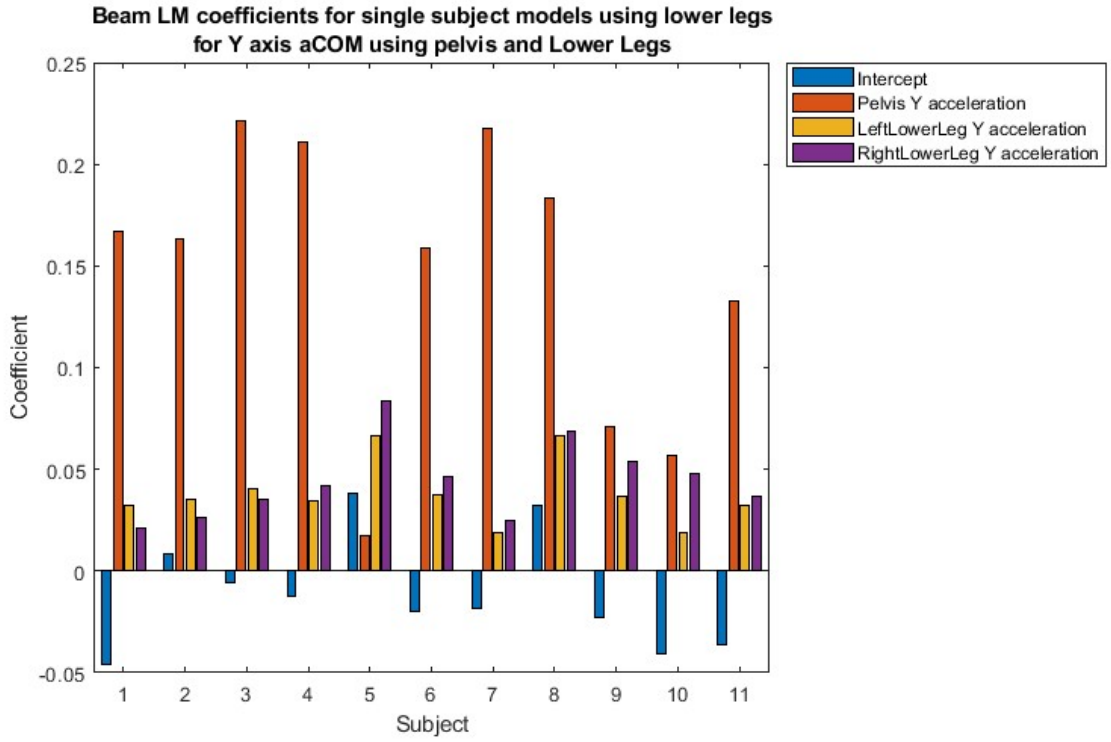

Figure F.10: A bar graph of the coefficients for subject specific models estimating mediolateral aCOM for the beam walking activity using the lower legs and pelvis.

F.4 Conclusion

While data from subject 5 was not found to be an outlier for all models, subject 5 is abnormal in multiple activities within the protocol and there is no clear chronological cutoff point for these abnormalities. The abnormalities also pertain to the pelvis acceleration, which is used in all models. Furthermore, the oscillations present in the pelvis acceleration for the natural walking activity do not seem to have a basis in the actual motion of the subject and are likely due to some sort of measurement error. As there is no clear cutoff point for where the abnormalities in the data from subject 5 appear, this data may is also exhibit abnormal behavior deviant in activities in between in a way that is not immediately visible from the plots. In order to avoid using faulty data unknowingly, the decision was made to exclude all recordings of subject 5 from the data used in the training and testing sets.

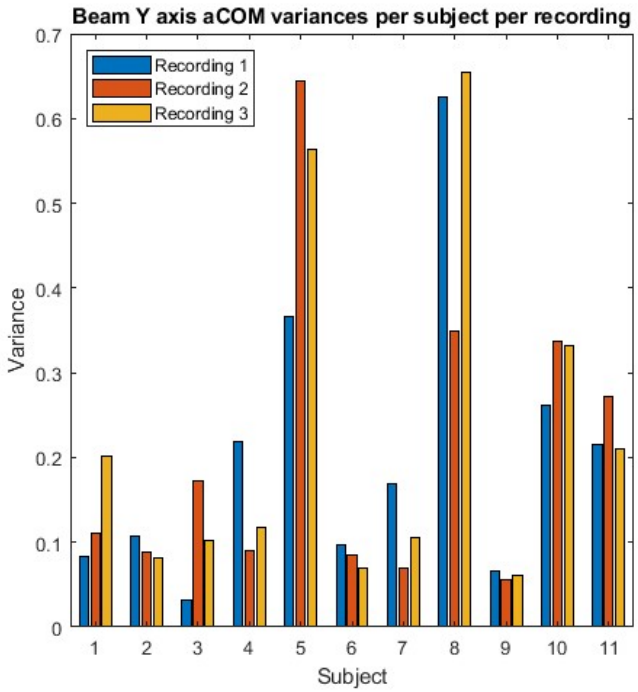

Figure F.11: A bar graph of the variances of the mediolateral aCOM of the subjects.

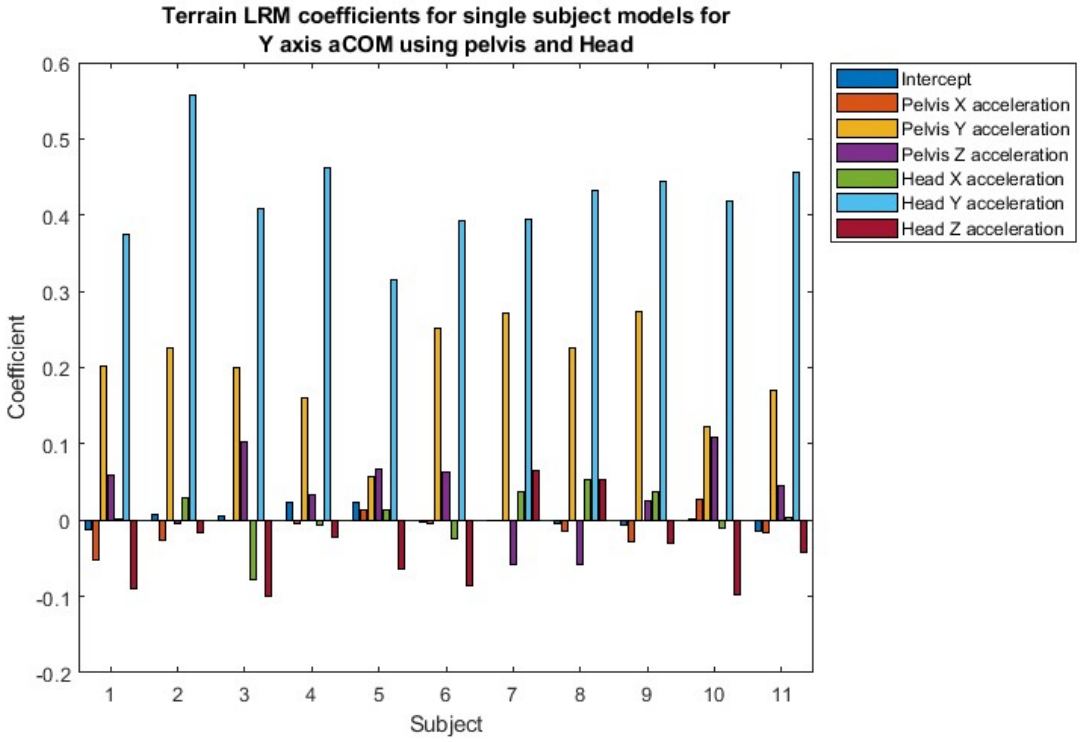

Figure F.12: A bar graph of the coefficients for subject specific models for the beam walking activity using the lower legs and pelvis.

G CONCEPT FOR A PHYSICS INFORMED MACHINE LEARNING MODEL

This unused model concept was meant to apply physics informed machine learning of a sort to the problem of estimating aCOM.

An introduction to physics informed machine learning

Physics informed machine learning(PIML) is a method that utilizes machine learning to simulate a system that is known to obey a certain equation such as a conservation law. This law is encoded as an additional loss term in the loss function of a machine learning algorithm, which can be seen as an addition to 2.2

$$E = \sqrt{(\bar{u} - u)^2} + f_c(\bar{u}) \tag{G.1}$$

Here f_c is a function that encodes the equation that the system should comform to. Encoding the law in this way causes the machine learning algorithm to produce results that (approximately) follow it.

PIML has two ways to be used, depending on whether the equation is known exactly or only the form of the equation is known. If the entire equation is known, a model can be created that simulates the system from an intial state. Used in this way, PIML can sometimes be a more efficient way to simulate a system than via numerical methods. If only the form of the equation is known, PIML can aditionally fit constants to the system. Often, training a model with an additional loss term like this will generalize better than model that is merely trained to best fit the training data.

The model

We would like to use PIML to estimate aCOM from minimal IMU data, but there is no exact equivalent to a conservation law when determining aCOM from IMU data. The one set relation between aCOM and IMU data is the equation for determining aCOM from segment movements. Using this equation requires full knowledge of the whole body, at which point machine learning is a redundant addition to the model. This can also be a way to simulate a system, or merely to estimate the constants in the equation.

To still use physics informed machine learning, we can go from the IMU data to a higher dimensional space where an additional loss term could be applied: An RBM of the whole body. The motion of the RBM can be transformed into aCOM data by using eq.2.12. The use of machine learning in this case is to determine the motion of the model from IMU data. Using a model that is trained only to minimize the error with the training data need not result in human-like motion at all, as it would be possible to keep the model in a static pose and apply a linear acceleration to the root segment to produce aCOM. To produce more human-like motion in the intermediate step, a constraint can be imposed to have the model comform to the input data. This constraint would work as follows: Every segment with an IMU that is used as input is simulated by the RBM. The difference between the angular velocity in these simulated segments and the angular velocity measured by the IMUs is used as an additional loss term when training the model. The difference between the linear acceleration in the simulated segment and the linear acceleration measured by the IMU is also used as a loss term.

By forcing the model to comform to the input motion in this way, the model may generalize better than normal machine learning methods.

Implementation considerations

There are several considerations in implementing a model like this.

Control

The first consideration in implementing this model is the actual means of controlling the RBM. The human body is normally controlled by muscle forces. The model could output muscle forces which would be integrated to simulate motion. When using muscles, the metabolic cost of muscle activation could be considered as an additional loss function to promote more realistic motion. However, when simulating control muscles, multiple ways of generating the same motion arise. These aditional ways of generating the same motion would add complexity to an already complicated model. A method using integration without this redundancy would be to use joint torques and integrate these. Since segment masses are constant, this would be equivalent to using the joint angle acceleration as output.

A model using joint torques would not be fully defined, as an RBM also has linear degrees of freedom in the root segment which are not accounted for by torques. To account for these, the linear acceleration in the root segment can be used as an additional output. Since the position and velocity of the root segment have no bearing on the aCOM of the RBM, this linear acceleration does not need to be integrated and only needs to be determined in each frame.

Creating a model without integration can also be considered. This would be a model that is free to determine the joint angles and joint angle velocities in addition to joint angular acceleration and root segment linear acceleration. The benefit of such a model would be that its output for one frame would not be able to negatively affect the outputs for future frames. However, the model would no longer truly describe motion, as the orientation, angular velocity and angular acceleration of the segmenets would be independent of each other. Aditionally, this would produce a model with far more output variables, making it (more) overdefined. As such, it would be best to control the model using angular acceleration outputs.

The usage of integration with respect to joint angles necessarily requires the model to have initial states for the angles and angular velocities of the RBM joints. These would need to be determined via a calibration of some sort, which is outside the scope of this concept.

Input

As mentioned, the machine learning model has the IMU linear acceleration and angular velocity data as input, and the model outputs joint angular accelerations for the purpose of determining aCOM. Since the angular velocity and orientation of the segments determine the relation between joint angular accelerations and aCOM, this information about the current state of the model should also be included in the input. Furthermore, the joint angular acceleration in the current frame determines the segment angular velocity in the following frame. Since the model is trained to replicate this angular velocity, the IMU data for the frame after the current one should also be used as input. Further future inputs may also be used provide more information. As the model outputs cannot affect the past, past data is not as likely to be useful.

Segments

As discussed in the model section machine learning model needs an RBM to control. As this model involves back and forth from a higher dimensional space, it would be best to keep the amount of variables in the rigid body model low. This would be done by limiting the amount of segments and the rotational degrees of freedom within the joints. Limiting the degrees of freedom can be done by merging segments, or by relating the motion of one segment to another. Reducing the amount of segments could be done by taking an existing model and dissallowing movement in the joints between the merged segmetns. For instance, the joints between the pelvis, sternum, head and neck segments could be removed in this way in order to treat these segments as a single 'torso' segment. Relating the motion of segments to others would involve defining the joint angular acceleration of one joint as a function of another. For instance the joint angular accelation of a leg could defined as a linear function of the joint angular acceleration of the shoulder.

The greatest simplification of this sort that still allows some freedom for the model would be to reduce the model to three segments, two of which are constrained by IMU input. One way to do this would be to make a model consisting of a torso segment, upper arm segment and lower arm segment. Here the torso torso segment would be made out of the strenum pelvis, the legs and an arm, the upper arm segment would consist of only the upper arm, and the lower arm would consist of the lower arm and the hand. The torso segment would be constrained by a pelvis IMU, the lower arm segment would be constrained by a lower arm IMU, and the upper arm segment would be unconstrained. This is shown in figure G.1

Modelling software

To implement this PIML model, a simulation of a rigid body model is required. There are several implementations available. Opensim is a commonly used piece of software for simulating rigid bodies, and it has been used in machine learning projects before. However, Opensim is not very well documented, and the program is relatively computationally expensive. Mujoco is a

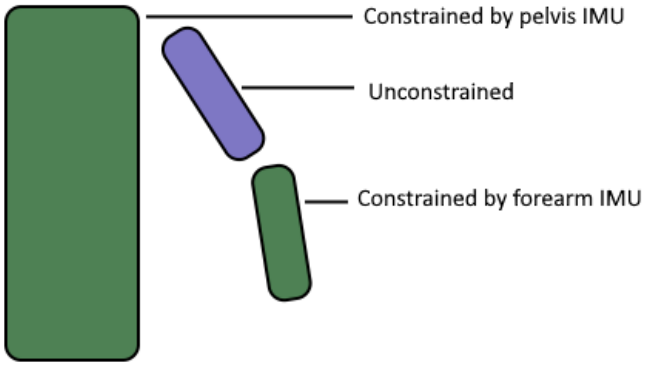

Figure G.1: A schematic depiction of the simple three segment rigid body model with two IMU constraints.

simpler, more lightweight alternative to Opensim, and has been implemented in the reenforcement learning software Gymnasium. This will likely make it easier to implement than Opensim, and the lower weight of the program should make it easier to optimize. Myosuite, another lightweight model, can also be considered. The main advantage that it offers over Mujoco is that Myosuite simulates muscles, while Mujoco does not. Of course, since muscle simulation would be an unnecessary element of complexity, there is no reason to choose Myosuite for this implementation.

Next steps

The first step in implementing this model would be to implement a basic model in Mujoco, using a custom error function to implement PIML. This would be done by first implementing a regular machine learning model to control a simplified rigid body model, and then adding the custom error function to that. To postpone the need for a calibration task, the model can be provided with the initial state from the MVN recording.